ANALYSIS OF SWIRLING FLOW IN ANNULAR DIFFUSER

A Thesis Submitted
In Partial Fulfilment of the Requirements
for the Degree of

DOCTOR OF PHILOSOPHY

by

PRIYA

(2K20/PHDME/501)

Under the Supervision of

Prof. B. B. ARORA
Professor, MED, DTU

Department of Mechanical Engineering

DELHI TECHNOLOGICAL UNIVERSITY
(Formerly Delhi College of Engineering)
Shahbad Daulatpur, Main Bawana Road, Delhi-110042, India

June, 2026

DELHI TECHNOLOGICAL UNIVERSITY
(Formerly Delhi College of Engineering)
Shahbad Daulatpur, Main Bawana Road, Delhi-110042, India

CANDIDATE'S DECLARATION

I, **PRIYA** hereby certify that the work which is being presented in the thesis, entitled **"Analysis of Swirling Flow in Annular Diffuser,"** in partial fulfilment of the requirements for the award of the Degree of Doctor of Philosophy, submitted in the Department of Mechanical Engineering, Delhi Technological University is an authentic record of my own work carried out during the period from January 2021 to April 2026 under the supervision of **Prof. B. B. Arora**, Professor, Department of Mechanical Engineering.

The matter presented in the thesis has not been submitted by me for the award of any other any degree of this or any other Institute.

Date : 22-06-2026 (**PRIYA**)

This is to certify that the student has incorporated all the corrections suggested by the examiners in the thesis and the statement made by the candidate is correct to the best of our knowledge.

Signature of Supervisor Signature of External Examiner

DELHI TECHNOLOGICAL UNIVERSITY

(Formerly Delhi College of Engineering)
Shahbad Daulatpur, Main Bawana Road, Delhi-110042, India

CERTIFICATE BY THE SUPERVISOR

Certified that **Priya** (**2K20/PHDME/501**) has carried out their search work presented in this thesis titled **"Analysis of Swirling Flow in Annular Diffuser",** for the award of **Doctor of Philosophy** from Mechanical Engineering, Delhi Technological University, Delhi, under my supervision. The thesis embodies results of original work, and studies are carried out by the student himself and the contents of the thesis do not form the basis for the award of any other degree to the candidate or to anybody else from this or any other University/Institution.

(**Prof. B. B. Arora**)
Professor
Department of Mechanical Engineering,
Delhi Technological University,
New Delhi, India.

Date: 22-06-2026

DELHI TECHNOLOGICAL UNIVERSITY
(Formerly Delhi College of Engineering)
Shahbad Daulatpur, Main Bawana Road, Delhi-110042, India

PLAGIARISM VERIFICATION

Title of the Thesis **"Analysis of Swirling Flow in Annular Diffuser",**

Total Pages - 153

Name of the Scholar: **PRIYA (2K20/PHDME/501)**

Supervisor: **Prof. B. B. Arora,**

Professor, Department of Mechanical Engineering

This is to report that the above thesis was scanned for similarity detection. Process and outcome are given below:

Software used: **TURNITIN** Similarity Index: **6%** Total Word Count**: 30,802.**

Date: 29-04-2026

Candidate's Signature **Signature of Supervisor**

ABSTRACT

In today's rapidly advancing world, there is an increasing demand for devices that are energy-efficient, safe, and cost-effective. Available usable energy resources are depleting quickly, creating an urgent need to address this challenge. One possible solution is to develop techniques that can convert otherwise unusable energy into useful forms. However, creating such methods often requires significant effort, and in many cases, the outcomes may not justify the cost or may lack economic feasibility.

An alternative and more practical approach is to conserve existing resources by designing energy-efficient systems that minimize energy losses. A diffuser is one such device that plays an important role in energy conservation. It converts the kinetic energy of a flowing fluid—energy that would otherwise be lost—into an increase in static pressure. In turbomachinery systems used for power generation, annular diffusers are commonly employed. These diffusers typically operate under conditions where the incoming flow may contain varying degrees of swirl. Therefore, improving their performance is essential and requires systematic investigation.

Experimental research on annular diffusers is often challenging due to the need for advanced instrumentation and complex, time-intensive procedures, making such studies costly and limiting the extent of research in this field.

The present study combines both experimental and analytical approaches to investigate the aerodynamic behaviour of axial annular diffusers. A specialized test setup was developed to introduce different levels of inlet swirl. Measurements were conducted

using a three-hole cobra probe to determine static pressure distribution, axial velocity, and swirl velocity profiles at various sections along the diffuser length.

In addition to experimental work, computational analysis was carried out using CFD modelling. The study includes grid independence testing and the selection of an appropriate turbulence model that closely matches experimental observations as well as results reported in existing literature. After validation, the CFD model was used to analyse flow characteristics in two types of annular diffusers: one with a parallel hub and diverging casing, and another with both hub and casing diverging at equal angles.

Both diffuser configurations were studied for equivalent cone angles of 10° and 20°, and area ratios of 2 and 3. The influence of inlet conditions—specifically velocity profiles with and without swirl angles of 7.5°, 12°, 17°, and 25° — was examined to evaluate diffuser performance. Detailed flow behaviour was analysed, and key performance parameters were calculated. The development of the flow was studied to identify regions of flow separation and reversal within the diffuser.

The effects of various factors, including inlet swirl, area ratio, diffuser geometry, and cone angle, were systematically analysed to understand their impact on flow separation and overall performance. The results indicate that inlet swirl has an optimal value that maximizes diffuser performance. This optimal swirl level depends on the geometry and configuration of the diffuser.

ACKNOWLEDGEMENTS

I would like to express my heartfelt gratitude to **Prof. B. B. Arora**, Professor and Head of Department, Department of Mechanical Engineering, Delhi Technological University, for his unwavering support, expert guidance, and continuous encouragement throughout the course of this research. Prof. B. B. Arora with his wide experience, sharp and incisive intellect, and maestro ability combined with astute research methodology and deep insight of the subject has unerringly steered the work on smooth and steady course. It has been a privilege to work under his mentorship, and I am truly grateful for the opportunity to learn from his vast knowledge and experience. I deeply appreciate the time and effort he has invested in guiding me during this journey.

I express my deepest gratitude to my grandparents Late Mr. Jai Gopal and Mrs. Pushpa Devi, my parents Dr. Vipin and Mrs. Parveen and my uncle Mr. Jitender Kumar for their unconditional love, unwavering support, and constant encouragement throughout my life. I am equally thankful to my sister Nishita for her understanding, support, and belief in me, which have been a source of strength during this journey.

Lastly, I express my heartfelt appreciation to all those — friends, mentors, and well-wishers—who, through their encouragement, thoughtful feedback, and kind words, have supported and influenced this work, whether directly or indirectly.

(PRIYA)

(2K20/PHDME/501)

TABLE OF CONTENTS

LIST OF TABLES

LIST OF FIGURES

LIST OF SYMBOLS

SYMBOL

A	:	Diffuser Annular Area
AR	:	Area Ratio
B	:	Blockage Factor
C_p	:	Pressure Recovery Coefficient
Θ_c	:	Casing Angle
Θ_h	:	Hub Angle
E	:	Effective Area Fraction
Re	:	Reynolds Number
T_u	:	Turbulence Intensity
x	:	Axial position from Inlet of Diffuser
L	:	Diffuser Axial Length
x/L	:	Nondimensional Axial Length
y	:	Traverse Position from Hub Surface
Ym	:	Annular Height
y/Ym	:	Normalized Diffuser Passage Height
R_h	:	Hub Radius
R_c	:	Casing Radius
L/R	:	Length To Radius
W_2/W_1	:	Aspect Ratio
S	:	Dimensionless Swirl Number
R_{hi}	:	Inlet Radius Hub
R_{ci}	:	Inlet Radius Casing
R_{hi}/R_{ci}	:	Inlet Radius Ratio
Φ	:	Swirl Angle

θ	:	Angle Of Divergence
2θ	:	Total angle of divergence or equivalent cone angle
ρ	:	Density
μ	:	Molecular Viscosity
η	:	Diffuser effectiveness
φ	:	Yaw angle
U	:	Velocity
U_m	:	Maximum Longitudinal Velocity
D_{eq}	:	Equivalent Diameter of Flow Passage
N/R_i	:	Non-Dimensional Length
P_t	:	Total Pressure
P_s	:	Static Pressure
P_{atm}	:	Atmospheric Pressure
K-ε	:	Kinetic energy, Eddy viscosity
K-Ω	:	Kinetic energy, Shear stress
V_z	:	Swirl Velocity

CHAPTER 1

INTRODUCTION

A diffuser is a device with a gradually expanding flow passage, commonly used in engineering applications to decrease the velocity of a fluid while simultaneously increasing its static pressure along the flow direction. Diffusers are widely employed in various internal flow systems such as aircraft engines inlets and combustion chambers, turbines, compressors, fans, blowers, and other rotating machinery. They are also found in wind tunnels, water channels, draft tubes, carburetors, flow meters, ejectors, and noise control devices. The design of a diffuser depends on specified inlet conditions and geometrical limitations, which ultimately define its configuration. Based on application requirements, diffusers can take different shapes, including rectangular, conical, annular, or radial forms.

In an ideal situation involving one-dimensional, incompressible, and inviscid flow, the pressure rise in a diffuser results solely from the increase in flow area, which reduces kinetic energy. However, real fluid flow behaves differently due to viscosity. As fluid passes through the diffuser, it encounters an adverse pressure gradient that slows it down. This effect is more pronounced near the walls, where boundary layers form and grow rapidly. The low-momentum fluid in these regions is especially affected, leading to energy losses and reduced efficiency. Consequently, the actual pressure recovery is always lower than the theoretical value. This is because of the reason that the flow dynamics of an actual fluid in the diffuser gradually slows down because of an adverse pressure gradient, creating a boundary layer against the solid surfaces that thickens quickly with the diffusion. This pressure gradient continuously slows the

fluid, especially affecting low momentum fluid close to the solid surfaces. The viscous energy loss in the slowed flow complicates the diffusion process, resulting in the diffuser not recovering as much pressure compared to ideal conditions.

The performance of a diffuser is influenced by two main categories: Geometric and Fluid dynamic. Geometric factors include parameters such as diffuser length, area ratio, divergence angle, and aspect ratio, all of which determine the optimal shape. Fluid dynamic factors include inlet velocity, turbulence intensity, Reynolds number, Mach number, flow uniformity, blockage ratio, and swirl. These factors significantly affect flow behavior and overall efficiency.

Many practical systems require diffusion to occur in annular passages. Annular diffusers are particularly important in turbomachinery, where the flow must adapt to annular combustion chambers and pass around central shafts, supports, and bearings. These diffusers are more complex due to the presence of both inner and outer walls, which introduce additional flow interactions. Furthermore, annular diffusers often operate under swirling flow conditions. This swirl may originate from upstream components such as compressors, inlet guide vanes, or rotating shafts.

The presence of swirl and annular geometry contribute to rapid boundary layer growth and uneven velocity distribution. This can lead to pressure losses, instability, and even flow seperation or recirculation. Because of these challenges, researchers focus on understanding the factors affecting diffuser performance and improving characteristics through detailed investigations.

Experimental studies play a key role in identifying ways to reduce energy losses and enhance pressure recovery. When combined with analytical methods and empirical correlations, these studies help improve diffuser design and performance. Improved diffuser efficiency directly enhances the overall performance of the fluid system in which it is used.

1.1 Problem considered

A review of existing research shows that most studies have focused on two-dimensional and conical diffusers, while annular diffusers have received comparatively less attention. Additionally, several important influencing factors have not been thoroughly investigated. These include inlet turbulence intensity, distorted velocity profiles, Mach number effects, equivalent cone angle, swirl, and flow pulsations.

Among these, swirl and equivalent cone angle are expected to have a significant impact on diffuser performance. Despite efforts to design annular diffusers that avoid flow separation, achieving consistent success has been difficult. These is also a lack of comprehensive, experimental, and analytical data regarding pressure recovery and energy loss coefficients across a wide range of geometries and swirl conditions. This gap exists mainly due to the complexity of swirling flows, which are difficult to measure and analyze.

Because experimental investigations require sophisticated equipment and are time-consuming and costly, research in this area has been limited. As a result, the present study only focuses on

analyzing specific aspects of swirling flow in annular diffusers using both experimental methods and Computational Fluid Dynamics (CFD).

This work examines annular diffusers with equivalent cone angles between 10° and 20° and area ratios of 2 and 3. It evaluates parameters such as pressure recovery, velocity distribution, and flow behavior under different swirl angles (0°, 7.5°, 12°, 17° and 25°). CFD simulations are also concluded to validate experimental results and predict flow characteristics for additional configurations.

1.2 Structure of the Study

The organization of the thesis is as follows:

Chapter 1 introduces the topic and outlines the research problem.

Chapter 2 reviews previous studies on diffusers and analyzes key influencing factors.

Chapter 3 describes the experimental setup, instruments, and measurement techniques used.

Chapter 4 explains the CFD modeling approach, including mesh generation and solution methods.

Chapter 5 presents validation of CFD results through comparison with experimental data.

Chapter 6 discusses the result and key findings.

Chapter 7 concludes the study and suggests directions for future research.

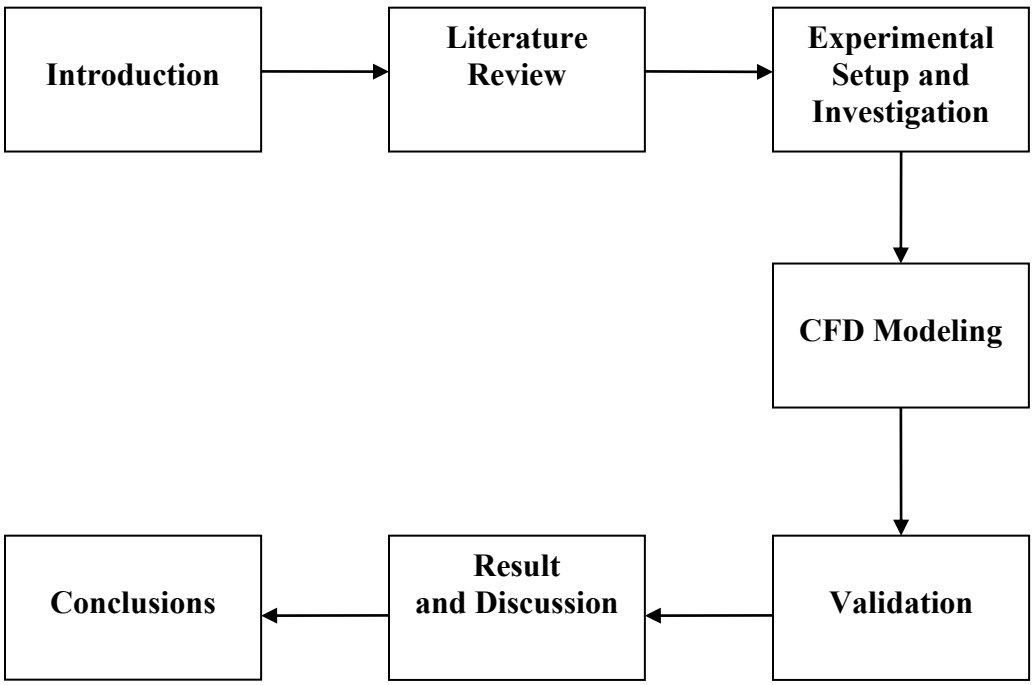

Figure 1.1 Flow chart of the thesis

CHAPTER 2

REVIEW OF DIFFUSER STUDIES

The movement of fluid passing through a diffuser experiences a steady slowing down, which leads to the transformation of kinetic energy into pressure energy. This process is known as Diffusion. The flow near the walls of the diffuser faces more significant slowing due to the creation and expansion of the Boundary layer. The growth of the boundary layer is especially noticeable in a diffuser because of the existing adverse pressure gradient. Given that diffusers typically function at high Reynolds numbers, the flow is almost always turbulent. The condition and growth of the turbulent boundary layer significantly impact how well a diffuser works. Therefore, it is essential to study the factors that affect the development of the boundary layer and how they relate to the performance of the diffuser when aiming for optimal diffuser design.

The initial quantitative research into diffusers dates back to the late 18th century when Venturi and his peers tried to define the shape of an effective diffuser for a specific flow scenario. Since that time, diffusers with various shapes have been extensively studied through many experimental and empirical research efforts. The different elements of diffuser flow that various researchers have looked at can be broadly grouped into these main categories:

1. Studies that explore the impact of various factors on pressure recovery and flow characteristics in diffusers;
2. Research aimed at enhancing the performance of diffusers by using special tools and techniques;

3. Analytical investigations to create semi-empirical methods for predicting diffuser performance.

This chapter focuses on revisiting these aspects of diffuser flow behavior. In this regard, the existing literature has been reviewed to provide insights on the current state of knowledge and to identify areas for further investigation on the topic.

2.1 Performance Parameters

The condition and evolution of the turbulent boundary layer significantly affect how well a diffuser works. Thus, exploring the factors that control the development of the boundary layer and how they relate to diffuser performance is crucial for enhancing diffuser design.

Choosing the "ideal" diffuser design for a specific use is complex due to the numerous factors that influence its performance. The performance is actually determined by the goals that the diffuser needs to achieve. Usually, one or more of the following criteria are set for a diffuser:

- Highest static pressure recovery
- Least stagnation pressure loss
- Limited length
- Defined area ratio
- Specific cross-sectional shape

Considering the above constraints, the various factors that affect pressure recovery and flow characteristics in diffusers can be categorized into:

- Geometric parameters

- Flow parameters

Diffusers can adopt numerous shapes by combining different wall parameters. The design of a symmetrical two-dimensional diffuser is established by its aspect ratio b/W_1, and any two from the following three independent geometric parameters: total angle of divergence 2θ, area ratio, aspect ratio W_2/W_1, and the non-dimensional length N_1/W_1. Conical diffusers are defined by the non-dimensional length N/R_1, the divergence angle, AR, or 2θ. To outline the shape of straight-walled annular diffusers, four factors are necessary: angles case angle (θ_c) and hub angle (θ_h), the inlet radius ratio Rh_1/Rc_1, and the non-dimensional length N/R_1. Figure 2.1 displays the types of axial diffuser geometries where the centerline is straight and the walls are flat surfaces connecting the entry and exit points. Figure 2.2 presents various models of straight-walled axial annular diffusers. The geometric features of the annular diffusers are depicted in Figure 2.3. The idea of equivalent cone angle for annular diffusers is shown in Figure 2.4.

Key flow parameters encompass certain aspects of the inlet boundary layer, including the inlet velocity profile, boundary layer thickness, blockage factor, turbulence characteristics, inlet flow Reynolds number, Mach number, and the swirl degree at the inlet.

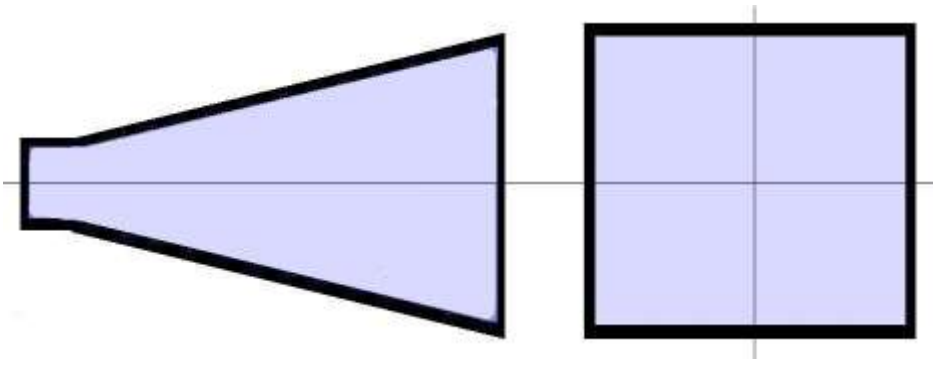

Rectangular Diffuser

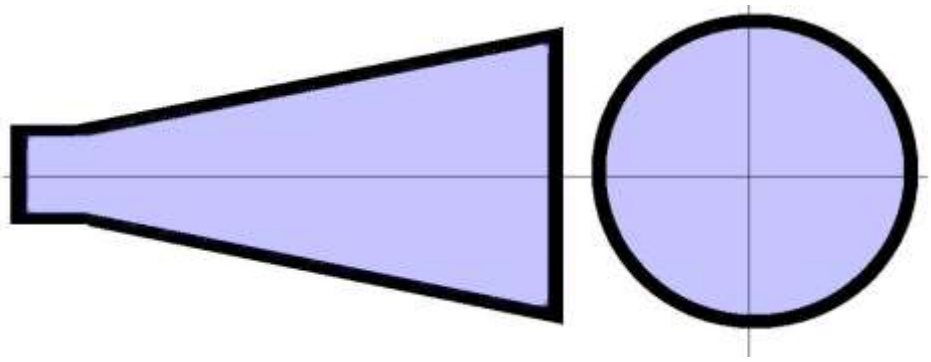

Conical Diffuser

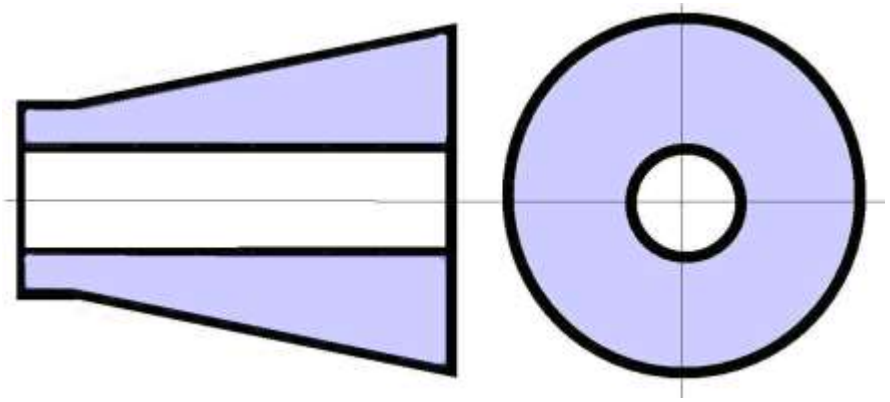

Annular Diffuser

Fig. 2.1 Types of Axial Diffusers

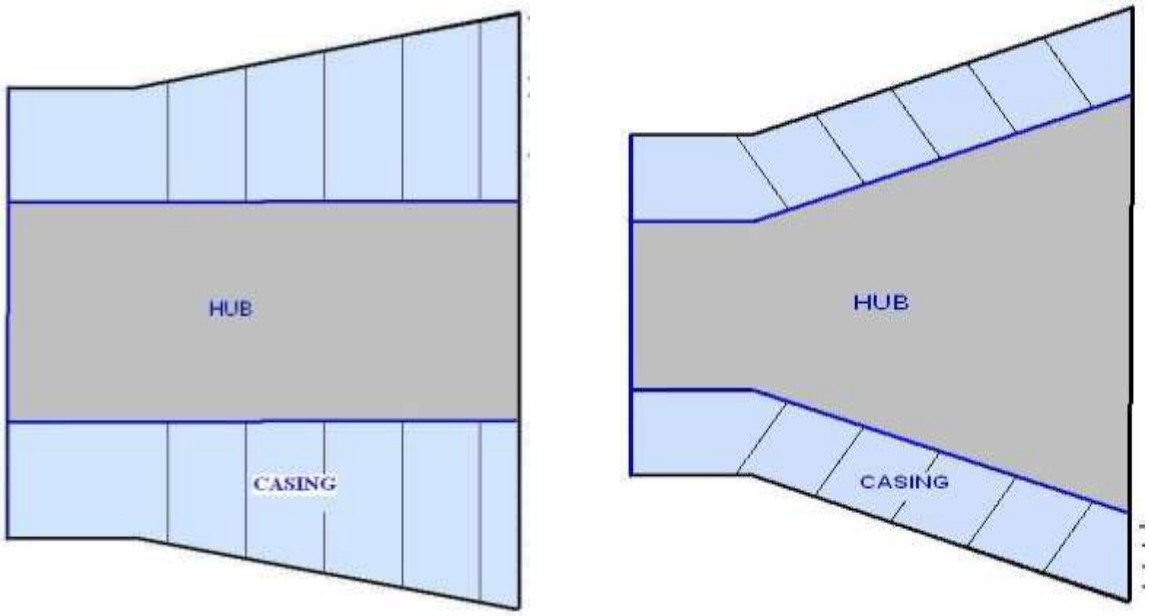

CASE A

Parallel Hub Diverging Casing

CASE B

Both Hub and Casing Diverging With equal angles

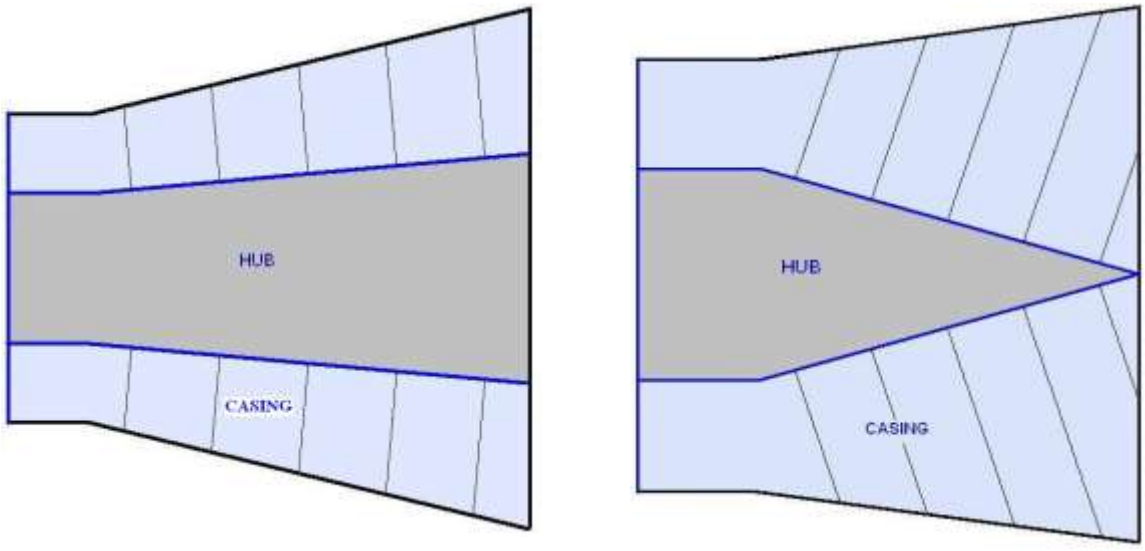

CASE C

Both Hub and Casing Diverging with unequal angles

CASE D

Hub converging and Casing Diverging

Fig. 2.2 Types of Axial Annular Diffusers

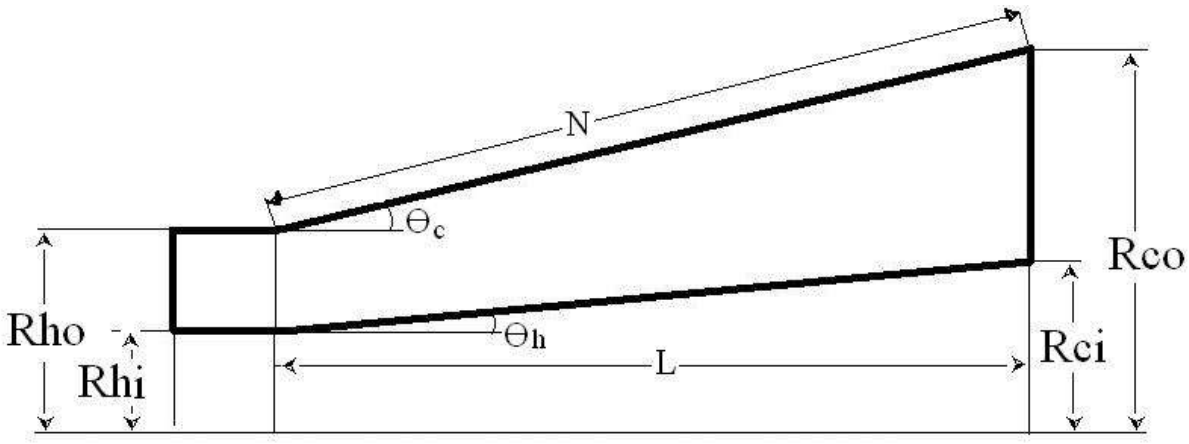

Fig. 2.3 Annular Diffuser Geometrical Parameters

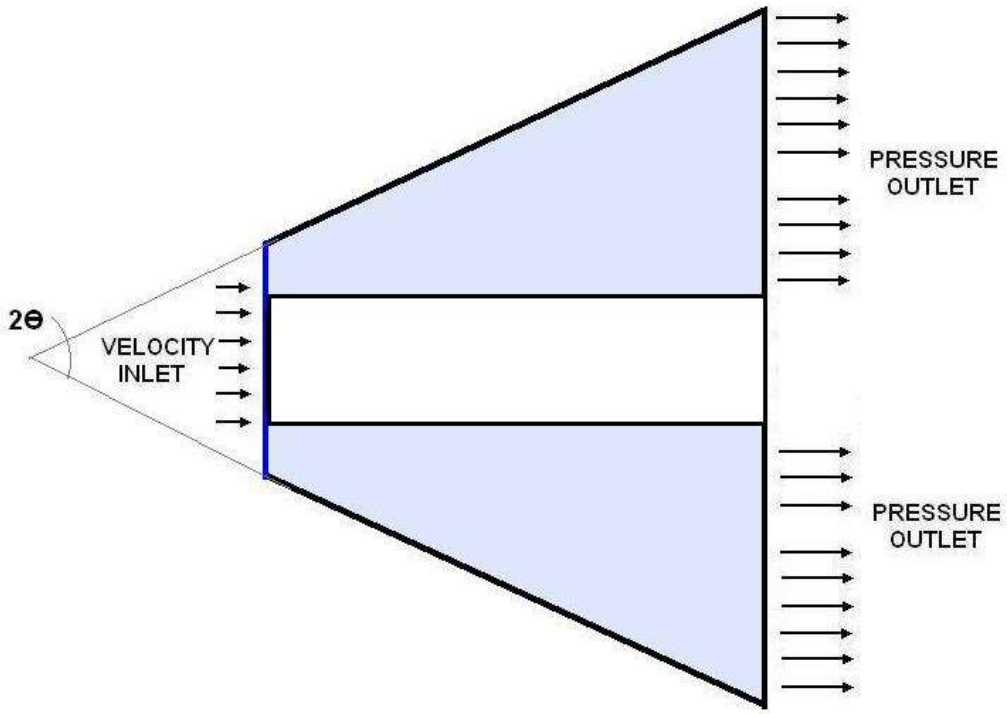

Fig. 2.4 Equivalent cone angle representation of Annular Diffuser

2.2 Effects of Geometric Parameters

2.2.1 Passage Divergence, Length and Area Ratio

Ashjee and Johnston conducted research in 1979 and 1980 on two-dimensional diffusers, finding that the best recovery occurs with a divergence angle between 8 and 9 degrees, with roughly two-thirds of this recovery happening in the first third of the diffuser length. Reneau and colleagues, in studies from 1964 to 1967, determined that for straight two-dimensional diffusers, maximum pressure recovery happens at a constant area ratio within the angle range of 6 to 8 degrees. Higher divergence angles revealed a similar pattern of reduced efficiency, as reported by Howard and colleagues in 1967, along with Stevens and Markland in 1968.

Sharan, in 1972 and 1976, noted that the performance of conical diffusers declines with an increasing divergence angle while maintaining a constant area ratio. Patterson observed in 1938 that for conical diffusers, the best efficiencies—in conjunction with the lowest loss coefficients—are found with cone angles ranging from 5 to 8 degrees and area ratios of 2.0 to 4.0. Conversely, for the same cone angle, performance improves when the area ratio increases. Cockrell and Markland, in their 1963 review of Patterson's earlier work, found that changing the area ratio from 2.5 to 8.0 has a minimal impact on the loss coefficient of conical diffusers. In 1965, McDonald and Fox researched conical diffusers using water and documented the contours of peak recovery based on the ratio of diffuser length to inlet radius, considering different area ratios. A follow-up study by Ishikawa and Nakamura in 1989 reported findings that closely matched those of McDonald and Fox from 1965. The results indicated effectiveness as a function

of cone angle for area ratios greater than 3, with effectiveness decreasing as the cone angle increased beyond 6 to 10 degrees.

Kanemoto and colleagues in 1982 and 1983, Lohmann and associates in 1979, and Yu and others in 1992 explored the effectiveness of annular diffusers with varying area ratios and angles for both inner and outer walls. Adkins in 1975 and Kwon and his team in 2002 investigated how the shape of the mixing chamber affected the performance of annular jet pumps at different jet flow rates using two-dimensional numerical simulations. The computational findings closely matched experimental results, with the RNG k-ε model showing slightly better alignment with the data than the standard k-ε approach.

Sovran and Klomp in 1967, created the first widely utilized maps for channel diffusers showing annular diffuser configurations. These maps illustrate the ideal diffuser shapes across various conditions. The optimal conditions generally stated include:

1. The C_p line: a graph representing diffuser area ratios that achieve maximum pressure recovery for specified non-dimensional diffuser lengths;

2. The C_p line: a graph indicating non-dimensional diffuser lengths that yield maximum pressure recovery for a given area ratio.

Sovran and Klomp [1967] defined the ideal lines C_p for two-dimensional diffusers. They also identified the position of these ideal lines for conical diffusers using findings from different

researchers like Ripple [1958], Cockrell and Markland [1963] and McDonald and Fox [1965], while Reneau et al. [1964] discovered the ideal lines for annular diffusers. The ideal lines for diffusers with different cross-sectional shapes were found to be closely clustered. This close clustering indicated that the area ratio and the non-dimensional length significantly influence the determination of the optimal geometry for diffusers, regardless of their type.

2.2.2 Down-Stream Ducting, Tail Pipe

A portion of the kinetic energy flow from a distorted profile is regained as an increase in static pressure when a non-uniform velocity pattern in a duct with consistent area transitions to a nearly uniform profile. This can be achieved by incorporating a tailpipe at the end of the diffuser, which aids in capturing some of the excess kinetic energy from a non-uniform exit profile. Cockrell and Markland [1963] and Lai and So [1989] studied a 15º conical diffuser with an area ratio of 2.5 functioning under fully developed flow conditions at its entrance and noted a 60% rise in pressure recovery due to the addition of a tailpipe. Meanwhile, Reneau and colleagues in 1964 observed that extending the length of the diffuser led to a pressure recovery enhancement of up to 30%. Experimental findings by Ainley [1946] and Stevens [1968] on annular diffusers indicated a similar pattern, where the diffusion process persisted for a certain distance downstream from the exit of the diffuser. A significant portion of the overall increase in pressure is likely to take place in the tailpipe, influenced by the angle of divergence and various other elements. Kelnhofer and Derick in 1971 demonstrated that the length of the tailpipe greatly affects not only the peak recovery level but also the ideal area ratio for achieving high efficiency in a diffuser. The greatest improvement ranged from 2 to 6 exit diameters for a stalled diffuser with non-uniform flow at the exit. Ishikawa and Nakamura in 1990 found that including a

tailpipe in a conical diffuser led to notable enhancements, with optimal efficiency occurring at a higher area ratio for a specified value of L/r1, suggesting a larger value of 2θ.

2.3 Effects of Flow Parameters

2.3.1 Inlet Profile and Distortions

The profile of the inlet caused by the development of the turbulent boundary layer along the diffuser walls shows the previous behavior of the flow. Different techniques can be utilized to manipulate the inlet profile, such as the addition of trip wires, central bodies, or an adequate length of constant diameter pipe in front of the diffuser.

Key factors that define the average velocity profile at the inlet include the length of the upstream pipe, and the thicknesses related to displacement and momentum, as well as the ‘peakiness’ of the profile. The peakiness of the inlet profile is understood as the ratio of maximum velocity to average velocity. An increased approach length results in a thicker boundary layer. The impacts of approach length and boundary layer thickness are similar. The effectiveness of a diffuser declines when the thickness of the boundary layer rises, as demonstrated by numerous studies. How the boundary layer has grown is as vital as its thickness in evaluating the diffuser's effectiveness.

The research conducted by Al-Mudhafar et al. [1982], Masuda et al. [1971, 1975], Waitman et al. [1961], Buice and Eaton [1997, 2000] and Wolf and Johnston [1969] on two-dimensional diffusers indicated that the recoveries were low with distorted inlet profiles. In fact, the wake

caused by an upstream disturbance near the wall continues into the diffuser, leading to reduced velocities along one wall. Chitambaran et al. [1984] examined the impact of an airfoil-shaped strut at the entrance, noting a significant drop in pressure recovery when placed at zero angle to the diffuser axis, while a steep increase was observed at 7º and 10º angles.

Yoshinaga et al. [1985] and Agrawal et al. [1991] characterized inlet distortion based on the velocity coefficient, which compares mass-averaged mean velocity to area-averaged mean velocity. Sajben et al. [1974], Shimizu et al. [1982] and Frendikov and Yanko [1972] researched inlet distortions in conical diffusers, concluding these distortions reduced pressure recovery. Keri et al. [2006] explored how inlet conditions affect image-based CFD models, finding that the real velocity profile produced improved results. Filipenco et al. [2000] investigated how inlet flow conditions impacted pressure recovery and the operational range of radial diffusers in centrifugal compressor stages, examining factors like diffuser inlet Mach number, flow angles, blockage, and non-uniform axial flow.

The overall pressure recovery coefficient of the diffuser, based on properly averaged inlet total pressure, showed a good correlation with the momentum-averaged flow angle entering the diffuser. The inlet dynamic pressure, which utilizes availability or mass-averaging combined with the definition of inlet flow angle based on the mass average of the radial and tangential velocities at the inlet of the diffuser, mitigates this sensitivity.

2.3.2 Inlet Blockage Factor

The inlet boundary layer influences how well a diffuser works, which is usually studied regarding the blockage factor B and the effective area fraction E. These concepts are described as

$$B = 1 - E = \frac{1}{A}\int (1 - \frac{U}{U_m})dA \tag{2.1}$$

$$E = \frac{1}{A}\int \frac{U}{U_m}dA \tag{2.2}$$

Reneau et al. [1964], Runstadler and Dean [1969], Runstadler and Dolan [1973], Sovran and Klomp [1967] and Waitman et al. [1961] demonstrated that the effectiveness of diffusers diminishes as the level of blockage rises in two-dimensional cases. Kano et al. [1982] and Kenny [1972] revealed that the impact of fluid dynamic blockage at the diffuser throat due to different factors in planar diffusers can be integrated into quasi-steady boundary layer calculations. It has been noted that increasing the inlet blockage four times, while keeping other variables unchanged, could lead to a 15 to 20% reduction in pressure recovery. Tyler and Williamson [1968, 1973] conducted experiments that showed a continued rise in inlet blockage resulted in the effectiveness increasing again, eventually surpassing one. This indicates that if the inlet distortion is severe enough, the positive effects of mixing can outweigh the negative consequences of increased blockage. Research by Reneau et al. [1964] along with the analysis by Sovran and Klomp [1967] suggested that optimally designed diffusers are only minimally influenced by inlet distortion.

Livesey and Odukewe [1973] and Sharan [1976] explored the aerodynamic blockage in conical diffusers based on approach length. Their findings indicated that the pressure recovery initially declines but later improves as the length increases due to growth in the boundary layer. Kline [1981] analyzed pressure recovery data in relation to inlet aerodynamic blockage in conical

diffusers, drawing from research by Cockrell and Markland [1963], Miller [1971], and Peters [1934] and comparing it to that of Runstadler and Dolan [1973]. He noted that Miller's results showed greater pressure recovery than those from Runstadler and Dolan for lower divergence angles, while results were similar for higher divergence angles.

Johnston's experimental findings [1954] indicated that for minor blockage fractions in annular diffusers, the reduction in effectiveness as blockage increases is minimal. However, when blockage factors exceed 0.15, there is a significant drop in effectiveness. Conversely, Bradshaw et al. [1963, 1964] and Steven and Williams [1971, 1980], along with Japikse [1986], discovered that after a slight decrease in static pressure recovery with the initial thickening of the boundary layer, the static pressure recovery actually increases again when the inlet boundary layer becomes thick enough to resemble fully-developed inlet flow. Bradshaw attributed this phenomenon to an enhanced level of radial momentum transfer. Klein [1995] compared the findings of Steven and Williams [1980] regarding annular diffusers with those of Sovran and Klomp [1967] for an inlet blockage of 0.02 and assessed predictions for higher blockage values. Ubertini and Desideri [2000] experimentally examined the performance of an annular diffuser with and without a strut, concluding that the performance improves with the strut in stalled diffuser scenarios.

The impact of inlet aerodynamic obstruction on an annular diffuser is more intricate compared to channel or conical diffusers since both the hub and casing surfaces can create boundary layers with notably distinct histories. Additional blockage on one side affects the effective flow area,

which in turn alters the core flow velocity, thus affecting the boundary layer's development on the wall across from it. As a result, intricate interactions arise within the annular diffuser.

2.3.3 Inlet Reynolds and Mach Numbers

Al-Mudhafar et al. [1982], Runstadler and Dolan [1973], and McMillan and Johnston [1973] examined how the Reynolds Number impacts the effectiveness of two-dimensional diffusers. They discovered that for high aspect ratios, this number was not a critical factor, but was significant at lower aspect ratios. Sprenger [1959] along with Cockrell and Markland [1963] and Raghunathan and Cooper [2000] found that when the inlet boundary layer parameters stay the same, changes in the inlet Reynolds number from 2x10^4 to 7x10^5 did not notably influence the performance of the diffuser. Runstadler and Dolan [1973] and Sharan [1972] pointed out that thick boundary layers did not show any change in pressure recovery as the Reynolds number increased. Conversely, the performance of thin boundary layers improved with a rise in the Reynolds number. This enhancement in performance was linked to a higher level of turbulence. Increased turbulence enhances radial momentum transfer, which delays flow separation and boosts pressure recovery.

Runstadler and Dolan [1973], as well as Duggins [1970, 1975], studying conical diffusers, reported that a Reynolds Number exceeding $2x10^5$ did not influence the pressure recovery coefficient. However, Bansal and Khanna [1977] noted a significant effect on the diffuser that was undergoing transitory stall. Thayer [1971], Japikse and Pamoreen [1979], Little and Wilbur [1954], Runstadler and Dean [1969], Adkins and Wardle [1992], Kwong and Dowling [1994] and Van Dewoestine and Fox [1966] concluded that an increase in the inlet Mach number

negatively impacts pressure recovery. These authors also indicated a slight improvement in pressure recovery when the Mach number rises from a low level to higher subsonic values. Yet, once sonic conditions are reached at the throat of the diffuser, local choking happens, causing performance to decline sharply with further increases in the Mach number within the diffuser.

Moller [1966]; Adenubi [1976]; Kibichov and Sayers [2008]; Nordin et al. [2015] examined how Reynolds number (Re) affects the increase of static pressure in both conical and radial diffusers, where the divergence angle was raised by a certain amount linked to static pressure recovery. The pressure recovery ratio grows with the rise in Reynolds number. For the radial diffuser, when the Reynolds numbers drop below 105, the pressure recovery declines quickly. Nordin et al. [2017] analyzed the flow characteristics of three-dimensional turning diffusers under various inlet conditions (Rein= 5.79E4-1.78E5) and different geometric parameters. The role of inlet boundary conditions allowed for the successful development of performance correlations through CFD with a deviation of around 7% from experimental results.

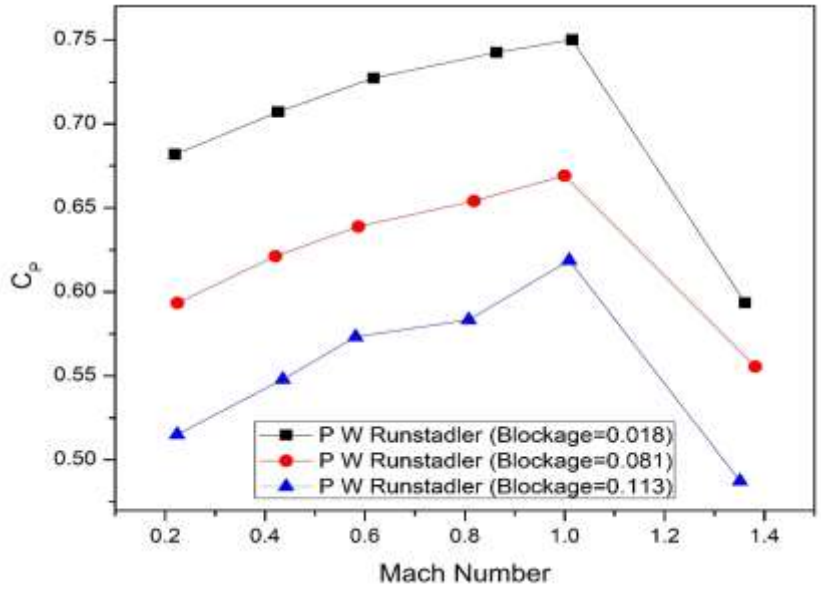

Figure 2.5: Static pressure recovery with Mach number. (Runstadler & Dean [1969]).

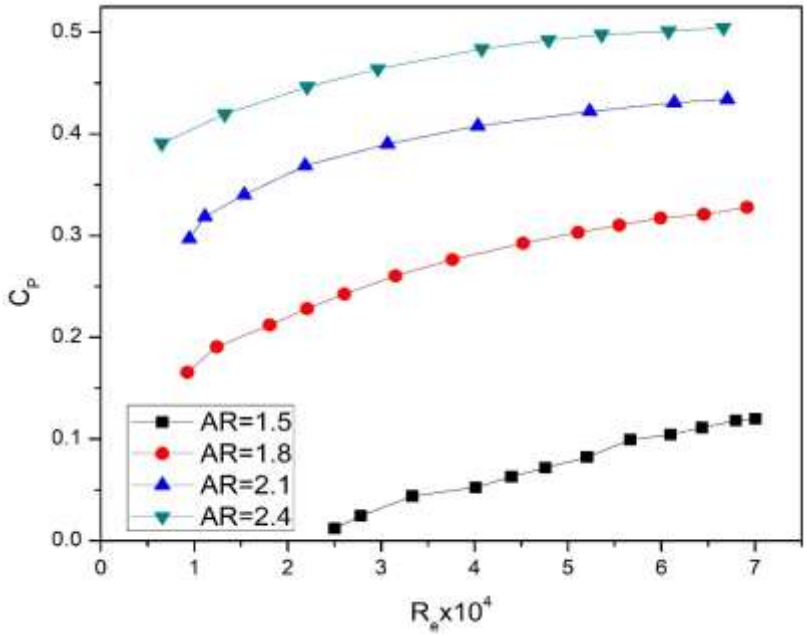

Figure 2.6: Static pressure recovery with Reynolds number. (Mcmillan & Johnston [1973].

Figure 2.5 illustrates how the Mach number changes with the recovery of static pressure for flows that are incompressible. Figure 2.6 demonstrates that the recovery of static pressure in

diffusers increases when the Reynolds number rises. Gartner & Amitay [2016] evaluated how well various passive and active actuators performed in a rectangular diffuser. Their studies examined how height, the arrangement of passive vortex generators located on the ramp's front, and the spacing between vortex generators impact these factors. Consequently, the AIP pressure recovery rose from 78.5% to 85.5%. According to Wen et al. [2012], a diffuser shock wave at the entrance was caused by the Mach number, resulting in a rapid decrease in total pressure as the static pressure and static temperature increased swiftly. Van & Fox [1966] found that the behavior of an incompressible fluid in a conical diffuser is influenced by the Mach number. The efficiency of the diffuser does not depend on the divergence angle, which rests just beneath the initial noticeable stall line at a particular Mach number and aspect ratio of the diffuser design. Little and Wilber [1950] and Dean et al. [1969] examined the significance of geometric factors, Mach number, aspect ratio, and obstruction at the diffuser's entrance. The performance of the diffuser, measured by pressure loss coefficient and efficiency, is greatly affected by the size of the boundary layer and the angle of the wall. Increasing these variables significantly reduces the effectiveness of diffusers.

2.3.4 Inlet Turbulence Level

The turbulence intensity is most frequently defined as an RMS value:

$$T_u = \frac{\left[1/3\left(u'^2 + v'^2 + w'^2\right)\right]^{1/2}}{U} \tag{2.3}$$

Hoffmann et al. [1981, 1984, 1988] carried out research on two-dimensional diffusers with angles of 2θ = 12° and 20°. The maximum pressure recovery occurred with turbulence levels of 10% for the 12° diffuser and 24% for the 20° diffuser. Hoffmann and Gonzalez [1984] demonstrated that turbulence decreased the effects of distortion and postponed flow separation.

Ginevsskiy et al. [1975] noted that the ideal divergence angle is improved by the presence of inlet turbulence Klein et al. [1981], Armfield and Fletcher [1986], Armfield [1990], Bradshaw [1972] and Sajben et al. [1974] stated that the efficiency of conical diffusers rises with higher turbulence at the inlet. Additionally, this improvement grows as the area ratio increases. Sharan [1972] reported that when Re=105, the rise in pressure recovery starts slowly and then becomes nearly constant at approximately 4% turbulence intensity. For greater Reynolds numbers, the increase in pressure recovery is quite rapid and levels off around a turbulence intensity of about 7%. The enhanced mixing caused by greater turbulence helps to make the speed profile at the inlet more consistent, thus improving pressure recovery. Adenubi [1975], Sharan [1972], and Stevens and William [1971] observed a rise of 10 to 12 percent in pressure recovery when the turbulence intensity in an annular diffuser increased from 4% to 10%. Sitaram and Treaster [1985], Ji-jun et al [1992], Johnston [1998] and Masahiro Ishida et al. [2001] investigated the reduction of rotating stall through controlling wall roughness in vaneless diffusers used in centrifugal blowers. They found that the turbulence intensity raised considerably in the boundary layer on the hub side due to the rough wall, which prevents three-dimensional separation; however, there was a slight pressure drop from the locally rough surface, which was noted to be under 1 percent of the total pressure increase of the blower. Hestermann et al. [1995] and Klein [1995] discovered that boosting turbulence levels to between 6-8.5% is advantageous for enhancing pressure recovery and also aids in eliminating separation in a stalled diffuser. Klein [1995] also indicated that the turbulence intensity in fully developed flow was approximately 3%. However, it is important to recognize that very high turbulence levels lead to greater energy losses. Hence, it is essential to find an appropriate balance between the positive effects of increased mixing or turbulence and the negative effects of excessive energy losses.

The swirl influences the flow properties, impacting elements such as the pass-through diffusing duct and how losses are distributed near the walls. Agrawal et al. [1994], Singh et. al. [1995], Arora and Pathak [2005, 2009, 2011], Arora [2007, 2014], Kumar et al. [2011], Arora et al. [2010] and Singh & Arora [2019, 2021, 2023] studied annular diffusers with area ratios between 2 and 4, and they experimentally derived inlet velocity profiles using computational fluid dynamics methods. To verify the experimental findings and forecast the performance of the annular diffusers, the RNG k-ε model was employed. Mansour et al. [1989] Choudhury [1993], Constantinescu et al. [2003] and Gorman et al. [2016] assessed five turbulence models based on experimental data involving swirl flow across various engineering applications. The SST κ–ω model proved to be the most effective for heat transfer scenarios. The predictions of speeds near the walls of the apparatus were particularly accurate when compared to those from other models. Azouz and Shirazi [1997] and Barbosa et al. [2015] created a mathematical model to analyze internal velocity behavior in three types of conical diffusers. A positive velocity gradient was observed, and the model aligned well with experimental results within the diffuser area at its peak velocity. However, at larger diffuser angles, the velocity gradient turned negative, leading to discrepancies between experimental data and theoretical predictions due to flow separation and viscous effects. El-Askary et al. [2015] demonstrated the numerical validation of two distinct flows through Eulerian-Lagrangian methods and the k-ε turbulence model. They tackled the issue using two different approaches: continuous and dispersed phases. Vlahostergios & Yakinthos [2015] documented two diverse Mach numbers in a converging-diverging diffuser experiencing transonic flow. Utilizing more complex turbulence models resulted in very accurate representations of flow behavior within a diffuser. Selvakarthick et al. [2016] claimed that the

greatest possible static pressure increase could be achieved in the shortest length possible with a gas turbine engine equipped with a dump diffuser design. Davis et al. [2002, 2003], Tsurusaki and Kinoshita [2001] and Lipeng et al. [2016] examined turbulent flow in a rectangular asymmetric diffuser through CFD using seven turbulence models. When it comes to evaluating static pressure, velocity, vortices, and flow features, the RSM turbulence model surpassed the performance of the other turbulence models.

2.3.5. Inlet Swirl

The presence of a swirling flow at the diffuser's entrance indicates that there is a tangential velocity component. This phenomenon has been studied in conical and annular diffusers; however, it also plays a significant role in two-dimensional diffusers commonly used in different pumps and compressors. Typically, the swirl is represented by the swirl angle at the inlet.

The swirling motion observed in a diffuser can be caused by residual swirl from a preceding compressor or turbine, or it may originate from guide vanes positioned at the entrance of the diffuser or a rotating object placed inside. Peters [1934], Sprenger [1959], Liepe [1960], McDonald and colleagues [1971], as well as So [1967], investigated swirling flows in conical diffusers. Peters [1934] noted that the performance of the diffuser improves with increased inlet swirl. Conversely, Liepe [1960] suggested that swirl could negatively impact diffuser performance with both free and forced vortex types, while it might prevent flow separation in wide-angle diffusers, thus providing benefits in such cases. Sprenger [1959] discovered that swirl helps redistribute excessive velocity from the center to near the walls, allowing for a better velocity profile at the diffuser entrance. So [1967] reported that certain swirl conditions led to

vortex breakdown and reverse flow at the center of the diffuser. He also identified a ‘stagnation bubble’ moving towards the entrance as swirl increased, using flow visualization methods. According to McDonald and associates [1971], introducing swirl could enhance the performance of diffusers that are moderately or severely stalled. Senno and colleagues [1978] noted the formation of a large solid vortex core at the center of the conical diffuser where the velocity was notably low. A similar solid vortex core was observed by Thakker in 1986 and by Thakker and others in 1991, although the decrease in axial velocity was not as pronounced as previously found. Clausen and colleagues in 1993 determined that the swirling flow's tendency to recirculate raises the velocity near the edge of the boundary layer and decreases the likelihood of separation.

Hoadlay [1970], Schwartz [1949], and Srinath [1968] conducted research on swirling flow in annular diffusers. Schwartz explored annular diffusers with a steady outer diameter, determining that optimal performance regions exist when swirl angles are similar to the total divergence angle of the annular walls; a significant drop in pressure recovery was noted for swirl angles exceeding the optimal levels. Srinath [1968] reached comparable conclusions while examining axial flow within equiangular annular diffusers, where the swirl ranged from 0° to 15°. The maximum recovery was observed at around 10°, followed by a swift decline. Hoadley and Hughes [1969] evaluated an annular diffuser featuring a diverging conical casing with 7.5° divergence, along with a cylindrical shaft running through it, identifying peak recovery again at 10° swirl. Dovzhik and Kartavenko [1975], along with Coladipietro et al. [1974], researched equiangular annular diffusers with 20° divergence, finding optimal performance occurring between 10° and 20° swirl across various diffusers. Batchelor [1967] and Coladipietro et al. [1974] indicated that pressure

recovery continued to rise even at the maximum swirl level tested. This variation is attributed to the formula for ideal pressure recovery coefficient.

The swirl component can only be diminished by creating a diffuser with either a large area ratio or maintaining the same height for the diffuser passage at both the inlet and exit, which applied to the investigations conducted by Coladipietro et al. [1974], Kumar [1977, 1978] and Sapre et al. [1987] performed experimental studies on the influence of inlet swirl in both equiangular and unequal angle diverging annular diffusers. He noted that the inclusion of inlet swirl generally enhances overall pressure recovery in annular diffusers, with a more notable increase in stalled diffusers when compared to well-performing ones. The impact of swirl on the diffusion mechanism is greater for short axial length diffusers. Adding inlet swirl decreases the chance of flow separation occurring at the wall of a stalled diffuser. Additionally, a significant inlet swirl may lead to shifting the stall from the casing to the hub.

Benedict et al. [1973], Bhaskarone [1991], Bose et al. [1992] and Yu et al. [1992] conducted an analytical study on the through flow with swirling inflow in an annular diffuser, assuming a minor cross-flow. The flow dynamics near the inner and outer wall surfaces were determined using the three-dimensional momentum integral equation related to the boundary layer. Agrawal et al. [1989] and Singh et al. [1994] investigated swirling flows within channels that have diverging inner and outer walls, including a scenario where the inner wall rotates in the swirl direction. Kanemoto et al. [1982, 1983] and Barker and Carrotte [2001] carried out experimental assessments of the internal flow and performance of an annular diffuser made up of a cylindrical casing and a conical hub. Their results indicated that when the inlet flow lacked a whirl

component, the optimal convergent angle of the hub for achieving maximum pressure recovery was approximately 24 degrees. However, as the whirl component increased, it transitioned into a free vortex pattern downstream, regardless of the initial flow pattern, with the axial velocity being greater on the hub side than on the casing side. Consequently, introducing a suitable whirl component at the inlet could prevent separation, even in cases where a significant convergent angle exists without a whirl component at the hub wall. When the whirl component intensifies, a reverse flow develops along the hub wall at a specific area ratio, independent of the convergent angle. The theoretical and experimental results were consistent, except for the influences of the boundary layer. Enhancing the thickness of the boundary layer on the casing wall and creating a gentle whirl flow at the inlet cross-section improved the diffuser's performance. Numerous researchers have examined the influence of inlet swirl through analytical and computational methods, which will be elaborated on in the following article.

2.4 Analytical and Computational Studies

Bardina et al. [1981], Neve [1993], Badawy and Aly [2000], Duncan et al. [2004], Kwon et al. [2002], Noui-Mehidi et al. [2004], Schlauter et al. [2003], Suzuki and Colonius [2003], Svetlana and Gianluca [2001], Lee et al [2000], Xu and Niu [2003], Michel and Engstrom [2004] and Yeung and Parkinson [2004] created models for two-dimensional diffusers. Badawy and Aly [2000] concentrated on a one-dimensional flow that is potential, incompressible, and inviscid in order to assess how Diffuser Augmented Wind Turbines perform. Tsui and Wang [1995], Spall and Ashby [2000], Vassiliev et al. [2002] and Duncan Walker et al. [2004] applied Reynolds-

averaged Navier-Stokes equations with the conventional high-Reynolds number two-equation k-ε model. The k-ε standard model and the RNG k-ε model were utilized by Kwon et al. [2002]. The computational findings were quite close to the experimental data, whereas the RNG k-ε provided slightly better agreement with the experimental results compared to the typical k-ε approach. Noui-Mehidi et al. [2004] conducted experimental studies on using perforated plates to manage the velocity distribution at the outlet of a wide-angle asymmetric diffuser. The diffuser was designed as a half pyramidal type, with one inner wall being parallel to the flow while the opposing wall was inclined. The opening angles of the diffuser measured 45° horizontally and 30° vertically, and the area ratio was 7. A setup of four perforated plates with 45% porosity led to various velocity distributions at the diffuser's outlet. Measurements taken by Laser Doppler Velocimetry and wall static pressure demonstrated the presence of different flow patterns depending on the placement of the perforated plates. The velocity distributions inside the diffuser exhibited complex flow patterns among various combinations of the perforated plates.

Schlauter et al. [2003] constructed a model integrating Reynolds average Navier-Stokes (RANS) with Large Eddy Simulations (LES). The flow solver was validated across various turbo machinery applications. Suzuki and Colonius [2003] created a reduced order model that addressed large-scale unsteady phenomena such as vortex shedding within a two-dimensional diffuser, examining ways to control active flow separation and gauge stagnation pressure loss in the diffuser. Svetlana and Gianluca [2001] concentrated on the equation for turbulent kinetic energy transport as well as the modeling parameters in the standard k-ε model, based on the linear Boussinesq assumption, identifying optimal values for the modeling coefficients applicable to separated flows. Xu and Niu [2003] explored the conventional k-ε simulation

technique for analyzing swirling air diffusers, with the aim to enhance diffuser design. Yeung and Parkinson [2004] examined and modeled average pressure recovery data for flows that separate and reattach, following diverse two-dimensional flows, in order to identify certain similarities.

Hah [1983] and Yongsen and colleagues [1992] examined conical diffusers. Hah [1983], Shulleray et al. [1992] and Shi and Tsukamoto [2001], created an algebraic model for Reynolds stress that forecasts different flow types in diffusers, taking into account the impact of inlet swirling and distortions while maintaining accuracy in measurements. Yongsen et. al [1992] conducted simulations of fully developed, incompressible turbulent flow within a conical diffuser that had an overall divergence angle of 8° and an area ratio of 4, employing a k-ε turbulence model suited for high Reynolds numbers and an opposing pressure gradient. They predicted the ideal combination of both resistance coefficient and the placement of the perforated screen to achieve optimal diffuser efficiency or consistent velocity distribution.

Yu et. al [1992], Mohan and others [1998], Su and Zhou [2000], and Kochevsky [2001, 2004], analyzed annular diffusers through calculations. Kochevsky [2001] explored a universal method for calculating strong swirling flows using finite difference techniques to solve the Navier-Stokes equations, referred to as TEACH 7. In 2004, Kochevsky examined the flow numerically in annular diffusers created by cylindrical casings and converging conical hubs, taking into account inlet swirl and/or rotation of the hub. Results indicate that rotating the hub in the opposite direction of the swirl helps prevent reverse flow. The study concluded that energy loss in the diffuser and downstream channel is minimized when there is a small inlet swirl against the

direction of the hub's rotation. Mohan et. al [1998] performed computational analysis to find the optimal performance of three annular diffusers, both with and without inlet swirling flow. They investigated three straight-walled annular diffusers, each having an area ratio of 3.0, and discovered that the absolute pressure recoveries were greatest with a 12.5° swirl angle. Su and Zhou [2000] simulated the interactions of combustor and diffuser flow using the KIVA-3V code, which is based on solutions to the Navier-Stokes turbulence models. They derived the static pressure recovery coefficients along both the inner and outer walls of the pre-diffuser and combustor casing from their numerical findings, which aligned well with the data obtained from measurements. Yu et. al [1992] analytically examined the flow through an annular diffuser with swirling inflow under the premise of minor cross-flow. They calculated the flow near the inner and outer wall surfaces based on the three-dimensional momentum integral equation governing the boundary layer. The potential flow outside the boundary layer was determined using the velocity gradient equation along the quasi-orthogonal direction of the meridional projection of the streamline on the meridional surface, along with the flux constancy equation. This approach proved useful for analyzing through flow with pre-swirl in the annular diffuser. The numerical outcomes showed good agreement with experimental results.

2.5 Cracks in Literature

- Impact of flow factors has gaps because of numerous variables
- Research only focuses on experimentation on limited Annular Diffusers
- Studies are restricted to experimental analysis only
- Influence of swirl examined solely limited diffusers
- Numerical studies are insufficient to validate the experimentation

- Impact of equivalent cone angle has been overlooked

2.6 Motivation for present work

A review has been conducted to reassess various elements of the flow characteristics of diffusers and to present them in an organized manner. The influence of different geometric and flow parameters on the effectiveness of a diffuser has been examined to reach specific conclusions. The impacts of the geometric factors concerning pressure recovery are fairly established for two-dimensional and conical diffusers, and to some degree for annular diffusers. In contrast, the influences of the flow factors have not been determined to the same extent as the geometric factors. This is due to the complex interactions among the different flow parameters and the development of the boundary layer under adverse pressure conditions. Several boundary layer control techniques and devices that are typically used to enhance the efficiency of diffusers have been summarized. From the literature review, it is clear that most research conducted so far has focused on two-dimensional and conical diffusers because of their simplicity. Annular diffusers, which consist of numerous geometric variables, have received much less focus and require more investigation. Additionally, past research on diffusers has primarily been centered on evaluating the overall performance, rather than analyzing the flow processes involved. A deeper understanding of the flow behavior in diffusers can be achieved by conducting thorough investigations focused on boundary layer development. Furthermore, an exploration of flow development with inlet-induced swirl is necessary to evaluate how well an annular diffuser performs, particularly when handling exit flow from a compressor that has a certain degree of swirl. It has also been observed that most research on axial annular diffusers has been limited to experimental findings, specifically focusing on only two diffuser types (i.e., Equiangular and

both hub and casing diverging at different angles). There is a lack of research on other types like Parallel hub, diverging casing, and diverging casing with converging hub. The effects of equivalent cone angles on these types of diffusers are also absent. Studies must connect diffuser performance with equivalent cone angle, diffuser type, and inlet swirl. Experimental examinations of annular diffusers demand advanced instruments and complex, time-intensive methods, which are not cost-effective and have consequently restricted research in this area. Computational models for annular diffusers are sparse. Future computational studies that can yield results close to experimental findings need to be created. Therefore, upcoming research should focus on a mix of experimental and computational studies.

2.7 Scope of the Current Research

The research on fluid movement in both conical and channel diffusers is well recorded in existing scholarly articles. The functionality of the diffuser is largely affected by the aspect ratio and the length of the channel where diffusion takes place. The shape of the wall affects the local pressure differences and the development of the boundary layer, which can greatly influence how well the diffuser operates. A review of the literature on flowing through diffusers indicates that previous studies have concentrated on flat and conical diffusers, paying less attention to annular diffusers. This research aims to explore how annular diffusers perform under various listed inlet conditions. The mentioned inlet conditions, such as divergence angle, swirl at the inlet, area ratio, inlet velocity profile, turbulence intensity, Reynolds number, and so on, are believed to notably impact the diffuser's efficiency. The performance and effectiveness of the annular diffuser rely on many geometric and flow-related factors. There have also been attempts to evaluate flow separation within the annular diffuser. There is limited experimental or analytical

data regarding the pressure coefficient (Cp) and lift coefficient (C_L) for a wide range of inlet conditions and swirl intensities. This scarcity may stem from the challenges of swirling flows in terms of measurement and analysis. Few experimental investigations have been conducted on annular diffusers in this field. Conducting experimental research calls for accurate measuring tools and is often intricate and lengthy, which makes it financially challenging. Hence, the present study focuses on experiments along with Computational Fluid Dynamics (CFD) modeling to explore aspects of flow behavior through annular diffusers with cone angles from 10º to 20º and area ratios of 2 and 3. This study was aimed at assessing velocity profiles, the static pressure recovery coefficient, and the total pressure loss coefficients across various sections of the annular diffuser, along with inlet swirl angles of 7.5°, 12°, 17°, and 25°, as well as cases without swirl (0°). CFD simulations of the test diffusers were performed for different setups. The intricate flow characteristics of annular diffusers were examined and compared with experimental findings. The model that best corresponded with experimental data was utilized for further analysis to forecast other flow behaviors in annular diffusers. Based on a thorough literature analysis, the main goals of the current study are as follows:

1. To analyze the region of flow separation
2. To visualize the flow development and separation of flow at different passage heights along the length of the axial diffuser
3. To study the variation of static pressure recovery, total pressure loss coefficient and velocity profiles at different area ratios, and divergence angles
4. To evaluate the effect of inlet swirl on performance

5. To assess the performance of the annular diffuser configurations, experimentally and computationally

CHAPTER 3

EXPERIMENTAL SETUP AND INVESTIGATION

The existence of an unfavorable pressure gradient in a diffuser contributes to the complexity of the flow within it. Additionally, the swirling motion of the flow adds to this intricacy. To understand the characteristics of the flow and its complexities in an annular diffuser, conducting experiments becomes essential. This current experimental study has been structured to collect comprehensive performance data regarding average flow parameters in two-dimensional axisymmetric boundary layer flows, both with and without swirling conditions at the diffuser's entrance for a range of annular diffusers. This section outlines the testing facility, the instruments used, and the uncertainties linked to the measurements taken. It also details the measurements of pressure distribution and velocity profiles carried out across the annular cross-section at different longitudinal points along the diffuser flow path, along with the findings from the experiments conducted.

3.1 Experimental Setup

The experimental study was conducted using a testing setup illustrated in figure 3.1 to 3.3 and explained in figure 3.4, which outlines the overall layout of the testing system that includes a blower, settling chamber, annular duct, and test diffuser.

A single-stage centrifugal blower provides an output of 1.5 m^3/s at a pressure of 1m water gauge, drawing air from the environment through a fine mesh filter and sending it into a settling chamber via a well-crafted conical expansion. A balanced damper located at the blower intake

regulated and maintained a steady flow rate throughout the system. A robust fabric acted as a flexible connector to close the gap between the blower and settling chamber, which helped stop vibrations from reaching the settling chamber. The settling chamber, with a diameter of 0.5 m and a length of 3.5 m, was linked to a constant area annular duct using a smooth converging section and included fine mesh screens along with a honeycomb section. The screens served several purposes, including making the flow more stable and straight, minimizing turbulence, and lowering losses. Two commercial pipes were utilized to create the annulus, featuring an outer pipe with an inside diameter of 15.5 cm and an inner pipe with an outside diameter of 7.6 cm, which resulted in an annulus height of 3.95 cm. To achieve a fully developed turbulent boundary layer flow at the entrance of the diffuser, the length of the annulus was approximately 50 times the hydraulic diameter. Fully developed turbulent flow devoid of swirl is seen as a better representation of real entry conditions than the thin boundary layer conditions observed by some researchers. The alignment of the inner pipe relative to the outer pipe was confirmed as the core was firmly secured by four radial streamlined struts positioned at two axial locations. A seamless transition from the annulus to the conical housing of the diffuser was guaranteed by placing appropriate metal shims between the flanges, with the inner surfaces finished with plasticine. The core of the diffuser was constructed from cast aluminum and polished smoothly, while the casing of the annular test diffusers was crafted from clear Plexiglass. This was done to allow visualization of the flow within the annulus. Ultimately, the air passing through the diffuser was released back into the atmosphere.

Figure 3.1 Experimental Setup

Figure 3.2 Manometers and Diffusers

Figure 3.3 Traversing Mechanism

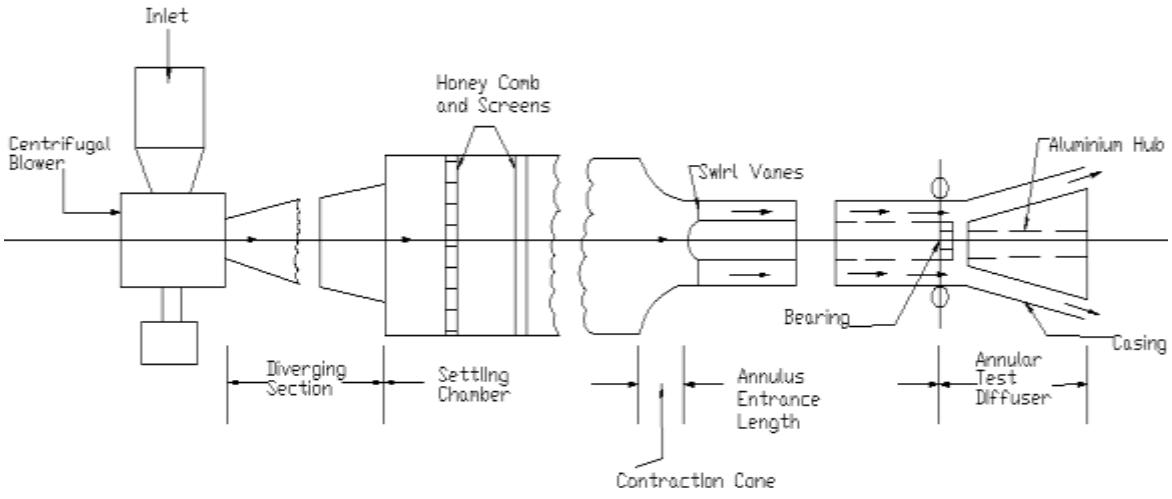

Figure 3.4 Block diagram of experimental setup

3.2 Swirl Generation and Specification

In previous studies, researchers have explored several techniques to create swirl for experimental examinations of swirling flow in jets, pipes, and diffusers. The methods outlined in existing literature for generating swirl are summarized below:

- Positioning the diffuser directly after a turbo machine
- Applying rotation to an axial stream using a spinning perforated plate
- Implementing twisted tapes
- Introducing a tangential airflow
- Allowing air to pass through a series of adjustable equiangular stator vanes

None of these approaches can be definitively classified as the optimal way to create swirl, as each has its own set of pros and cons. In this study, swirl was produced in the air stream by directing it through stator vanes made from a swirl plate, which comprised a flat steel plate with twelve radial slits. Different amounts of swirl were achieved by adjusting the angle of the vanes. When a specific swirl amount was needed, the respective swirl plate was positioned at the entrance of the annular passage. This upstream placement was chosen to minimize the likelihood of wake formation at the diffuser's entry. Wake could have lingered within the diffuser, which would negatively impact its efficiency.

Swirl can be defined based on either the design characteristics of the device that generates it or the mass-averaged or area-averaged swirl angle value. The latter approach is viewed as a more effective method of describing swirl compared to the former. Averaging becomes essential

because the swirl angle might vary within a section. Swirl can be represented using a dimensionless swirl number S, defined as the ratio of the axial angular momentum flux to the axial momentum flux.

$$S=\left(\int r^2 uwdr \Big/ \int r u^2 dr\right)\cdot\frac{1}{D_{eq}} \tag{3.1}$$

Where D_{eq} is the equivalent diameter of the flow passage.

3.3 Geometry of the Test-Diffusers

Table 3.1 outlines the diffusers that were tested in this research. Each diffuser featured identical hub and casing radii at the inlet. The various tested geometries, which include the angles of the hub and casing walls, the exit radii for both the hub and casing, the area ratios, the ratios of length to annulus height, and the equivalent cone angles of the different diffusers examined, are documented in a table. The choice of diffuser geometries aimed to ensure a consistent equivalent cone angle across all four diffuser types, as detailed in chapter 2. The goal was to investigate how swirl affects the flow within the diffusers and to identify any potential zones of separation or flow reversal.

Table 3.1 Diffusers

Diffuser Name	R_{h1}=3.8		R_{c1}=7.75		R_{h1}/R_{c1}=0.49		N/ΔR	Equivalent cone angle
	Wall Angles		Exit Radius					
	Hub	Casing	Hub	Casing	AR	N		
E1	0	4.6	3.8	10.3	2.01	32	8.1	10.09
E2	10	10	12	16.41	3	56	13.9	10.11
E3	5	7	8.7	14.6	3.01	56	14.2	10.14
E4	- 6.8	3.2	0	9.6	2.02	32	8.1	10.14

3.4 Diffuser Inlet Location

The flow conditions at the beginning should ideally match those at the true or geometric entry of the diffuser; however, since placing a pressure tap right at the transition is challenging, the inlet position was selected to be a location somewhat upstream of the geometric entry. The chosen inlet position results in friction losses along the annular duct section between this inlet point and the actual entry of the diffuser, but it also lessens the streamline curvature effects at the start of a geometric expansion by reducing the pressure near the wall below that of the core flow area. To strike a balance, the reference section was placed 5 cm upstream of the geometric beginning of the diffuser to decrease any unnecessary impact on the diffusion process, and the friction loss is anticipated to be very minimal compared to the losses within the actual diffuser. Additionally, the inlet velocity profile would only differ slightly from that at the geometric start of the diffuser.

3.5 Instrumentation

The static pressure and yaw angle were recorded by hand using the Cobra probe, Traversing Mechanism, and Manometers. The tools employed are detailed below.

3.5.1 Three-Tube Impact Pressure Probe (Cobra Probe)

The three-tube impact pressure probe (such as the cobra probe) was utilized to measure pressure and velocity components at the same time in the flow field being studied in this research. The probe was made using standard hypodermic stainless tubes with an outer diameter of 0.8 mm. The dimensions of the pressure probe were selected to optimize both the delay in pressure

transmission and the accuracy of measurements, as noted by Bryer et al. [1958, 1971] and Dellenback et al. [1988].

A square cut was created on the front edge of the central tube of the cobra probe, while the two outer tubes were cut at angles of 40º to 45º in relation to their respective axes. This design aimed to maximize sensitivity to yaw. Since the probe assembly needed to be attached to the traversing mechanism, the three tubes were aligned parallel and on the same plane, then soldered into a steel tube with a diameter of 3 mm. To reduce potential errors caused by flow interference, the probe assembly's stem was constructed 50 mm from the tip.

3.5.2 Traversing Mechanism

The traversing mechanism was created to provide two degrees of freedom for examining the average turbulence velocity field. This setup allowed the probe to both move across and rotate around its long axis. The smallest measurement unit for the traversing mechanism in the longitudinal direction was set to 0.1 mm, while the rotation had a minimum measurement of 0.5°. Initially, the cobra probe was attached to the traversing mechanism before being placed into the flow passage to analyze the flow field. The probe was set to align parallel to the reference direction with an accuracy of ± 2° and was positioned to contact the surface of the diffuser hub. Measurements closer than 0.5 mm from the hub and the casing wall could not be taken since the probe head had a diameter of 1 mm. In the boundary layer area near the walls, measurements were taken in increments of 0.5 mm. Conversely, further away from the wall, larger increments were selected, and the step size was modified to obtain around 10 to 20 measurements at specific traversing stations based on the height of the diffuser passage. There was a risk of backlash error

linked to the mechanisms, which was resolved by moving the traversing system in the same way during the collection of a single set of data.

3.5.3 Manometers

The static pressures of the wall and the readings from the cobra probe were obtained using a water manometer with 36 tubes, designed to measure up to the nearest tenth of a centimeter. To enhance the sensitivity of the manometer, it was tilted at a 10° angle relative to the horizontal plane. Distilled water served as the liquid for measurement. When the manometer was set at an angle, the menisci in the tubes were noted to be at varying heights. This slight error was accounted for while converting the pressure data into the corresponding flow parameters. Furthermore, measures were taken to ensure that stable conditions were reached within the flow passage before data collection began. A waiting period of four to five minutes was implemented between each reading, allowing the probe system to reach steady equilibrium. The potential for debris obstructing the thin hypodermic tube was regularly assessed by immersing the probe in carbon tetrachloride and using compressed air to blow through it. Leakage tests were also conducted frequently on the manometer heads and the PVC tubing. The manometer board enabled direct observation of the pressure distribution, which made it easier to establish the intended test conditions.

3.6 Analysis of the Asymmetric Response

The position of the probe in relation to the speed vector, the dynamic head, and the overall pressure were the elements that affected the pressures shown by a specific three-hole probe. As a result, the pressure measurements can be categorized into three distinct dimensionless

parameters, each illustrating the flow direction, the dynamic head, and the stream's total pressure individually. For consistent incompressible flow along a streamline, the total pressure is expressed as

$$p_t = p_s + \frac{1}{2}\rho U^2 \tag{3.2}$$

The equation for energy balance at a point in the free stream and any of the openings in the three-tube probe was utilized to create appropriate functional relationships. The energy conservation equation connects the pressure *Pi* shown by one of the cobra probe tubes as

$$p_i = p_s + K_i + \frac{1}{2}\rho U^2 \tag{3.3}$$

Where *Ki* is a variable that relies on the shape of the probe, the direction of the stream in relation to the tube, and the classification of the tube, meaning i equals 2 for the center tube and i equals 1 and 3 for the tubes on the side. Therefore:

$$\frac{p_2 - p_1}{p_2 - p_3} = \frac{K_2 - K_1}{K_2 - K_3} = f_1(\theta) \tag{3.4}$$

The functional relationship for the dynamic head can be found from the relationship

$$p_j - p_1 = \left(K_j - K_2\right) \times \frac{1}{2}\rho U^2$$

Where j = 1 & 3

$$\frac{p_j - p_2}{p_t - p_s} = K_j - K_2 = f_2(\theta) \tag{3.5}$$

The total pressure's functional connection was established by applying equations (3.2) and (3.3). The resulting formula for the total pressure is

$$p_t - p_2 = \frac{1}{2}\rho U^2\left(1 - K_2\right) = \frac{p_j - p_2}{K_j - K_2}\left(1 - K_2\right)$$

or $$\frac{p_t - p_2}{p_j - p_2} = \frac{1 - K_2}{K_j - K_2} = f_3(\theta) \qquad (3.6)$$

The tube 'j' is selected to enhance both the sensitivity to direction and to broaden the velocity range. The calibration functions mentioned earlier were found through experiments by recording the pressure values of the tubes when the probe was at a specific angle to the free stream velocity. The method detailed and applied in this study was the same as that presented by Dau et.al [1968] and Perry [1974] for analyzing the asymmetric response of a cobra probe with three tubes.

3.7 Probe and its Calibration for Asymmetric Orientation

The process of calibrating the probe was performed to assess how the non-dimensional pressure coefficients (as described in equations 3.4, 3.5, and 3.6 previously) change with different yaw angles. This calibration was conducted in a low-speed suction open circuit wind tunnel. To start, the probe was aligned with the flow direction. The alignment was verified by adjusting the probe until both side tubes indicated equal pressure. After this, the probe was positioned relative to the direction of the flow and the pressure measured by the three tubes was recorded. The angle was changed up to 40° in increments of 2°. To confirm the consistency of the probe's response, the orientation was altered back and forth from 0° to 40° and then reversed from 40° back to 0°. Once the calibration process was finished, it was tested at various random angles. The calibration data collected in this manner was then utilized to compute the functions f_1, f_2, and f_3.

While conducting actual measurements in the diffuser, the orientation of the probe remained unchanged, and the readings from the three tubes were noted at each measurement point. The flow variables were analyzed as follows:

I. The probe pressure readings P_1, P_2, and P_3 were employed to calculate the probe geometry constants and subsequently the functional parameter f_1 as outlined in equation 3.4.

II. The functional constant for dynamic head was then calculated as stated in equation 3.5, followed by the calculation of the functional parameter f_2. The yaw angle that corresponded to the computed f1 was identified using the calibration constant derived from equation 3.4. The values for functions f_1 and f_3, associated with this yaw angle, were then determined as described in equations 3.5 and 3.6.

III. The values of f_2 and f_3 obtained in step (ii), alongside the pressure readings P_1, P_2, and P_3, were employed to determine the values of $(P_t - P_s)$, P_t and P_s.

This method of measurement and calculation offered an effective and quick approach for obtaining the required flow parameters with acceptable accuracy.

3.8 Initial conditions

The starting conditions involve the physical circumstances of the fluid as it approaches the diffuser. Before reaching the diffuser, the fluid travels through an annulus pipe that has a ratio of length to hydraulic diameter of 50, which guarantees that a fully developed turbulent boundary layer flow occurs at the inlet of the diffuser. A fully developed turbulent boundary layer flow

without any swirl has been selected because it is thought to better reflect the real entry conditions for a turbo machinery diffuser compared to the thinner boundary layer conditions used by some researchers. The pressure at the diffuser's exit was atmospheric since there was no tailpipe connected to it. All the measurements taken in this experimental study were within the incompressible flow range at an average Reynolds number of 2.5×10^5, calculated using the equivalent flow diameter at the diffuser entrance. This Reynolds Number was deemed adequate to eliminate the chance of transition flow occurring at the diffuser entrance. Prior to conducting actual measurements in the test diffusers, the boundary layer was verified for axial symmetry. This verification involved checking for lateral changes in static pressure. The inlet velocity profiles collected experimentally for various inlet swirls can be seen in figure 3.2.

3.9 Experimental Method

Data was collected for each diffuser in the following order:

- static wall pressure
- inlet velocity profiles
- velocity profiles in the diffuser at different locations using the three-hole cobra probe
- Flow visualizations

3.9.1 Measurement of the wall Static Pressure

Static pressure tapings on the walls were installed on the test diffusers along the casing's generatrix and on the hub wall. Carefully, holes measuring 3 mm in diameter were drilled, and

stainless-steel tubes with an outer diameter of 3 mm and an inner diameter of 1.5 mm were pressed into these openings, aligning flush with the internal surface. These pressure taps were connected to an inclined multi-limb manometer using polythene tubes. Wall static pressure measurements were taken at diametrically opposite locations at both the first and last measurement stations along various circumferential tapings to confirm the axial symmetry of the flow. A variation in the readings was noted, reaching up to ±3% of the average inlet dynamic flow. Since this deviation was minor, the flow was considered axisymmetric.

3.9.2 Measurement of the Mean Velocity Field

Mean velocity profiles were determined at various cross-sections along the diffuser length. The velocity traverses were made normal to the diffuser hub by means of a cobra probe. Holes of 3 mm diameter were drilled on the diffuser casing at suitable intervals along its length to introduce the probe. The free holes were plugged with carefully shaped inserts to prevent air from leaking into the flow passage. To determine the velocity profiles, one needs to measure total pressure, static pressure and the yaw angle at various locations in the flow field. The three quantities were obtained with the help of cobra probe along the various transverses of the diffuser passage length. The flow was assumed to be steady, incompressible and in viscid. The velocity U at each location of the flow field was computed with the help of law of conservation of energy as given in eq. 3.2. The longitudinal and swirl velocity was then computed as follows

$$u = U \cos \varphi$$

$$w = U \sin \varphi$$

where φ represents the yaw angle related to the long direction on the surface of the hub. The longitudinal and swirl velocities were then normalized in relation to the maximum longitudinal

velocity Um of any cross-section. The normalized velocity profiles u/Um and w/Um for the longitudinal and swirl components were graphed against the normalized diffuser passage height y/Ym. This normalized height y/Ym was calculated by taking the diffuser passage height y at any point along the traverse from the hub surface to the maximum height Ym of the diffuser passage (which is the distance from the hub to the casing). Measurements of the flow field were taken at different sections of the diffuser passage length for varying inlet swirl conditions. The different normalized longitudinal and swirl velocity profiles for several inlet swirls at the inlet of the experimental diffusers are illustrated in figure 3.5.

3.9.3 Flow Visualization

Small pieces of wool, measuring 2.5 cm and able to turn freely in all directions, were utilized to examine the flow patterns in the test diffusers. These pieces were placed along four lines, roughly 90° apart, on both the hub and casing sides of the diffusers. The motion of the wool pieces could be observed through the clear casing of the diffuser test area. Categorizing flow types based on the motion of the wool pieces could be subject to significant personal interpretation. Nevertheless, a review of the current literature on the topic shows a classification proposed by Carlson and Johnston [1967].

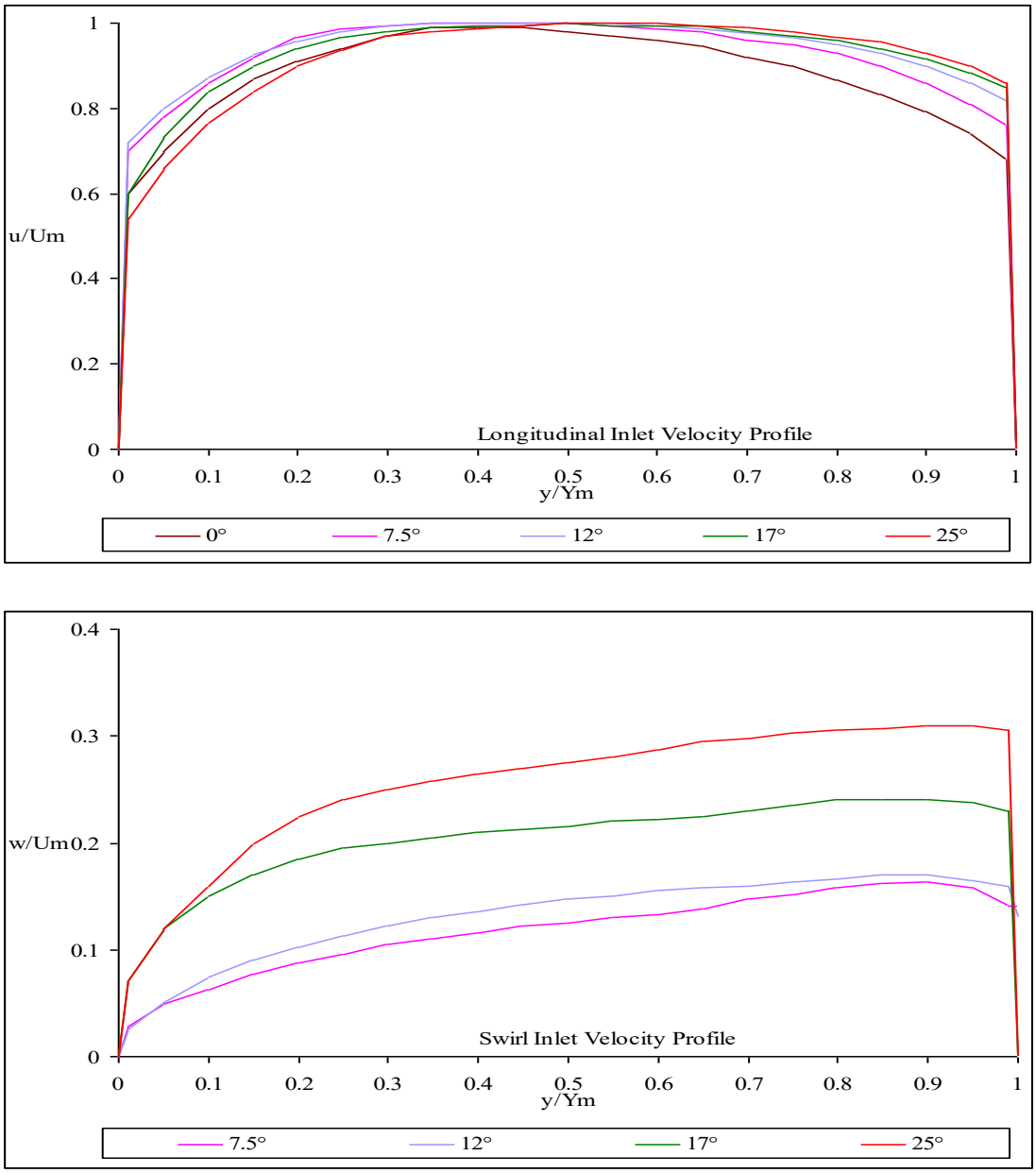

Fig. 3.5 Experimentally obtained Inlet velocity Profiles at various inlet swirl

3.10 Uncertainty in Measurements

Regardless of the extensive attention and precautions that an experimenter may implement to remove all potential mistakes from their observations, some experimental inaccuracies can arise

from geometric flaws in the testing equipment, while others might stem from imprecisions in the measurement tools.

The housing for the test diffusers was constructed using a 4 mm Perspex sheet, which was first warmed in an oil bath before being shaped around a wooden conical mold that had the necessary measurements. The lengthwise joint of the casing was reinforced by attaching a Perspex strip along the entire seam and adding flanges at both ends. The flange located at the inlet of the diffuser also acted as the connection point between the casing and the straight annular section that comes before it. The rolling method inevitably caused the casing to become ‘out of round’, leading to a diameter that was not perfectly conical, which in turn resulted in a discrepancy in the divergence angle. In contrast, the hub was made from aluminum and then machined, resulting in greater accuracy regarding both diameter and divergence angle. The variations mentioned above influenced the height of the flow passage that exists between the casing and the hub of the diffuser assemblies. Additionally, this passage height was affected by how the hub was positioned within the casing. Similarly, the height of the straight annular duct was impacted by any inconsistencies in the pipe dimensions used and by any misalignment that occurred when one pipe was fitted inside another.

Several factors, such as leaks in the pressure tubing, misalignment of the probe, variations in the bore or surface condition of the manometer, and changes in atmospheric and flow stream pressures, may knowingly or unknowingly influence the readings from the probe. There is a likelihood of near wall displacement effects, which might cause the pressure probe to yield readings from a location further from the wall than where the probe actually sits. Furthermore, since the probe was relatively small, its response to the applied pressures was relatively slow.

Although significant effort was made to allow sufficient time before taking a reading due to the probe's slow response, there was always a chance for human error when noting a reading without ensuring the pressure had stabilized. The backlash effect in the micrometer screw cannot be completely dismissed, despite the fact that all readings were taken in the same direction.

The uncertainties related to the measured values are detailed in Table 3.2.

Table 3.2 Uncertainties of the measured values

Physical Quantity	Symbol	Formula	Uncertainity
Hub Radius	R_h		± 1%
Casing Radius	R_c		± 2%
Annular Height	Ym	$R_c - R_h$	± 3%
Traverse position	Y		± 0.05 mm
Angle of Divergence	Θ		± 0.5%
Swirl angle	Φ		± 2°
Total Pressure	P_t		± 1%
Static Pressure	P_s		± 1%
Atmospheric Pressure	P_{atm}		± 1%
Velocity	U	$\left[\frac{2}{\rho}(P_t - P_s)\right]^{1/2}$	± 1%
Mean Velocity	$\bar{U}$	$\int \rho U dA / \int \rho A$	± 3%
Reynolds Number	Re	$U D_{eq}/\nu$	± 4%
Dynamic head	$\overline{q_1}$	$\rho U_1^2/2$	± 6%
Pressure Recovery Coefficient	Cp	$(P - P_1)/\overline{q_1}$	± 6%

CHAPTER 4

CFD MODELING

Flow in axisymmetric diffusers can be examined mathematically by solving the governing partial differential equations. In two-dimensional flows where there is a primary direction of movement, the governing equations are parabolic, and solutions for such equations do exist. However, in general two-dimensional flows, like those addressed in this study, there may not be a primary flow direction, and flow reversal can occur. These types of flows are represented by elliptic partial differential equations. There are limited solution methods available for such flows in annular diffusers. This chapter focuses on the Computational Fluid Dynamics (CFD) modeling used to forecast the flow behavior in an annular diffuser, both with and without inlet swirl. This chapter presents an overview of the method developed and the computational approaches utilized to estimate the flow variables in annular diffusers.

4.1 CFD Procedure

The suggested forecasting approach relies on the CFD resolution of the main partial differential equations. The turbulence model implemented is the two-equation k-ε model, used as the closure assumption. In this study, the commercial software FLUENT was utilized for solving flow, while GAMBIT was used for designing the geometry and generating the mesh. The software was appropriately adjusted to meet the modeling needs. CFD modeling should be separated into two segments as follows:

- Developing and meshing the fundamental geometry
- Addressing the fluid flow issue

4.2 Developing and meshing the fundamental geometry

The steps outlined below were executed for the creation of geometry and the generation of mesh utilizing GAMBIT.

- Designing the model geometry and grid.
- Creating a boundary layer mesh.
- Generating the mesh.
- Defining boundary types.

4.2.1 Designing the model geometry and grid

The designs of the annular diffusers were developed in two stages. The first stage involved creating models that matched the configurations of the experimental diffusers as mentioned in the previous chapter to confirm the CFD model's accuracy. In the second stage, the designs to be examined with the confirmed CFD model were derived from the equivalent cone angle and types of diffusers listed in Table 4.1. To maintain symmetry, the inlet of the annular diffusers used the equivalent cone angle for every diffuser type, similar to the inlet of the experimental diffuser; the outlet was determined using the equivalent cone angle. An equivalent cone angle diffuser is defined as one that shares the same length and area ratio as a conical diffuser. This angle corresponds to that of the conical diffuser. The approach length for all diffuser cases was set to 5 cm. This choice was made because the inlet parameters were recorded at a distance of 5 cm upstream during experimental studies. After settling on the geometry based on calculations, it was drawn using GAMBIT software.

Table 4.1 Diffusers' geometry for computational investigation

Area Ratio (AR)	Equivalent Cone angle (Θ_e)	Hub angle (Θ_h)	Casing angle (Θ_c)	Length to Radius (L/r)	Swirl (S)	Type of Diffuser
2	10	0	2.140035	8.095896	0-25	Parallel Hub Diverging Casing (A)
2	10	10.23663	10.23663	8.095896	0-25	Both Hub and Casing Diverging With equal angles(B)
2	20	0	4.313083	4.016964	0-25	Parallel Hub Diverging Casing (A)
2	20	19.99962	19.99962	4.016964	0-25	Both Hub and Casing Diverging With equal angles(B)
3	10	0	1.373153	14.3081	0-25	Parallel Hub Diverging Casing (A)
3	10	11.55012	11.55012	14.3081	0-25	Both Hub and Casing Diverging With equal angles(B)
3	20	0	2.767489	7.09929	0-25	Parallel Hub Diverging Casing (A)
3	20	22.38575	22.38575	7.09929	0-25	Both Hub and Casing Diverging With equal angles(B)

4.2.2 Creating a boundary layer mesh.

All the designs of the diffuser located at the hub and casing walls underwent boundary layer meshing. This was performed to achieve a detailed mesh along the diffuser walls due to the significant shear stresses present at these surfaces. The boundary layer meshing was executed with 10 rows on each wall, beginning with the first row positioned 0.01 cm away from the wall, while each following row had a growth factor of 1.01. The internal continuity and the shape of the wedge corner were considered as well for the boundary layer meshing.

4.2.3 Generating Mesh

After the completion of the boundary layer mesh, the face mesh was generated. Throughout the preliminary analysis, different mesh dimensions were tested for grid independence, and ultimately a mesh size of 0.07 cm was selected. During the preliminary analysis, the element types examined included quadrilateral, triangular, and a combination of quadrilateral-triangular. The meshing methods explored were map, sub map, pave, and primitive wedge. Nevertheless, the optimal results were achieved using the quadrilateral and pave meshing types, which were then applied to all the diffusers.

4.2.4 Defining Boundary Types

The entrance of the diffuser was regarded as a velocity inlet, while the exit was designated as a pressure outlet. The hub and casing were considered as solid surfaces. The fluid was classified as air.

4.3 Addressing the fluid flow issue

Once the diffuser's geometry was designed using GAMBIT, the geometry was exported to the FLUENT processor as a case file. The option of 2D double precision solver was selected. The mesh was examined for quality, scaled, smoothed, and any necessary swapping of mesh cells was performed. Next, the cell-based segregated solver model (2D axisymmetric with swirl) was chosen. Different viscous models, including Inviscid, Spalart-Almaras, k-ε (standard, RNG, and realizable), k-Ω (Standard and Shear-Stress Transport), and Reynolds stress, were evaluated in the pre-study and matched with the experimental results available for the geometries tested. Air was used as the working fluid for the model's analysis. The boundary conditions at the diffuser's inlet included velocity, with a profile matching the experimental findings, along with a turbulence specification of 3% intensity and a hydraulic diameter calculated from the inlet geometry. The outlet boundary conditions were set as atmospheric pressure normal to the pressure outlet, featuring a backflow turbulence specification of 3% and a hydraulic diameter derived from the outlet geometry. The solution controls for momentum, swirl velocity, turbulence kinetic energy, and turbulence dissipation rate were set to second-order upwinding. The discretization criterion for pressure was designated as PRESTO, while the pressure-velocity coupling utilized PISO. The solution initialization occurred at the inlet of the diffuser. The convergence criteria for the residuals were set to 10^{-6} for various parameters relevant to the study, such as continuity, x and y velocity, swirl, k, and ε; results were deemed stable.

The modeling was conducted multiple times with mesh sizes ranging from 50,000 to 500,000 mesh cells in order to achieve grid independence. It was determined that the

model yielding the closest alignment with experimental results was the 2D, double precision, axisymmetric swirl RNG “Renormalization Group” k-ε turbulence model, utilizing a moderate mesh size of 0.07 cm. The RNG-k-ε turbulence model is based on the instantaneous Navier-Stokes equations and employs a mathematical approach known as "Renormalization Group" (RNG) methods. This same model was also applied to the analysis of other geometries deemed relevant for this study.

4.4 Governing Equations

Turbulent flows exhibit fluctuating velocity fields. These fluctuations mix transported quantities like momentum, energy, and concentration of species, causing variations in these transported quantities as well. Since these fluctuations may be small in scale and high in frequency, simulating them directly can be computationally expensive for practical engineering applications. Instead, the exact governing equations can be adjusted through time-averaging, ensemble-averaging, or other modifications to eliminate the small scales, allowing for a less costly set of equations to solve computationally. Nevertheless, these modified equations have additional unknown variables, thus necessitating turbulence models to express these variables in terms of known quantities.

FLUENT resolves equations for the conservation of mass and momentum. When the flow is turbulent, additional transport equations are also solved. The governing equations relevant to 2D axisymmetric geometries are expressed in the following manner:

Continuity equation is

$$\frac{\partial \rho}{\partial t} + \frac{\partial}{\partial x}(\rho v_x) + \frac{\partial}{\partial r}(\rho v_r) + \frac{\rho v_r}{r} = 0 \tag{4.1}$$

Where x is the axial coordinate, r is the radial coordinate, v_x is the axial velocity, and v_r is the radial velocity.

Conservation of momentum within a stationary (non-accelerating) reference frame is described by

$$\frac{\partial}{\partial t}(\rho \vec{v}) + \nabla \cdot (\rho \vec{v} \vec{v}) = -\nabla p + \nabla \cdot (\bar{\bar{\tau}}) + \rho \vec{g} + \vec{F} \tag{4.2}$$

Where p is the static pressure, $\bar{\bar{\tau}}$ is the stress tensor (described below), and $\rho \vec{g}$ and $\vec{F}$ are the gravitational body force and external body forces (e.g., that arise from interaction with the dispersed phase), respectively.

The stress tensor $\bar{\bar{\tau}}$ is given by

$$\bar{\bar{\tau}} = \mu \left[\left(\nabla \vec{v} + \nabla \vec{v}^{T} \right) - \frac{2}{3} \nabla \cdot \vec{v} I \right] \tag{4.3}$$

Where μ represents the molecular viscosity, I, the unit tensor, and the second term on the right hand side represents the effect of volume dilation.

For 2-D axisymmetric geometries, the axial and radial momentum conservation equations are given by

$$\frac{\partial}{\partial t}(\rho v_x) + \frac{1}{r}\frac{\partial}{\partial x}(r \rho v_x v_x) + \frac{1}{r}\frac{\partial}{\partial r}(r \rho v_r v_x) = -\frac{\partial p}{\partial x} + \frac{1}{r}\frac{\partial}{\partial x}\left[r\mu \left(2\frac{\partial v_x}{\partial x} - \frac{2}{3}(\nabla \cdot \vec{v}) \right) \right]$$

$$+ \frac{1}{r}\frac{\partial}{\partial r}\left[r\mu \left(\frac{\partial v_x}{\partial r} + \frac{\partial v_r}{\partial x} \right) \right] + F_x \tag{4.4}$$

and

$$\frac{\partial}{\partial t}(\rho v_r)+\frac{1}{r}\frac{\partial}{\partial x}(r\rho v_x v_r)+\frac{1}{r}\frac{\partial}{\partial r}(r\rho v_r v_r)=-\frac{\partial p}{\partial r}+\frac{1}{r}\frac{\partial}{\partial x}\left[r\mu\left(\frac{\partial v_r}{\partial x}+\frac{\partial v_x}{\partial r}\right)\right]$$

$$+\frac{1}{r}\frac{\partial}{\partial r}\left[r\mu\left(2\frac{\partial v_r}{\partial r}-\frac{2}{3}(\nabla\cdot\vec{v})\right)\right]-2\mu\frac{v_r}{r^2}+\frac{2}{3}\frac{\mu}{r}(\nabla\cdot\vec{v})+\rho\frac{v_z^2}{r}+F_r \qquad (4.5)$$

where $$\nabla\cdot\vec{v}=\frac{\partial v_x}{\partial x}+\frac{\partial v_r}{\partial r}+\frac{v_r}{r} \qquad (4.6)$$

The tangential momentum equation for 2D swirling flows may be written as

$$\frac{\partial}{\partial t}(\rho\, v_z)+\frac{1}{r}\frac{\partial}{\partial x}(r\rho\, v_x\, v_z)+\frac{1}{r}\frac{\partial}{\partial r}(r\rho\, v_r\, v_z)$$
$$=\frac{1}{r}\frac{\partial}{\partial x}\left[r\mu\frac{\partial v_z}{\partial x}\right]+\frac{1}{r^2}\frac{\partial}{\partial r}\left[r^3\mu\frac{\partial}{\partial r}\left(\frac{v_z}{r}\right)\right]-\rho\frac{v_r\, v_z}{r} \qquad (4.7)$$

and V_z is the swirl velocity

4.5 RNG k - ε Model Transport Equations

The equations for transport yield the turbulence kinetic energy, k, along with its dissipation rate, ε are as under:

$$\frac{\partial}{\partial t}(\rho k)+\frac{\partial}{\partial x_i}(\rho k u_i)=\frac{\partial}{\partial x_j}\left(\alpha_k\,\mu_{eff}\frac{\partial k}{\partial x_j}\right)+G_k+G_b-\rho\varepsilon-Y_M+S_k \qquad (4.8)$$

and

$$\frac{\partial}{\partial t}(\rho\varepsilon)+\frac{\partial}{\partial x_i}(\rho\varepsilon u_i)=\frac{\partial}{\partial x_j}\left(\alpha_\varepsilon\,\mu_{eff}\frac{\partial\varepsilon}{\partial x_j}\right)+C_{1\varepsilon}\frac{\varepsilon}{k}(G_k+C_{3\varepsilon}G_b)-C_{2\varepsilon}\rho\frac{\varepsilon^2}{k}-R_\varepsilon+S_\varepsilon \qquad (4.9)$$

In these equations,

G_k is the generation of turbulence kinetic energy due to the mean velocity gradients,

G_b is the generation of turbulence kinetic energy due to buoyancy,

Y_M is the contribution of the fluctuating dilatation in compressible turbulence to the overall dissipation rate.

$C_{1\varepsilon}$, $C_{2\varepsilon}$ and $C_{3\varepsilon}$ are constants.

α_k and α_ε are the inverse effective Prandtl numbers for k and ε, respectively.

S_k and S_ε are source terms for k and ε , respectively.

4.6 Effective Viscosity Modeling

The process of scale exclusion in RNG theory leads to a differential equation related to turbulent viscosity.:

$$d\left(\frac{\rho^2 k}{\sqrt{\varepsilon\mu}}\right) = 1.72\frac{\hat{\nu}}{\sqrt{\hat{\nu}^3 - 1 + C_\nu}}d\hat{\nu} \qquad (4.10)$$

$$\hat{\nu} = \mu_{eff}/\mu$$

$$C_\nu \approx 100$$

The equation is combined to provide a precise explanation of how the effective turbulent transport changes with the effective Reynolds number (or eddy scale), enabling the model to improve its management of flows that have low Reynolds numbers and those close to walls.

In the limiting high-Reynolds-number, Equation 4.10 gives

$$\mu_t = \rho C_\mu \frac{k^2}{\varepsilon} \tag{4.11}$$

with $C_\mu = 0.0845$, obtained through RNG theory. It is noteworthy that this value of C_μ is quite similar to the empirically found value of 0.09 utilized in the conventional k-ε model.

In FLUENT, the standard method for calculating the effective viscosity employs the high-Reynolds-number equation stated in Equation 4.11. Nonetheless, there is a choice that enables us to utilize the differential relationship presented in Equation 4.10 when it is necessary to take low-Reynolds-number influences into account.

$$\mu_t = \mu_{t0} f\left(\alpha_s, \Omega, \frac{k}{\varepsilon}\right) \tag{4.12}$$

where μ_{t0} is the turbulent viscosity value determined without the swirl adjustment by utilizing either Equation 4.12 or Equation 4.13.

Ω is a characteristic swirl number evaluated within FLUENT.

α_s a swirl constant that takes on various values based on whether the flow is primarily influenced by swirl or just slightly swirling.

This swirl adjustment is consistently applied to axisymmetric, swirling flows and three-dimensional flows whenever the RNG model is chosen. For slightly swirling flows (where FLUENT is the standard), α_s is established at 0.05 and is

unchangeable. Nevertheless, a greater value of of α_S are applied for flows that exhibit strong swirling.

4.7 Model Constants

The constants $C_{1\varepsilon}$ and $C_{2\varepsilon}$ in Equation 4.9 are values that have been calculated using RNG theory. These values, which FLUENT uses as standard, are $C_{1\varepsilon}$ = 1.42 and $C_{2\varepsilon}$ = 1.68

4.8 Discretization

The governing equations are transformed into algebraic forms using the finite volume method, which allows for numerical solutions. This control volume approach involves integrating the governing equations around each control volume, resulting in discrete equations that preserve each quantity based on the control volume.

The discretization process for the governing equations can be most clearly shown by examining the steady-state conservation equation for the movement of a scalar quantity φ. This is exemplified through the subsequent equation presented in integral form for any chosen control volume V as follows:

$$\oint \rho\phi\bar{v}.d\bar{A} = \oint \Gamma_\phi \nabla\phi.d\bar{A} + \int_V S_\phi dV \qquad (4.13)$$

where

ρ = density

v = velocity vector A = surface area vector

Γ_φ = diffusion co-efficient for φ

$_\varphi$ = gradient of φ

S_φ = source of φ per unit volume

The above formula is used for each control volume, or cell, within the computational area. Breaking down the equation for a specific cell results in

$$\sum_{f}^{N_{faces}} \rho_f \nu_f \phi_f . \vec{A}_f = \sum_{f}^{N_{faces}} \Gamma_\phi \left(\nabla \phi\right)_n . \vec{A}_f + S_\phi V \qquad (4.14)$$

Where

N_{faces} = number of faces enclosing cell

φ_f = value of φ convected through face f

ρ_f, v_f, A_f = mass flux through the face

A_f = area of face f, A

$(\nabla\varphi)_n$ = magnitude of ∇φ normal to face f

V = cell volume

The equations take share a similar structure to the one presented earlier and easily adapt to multi-dimensional, non-uniform meshes made up of various polyhedral, representing the discrete values of the scalar φ located at the center of the cells. However, face values φ_f is required for the convection terms in Equation and need to be estimated from the values at the cell centers. This is done through an upwind method.

Upwind implies that the face value φ_f is obtained from the quantities in the adjacent cell upstream, or "upwind," in relation to the normal velocity V_n direction.

4.9 Convergence Criteria

To conclude, it is necessary to establish the convergence standards for the iterative technique. Typically, there are two stages of iterations: one focuses on solving the linear equations, while the other addresses the non-linearity and interactions of the equations. It is crucial to determine when to end the iterative process at each stage for reasons of both effectiveness and precision. A numerical approach is considered convergent when the solution of the discretized equations approaches the exact solution of the differential as the grid size approaches zero. For a convergence criterion set around 10^{-6} for the X velocity variable, the outcomes are stable in the current scenario.

CHAPTER 5

VALIDATION

The earlier chapters have described the experimental and computational approaches used to derive detailed performance data concerning average flow characteristics in two-dimensional axisymmetric boundary layer flows, both under normal conditions and with swirling flows at the inlet of axial annular diffusers. Nonetheless, it is essential to evaluate the relationship between these two methods and their mutual dependence for further study. This chapter illustrates the process of validating the results obtained from computational methods against the experimental findings. The validation aims to confirm grid independence and identify the most appropriate model for the current study, based on how closely the computational outcomes align with the experimental data regarding inlet flow conditions, velocity profile development, and pressure recovery coefficients.

5.1 Grid Independence

The outcomes of any computational model depend on the meshing established within the defined geometry. Meshing is comprised of nodes, cells, or grids. The dimensions of the grid are crucial for influencing the results of the physical model. A coarser mesh size, which entails a smaller quantity of meshes, often leads to less accurate results. Conversely, employing a finer mesh or a larger number of meshes typically yields improved results. Nevertheless, utilizing finer meshes leads to a significant increase in computation time. Thus, optimizing grid size is essential to achieve results promptly while ensuring the predetermined level of accuracy is maintained.

In this study, grid independence was assessed across various geometries utilizing multiple models. A specific example of this grid independence testing is presented here. An annular diffuser, characterized by both the hub and casing diverging at equal angles, was selected, on which experiments were also conducted. The inlet velocity profile for the computational model was derived from the same profile obtained experimentally. The turbulence model investigated in this test was the RNG k-ε model. Four distinct grid sizes were utilized to assess the sensitivity related to grid specifications. Different diffusers, with varying geometric parameters, will require a different number of grids that depend on the grid size and the geometrical features. For this investigation, the grid size was considered as a parameter to maintain symmetry among various annular diffusers. The grid size was expressed in relation to the dimensions of the sides of a quadrilateral cell. Mesh sizes ranging from 0.05 to 0.09 cm were implemented to analyze the influence of grid size on the accuracy achieved when compared to experimental results, as well as the computational time required to attain those results. An example of this is illustrated in Table 5.1, which details the mesh size along with the associated number of cells, faces, nodes, and the time taken to reach the converged solution.

Table 5.1 Mesh size

	Element Type	Mesh Size (Cm)	No. of Cells	No. of Face	No. of Nodes	Computation Time (hrs)
Coarse mesh	**Quad./Pave**	**0.09**	**47076**	**94812**	**47737**	**2.5**
Fine mesh	**Quad./Pave**	**0.08**	**85024**	**170787**	**85764**	**8.15**
Finer mesh	**Quad./Pave**	**0.07**	**156064**	**312969**	**156906**	**19.2**
Finer mesh	**Quad./Pave**	**0.06**	**273554**	**548087**	**274534**	**49.9**

Figure 5.1 illustrates the outcomes obtained using the k-ε RNG model with mesh sizes of 0.06, 0.07, 0.08 and 0.09 cm. The results for mesh sizes 0.06 and 0.07 are nearly identical, which is why a mesh size of 0.07 cm has been chosen for the current CFD analysis to shorten computational duration while still maintaining precision.

5.2 Turbulence Model Validation

Choosing a model can be a complex task because it requires managing many known and unknown factors to forecast outcomes that align closely with actual experimental data. In the preliminary study, various models were examined to determine the turbulence model that best represented the real-world scenario by being closest to the experimental findings.

- **k- ε models**
  - Standard k- ε model
  - Renormalization-group (RNG) k- ε model
  - Realizable k- ε model

- **Reynolds stress model (RSM)**

- **The Spalart-Allmaras Model**
  - Vorticity based production
  - Strain/ Vorticity based production

- **Standard k- ω Model**
- **Shear-Stress Transport (SST) k- ω Mode**l

5.2.1 k- ε models

The Standard, RNG, and Realizable k-ε Models

All three models exhibit comparable structures, featuring transport equations for k and ε. The different categories of models include:

- A method for computing turbulent viscosity
- The turbulent diffusion of k and ε, regulated by turbulent Prandtl numbers
- The transport equations, approaches for determining turbulent viscosity, and model constants are introduced individually for each model.

5.2.1.1 The Standard k-ε Model

In computational fluid dynamics (CFD), turbulence models typically employ two equation frameworks. Both of these frameworks calculate the Reynolds Stresses through the Eddy Viscosity method, which is used to resolve two transport equations. Since it was introduced by Launder and Spalding, the standard k-ε model in ANSYS Fluent belongs to this group of models and has become essential for engineering flow calculations in practice.

In ANSYS Fluent, it is advised to choose the Realizable k-ε model over other options within the k-ε category. Using the k-ε model alongside the Enhanced Wall Treatment (EWT) is suggested. However, in situations where the flow detaches from smooth surfaces like airfoils due to unfavorable pressure gradients, k-ε models are usually not recommended.

5.2.1.2 Transport Equations for the Standard k-ε Model

The following transport equations provide the turbulence kinetic energy (k), and the rate at which it is dissipated (ε) are:

$$\frac{\partial}{\partial t}(\rho k)+\frac{\partial}{\partial x_i}(\rho k u_i)=\frac{\partial}{\partial x_j}\left[\left(\mu+\frac{\mu_t}{\sigma_k}\right)\frac{\partial k}{\partial x_j}\right]+G_k+G_b-\rho\varepsilon-Y_M+S_k \quad (5.1)$$

and

$$\frac{\partial}{\partial t}(\rho \varepsilon)+\frac{\partial}{\partial x_i}(\rho \varepsilon u_i)=\frac{\partial}{\partial x_j}\left[\left(\mu+\frac{\mu_t}{\sigma_\varepsilon}\right)\frac{\partial \varepsilon}{\partial x_j}\right]+C_{1\varepsilon}\frac{\varepsilon}{k}(G_k+C_{3\varepsilon}G_b)-C_{2\varepsilon}\rho\frac{\varepsilon^2}{k}+S_\varepsilon \quad (5.2)$$

In this context, Y_M denotes the part of the varying expansion in compressible turbulence that contributes to the total dissipation rate. G_b refers to the production of turbulence kinetic energy resulting from buoyancy. G_k indicates the production of turbulence kinetic energy due to the gradients in average velocity. The values $C_{1\varepsilon}$, $C_{2\varepsilon}$, and $C_{3\varepsilon}$ are constant numbers. σk and σε are the turbulent Prandtl numbers related to k and ε respectively.

5.2.1.3 Modelling the Turbulent Viscosity

The turbulent (or eddy) viscosity (μ_t) is computed by combining k and ε as follows:

$$\mu_t=\rho C_\mu\frac{k^2}{\varepsilon} \quad (5.3)$$

where C_μ is a constant.

The model constants

$C_{1\varepsilon}$, $C_{2\varepsilon}$, C_{μ}, σ_k, and σ_v have the following default values:

$C_{1\varepsilon} = 1.44$, $C_{2\varepsilon} = 1.92$, $C_{\mu} = 0.09$, $\sigma_k = 1.0$, $\sigma_{\varepsilon} = 1.3$

5.2.2 The RNG k-ε Model

It is similar to the k- ε model within the Navier-Stokes equations, and the RNG-based k- ε turbulence model is developed utilizing a method known as "renormalization group" (RNG). However, it includes these enhancements:

- For flows that are increasingly strained, the RNG model incorporates an additional term in its equation that helps improve accuracy.
- To enhance the precision regarding the impact of swirl on turbulence, it considers swirling flows.
- It provides a mathematically derived differential equation for viscosity that takes into account the lower Reynolds-number effects, thus making the RNG k- ε model more accurate.
- These enhancements apply to a broader range of flows compared to the standard k- ε model.

These enhancements render the RNG k- ε model dependable and more precise for a wider variety of flows than the standard k- ε model.

5.2.2.1 Transport Equations for the RNG k-ε Model

The RNG k-ε model is an upgraded version of the standard k-ε turbulence model, created through Renormalization Group (RNG) theory. It addresses two transport

equations: one for turbulent kinetic energy (k) and a second for its dissipation rate (ε), while adding extra terms and changing constants to enhance precision in specific flow situations.

$$\frac{\partial}{\partial t}(\rho k) + \frac{\partial}{\partial x_i}(\rho k u_i) = \frac{\partial}{\partial x_j}\left[\alpha_k \mu_{eff} \frac{\partial k}{\partial x_j}\right] + G_k + G_b - \rho\varepsilon - Y_M + S_k \quad (5.4)$$

and

$$\frac{\partial}{\partial t}(\rho \varepsilon) + \frac{\partial}{\partial x_i}(\rho \varepsilon u_i) = \frac{\partial}{\partial x_j}\left[\alpha_k \mu_{eff} \frac{\partial \varepsilon}{\partial x_j}\right] + C_{1\varepsilon}\frac{\varepsilon}{k}(G_k + C_{3\varepsilon}G_b) - C_{2\varepsilon}\rho\frac{\varepsilon^2}{k} - R_\varepsilon + S_\varepsilon \quad (5.5)$$

In these equations, G_b is generation of turbulence kinetic energy (G_k) represents generation of turbulence kinetic energy (Y_M) represents the contribution of fluctuating in compressible turbulence overall dissipation rate.

5.2.2.2 Modelling the Effective Viscosity

RNG theory provides a differential equation for turbulent viscosity through the scale elimination method as follows:

$$d\left(\frac{\rho^2 k}{\sqrt{\varepsilon\mu}}\right) = 1.72\frac{\hat{\nu}}{\sqrt{\hat{\nu}^3 - 1 + C_\nu}} \quad (5.6)$$

where

$$\hat{\nu} = \mu_{eff}/\mu \qquad C_{\hat{\nu}} \approx 100$$

to acquire a highly precise detail regarding how the effective turbulent transport relates to the effective Reynolds number, with the equations for near-wall flows

incorporated, enabling the model to improve its handling of low-Reynolds-number situations. The equation provided in the high-Reynolds-number condition offers

$$\mu_t = \rho C_\mu \frac{k^2}{\varepsilon} \tag{5.7}$$

with $C_\mu = 0.0845$, obtained through RNG theory. It is noteworthy that this Cμ value is quite similar to the experimentally found value of 0.09 applied in the standard k- ε model.

5.2.3 The Realizable k-ε Model

A different formulation for turbulent viscosity is found in the Realizable k-ε model, setting it apart from the conventional k-ε model.

The phrase "Realizable" positively addresses mathematical modelling. Both the conventional k-ε model and the RNG k-ε model lack realizability. This is due to the specific reason that it takes into account the influences of average rotation in how turbulent viscosity is defined.

5.2.3.1 Transport Equations for the Realizable k-ε Model

The transport equations for k and ε in the realizable k-ε model are modeled as:

$$\frac{\partial}{\partial t}(\rho k) + \frac{\partial}{\partial x_i}(\rho k u_i) = \frac{\partial}{\partial x_j}\left[\left(\mu + \frac{\mu_t}{\sigma_k}\right)\frac{\partial k}{\partial x_j}\right] + G_k + G_b - \rho\varepsilon - Y_M + S_k \tag{5.8}$$

And

$$\frac{\partial}{\partial t}(\rho\varepsilon) + \frac{\partial}{\partial x_i}(\rho\varepsilon u_i) = \frac{\partial}{\partial x_j}\left[\left(\mu + \frac{\mu_t}{\sigma_\varepsilon}\right)\frac{\partial \varepsilon}{\partial x_j}\right] + \rho C_1 S_\varepsilon + C_{1\varepsilon}\frac{\varepsilon}{k}(C_{3\varepsilon}G_b) - C_2\rho\frac{\varepsilon^2}{k+\sqrt{\nu\varepsilon}} + S_\varepsilon \tag{5.9}$$

where

$$C_1 = \max\left[0.43, \frac{\eta}{\eta+5}\right] \qquad \eta = S\frac{k}{\varepsilon}$$

5.2.3.2 Modelling the Turbulent Viscosity

The eddy viscosity is computed from

$$\mu_t = \rho C_\mu \frac{k^2}{\varepsilon}$$

$$C_\mu = \frac{1}{A_0 + A_s \dfrac{kU^*}{\varepsilon}}$$

as in other k-ε models,

where

$$U^* = \sqrt{S_{ij}S_{ij} + \tilde{\Omega}_{ij}\tilde{\Omega}_{ij}}$$

and

$$\tilde{\Omega}_{ij} = \Omega_{ij} - 2\varepsilon_{ijk}\omega_k$$
$$\tilde{\Omega}_{ij} = \bar{\Omega}_{ij} - \varepsilon_{ijk}\omega_k$$

Model Constants

The constants C_2, σ_k, and $\sigma\varepsilon$ have been set to ensure that the model operates effectively under standard flow conditions. The constants in the model are

$\sigma_k = 1{:}0$; $\sigma_\varepsilon = 1{:}2$ $C_{1\varepsilon} = 1{:}44$; $C_2 = 1{:}9$;

5.2.4 Reynolds stress model (RSM)

The Reynolds Stress Models, also referred to as the Reynolds Stress Transport Models, represent an advanced type of turbulence closure and are considered the most thorough classical turbulence model. The closure technique used is typically known as a Second Order Closure. This modeling concept was developed from the research conducted by Chou in 1945 and Rotta in 1951. In these models, the eddy viscosity method is not utilized, and the individual elements of the Reynolds stress tensor are calculated directly. These models are based on the precise transport equation for Reynolds stress. They can incorporate intricate interactions present in turbulent flow situations, including the directional influences of the Reynolds stresses.

The Reynolds Stress Model serves as an effective method for modeling turbulent flows in different engineering scenarios. Due to its capacity to consider intricate interactions and directional effects, it is often favored by numerous CFD professionals aiming for precise and dependable outcomes in the analysis of turbulent flows.

5.2.5 The Spalart-Allmaras Model

The Spalart-Allmaras approach is a single-equation turbulence model intended for the precise and effective forecasting of aerodynamic flows near walls. The model is clearly influenced by the distance from the wall, which allows it to perform very well in boundary layers and attached flows. The flow can be modelled on the following two basis

- Vorticity based production
- Strain/ Vorticity based production

5.2.6 Standard k-ω Model

The standard model utilized in Ansys Fluent relies on a model introduced by Wilcox, which includes changes for effects related to low Reynolds numbers, compressibility, and the spreading of shear flow. A limitation of the Wilcox model from 1998 is how sensitive its results are to the values of k and ω beyond the shear layer (freestream sensitivity). This sensitivity can greatly influence the outcome, particularly in free shear flows. There is a newer iteration of this model, known as the Wilcox 2006 k-ω model, which also has not entirely addressed the issue of freestream sensitivity.

The standard model is an empirical framework based on transport equations for turbulence kinetic energy (k) and the specific dissipation rate (ω), which can be seen as the ratio of ω to k.

Over the years, the k-ω model has undergone modifications, leading to the inclusion of production terms in both the k and ω equations, thereby enhancing the model's effectiveness in predicting free shear flows.

5.2.7 The Shear Stress Transport (SST) model

The Shear Stress Transport (SST) model is a popular turbulence model in computational fluid dynamics (CFD) that merges the advantages of the k-ω and k-ε models to offer precise predictions of turbulent flows, particularly when facing unfavorable pressure gradients.

For validating the experimental results obtained were tested against the above turbulence models. These models underwent testing using an inlet velocity profile that

was derived through experiments for a fully developed flow in an annular diffuser with an equivalent cone angle of 10°. Both the casing and hub of the diffuser were diverging at the same angle of 10°. The findings related to longitudinal velocity profiles and pressure recovery coefficients are illustrated in figures 5.2 and 5.3, respectively. It can be observed from these figures that the turbulence model aligning most closely with the experimental findings is the Renormalization-group (RNG) k- ε model. This model has been applied for additional analyses in the current study.

5.3 Validation of Development of velocity profile

The k- ε model utilizing the renormalization-group (RNG) approach was applied to analyze the development of flow in different diffusers. Before advancing, the outcomes retrieved from this model for the identical setup were compared with the current experimental findings and those from Kumar [1977].

The comparison is displayed in figure 5.4, which shows the results for non-swirling flow at different sections of the diffuser passage length. Figures 5.5 and 5.6 present the outcomes related to axial and swirling velocities for inlet swirl angles of 12° and 17° respectively. The results achieved through CFD modeling align well with both the current experimental data and Kumar's findings from 1977.

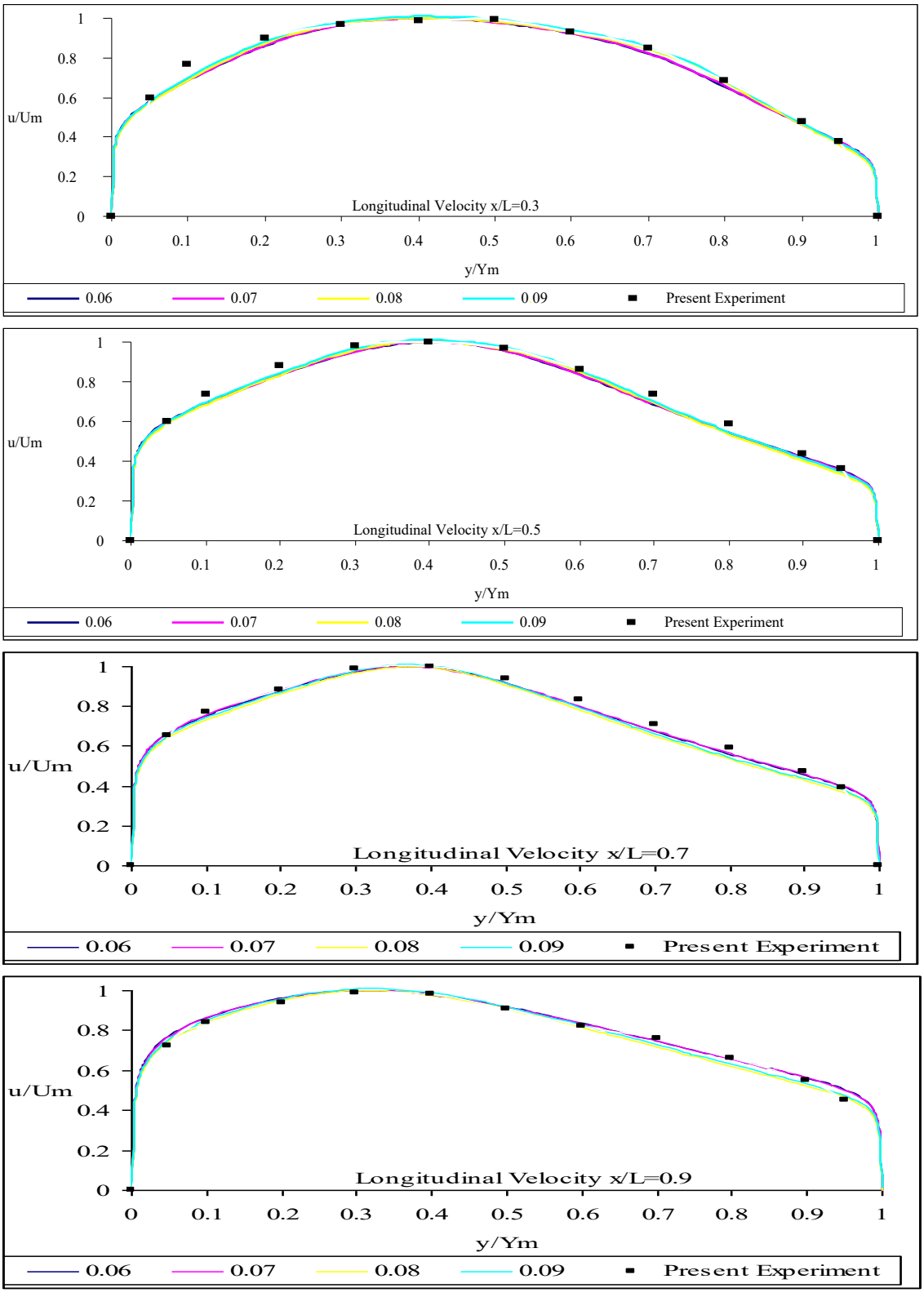

Figure 5.1: Grid Independence Test of Longitudinal Velocity (0°) for 10° equivalent cone angle diffuser

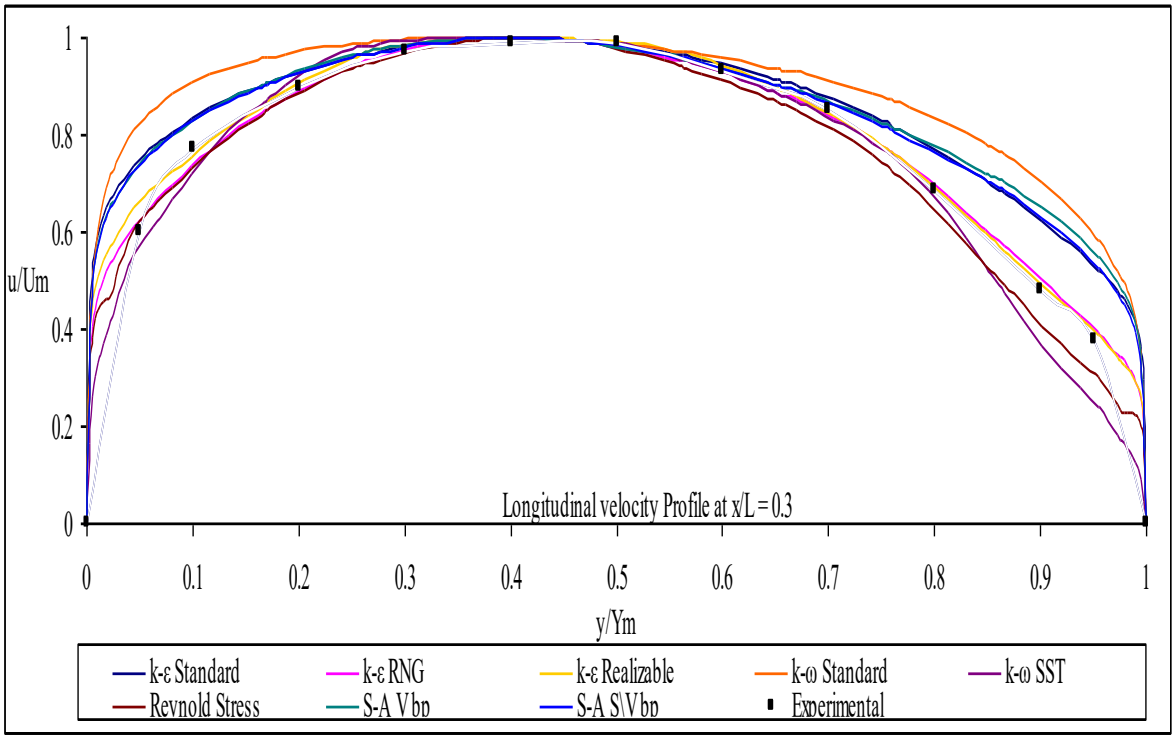

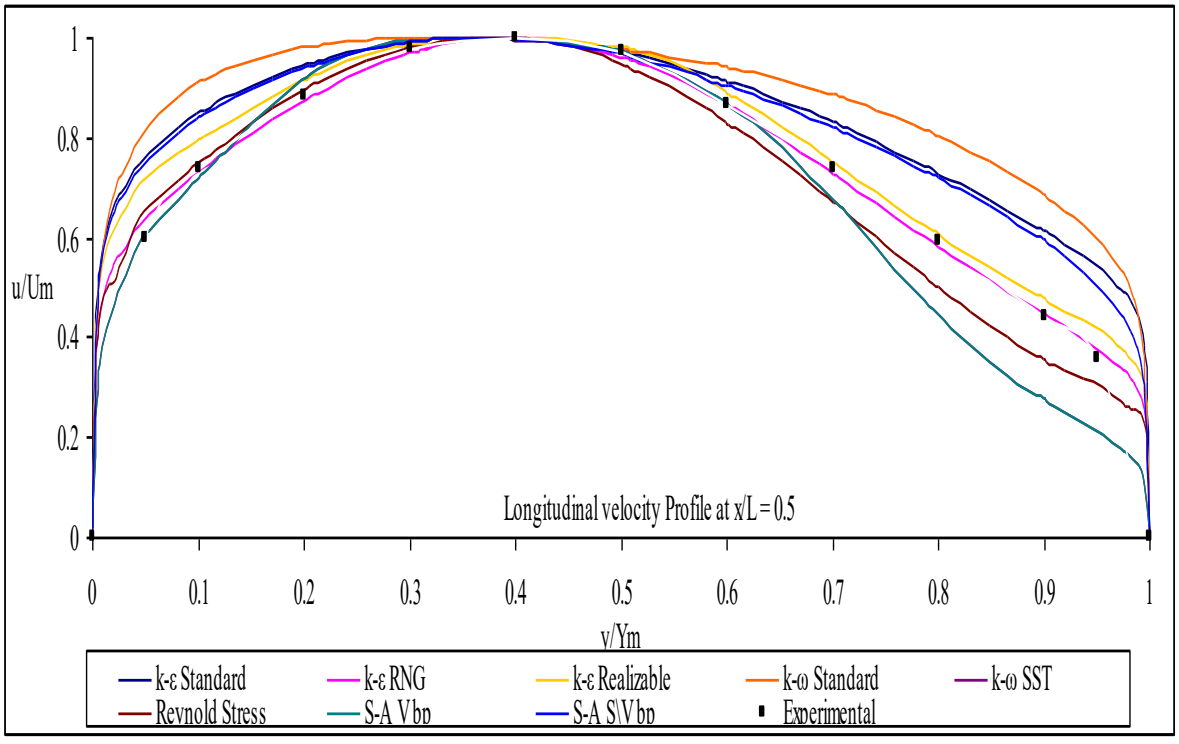

Fig. 5.2(a) Validation of Turbulence Model with Experimental Results at x/L = 0.3 and 0.5

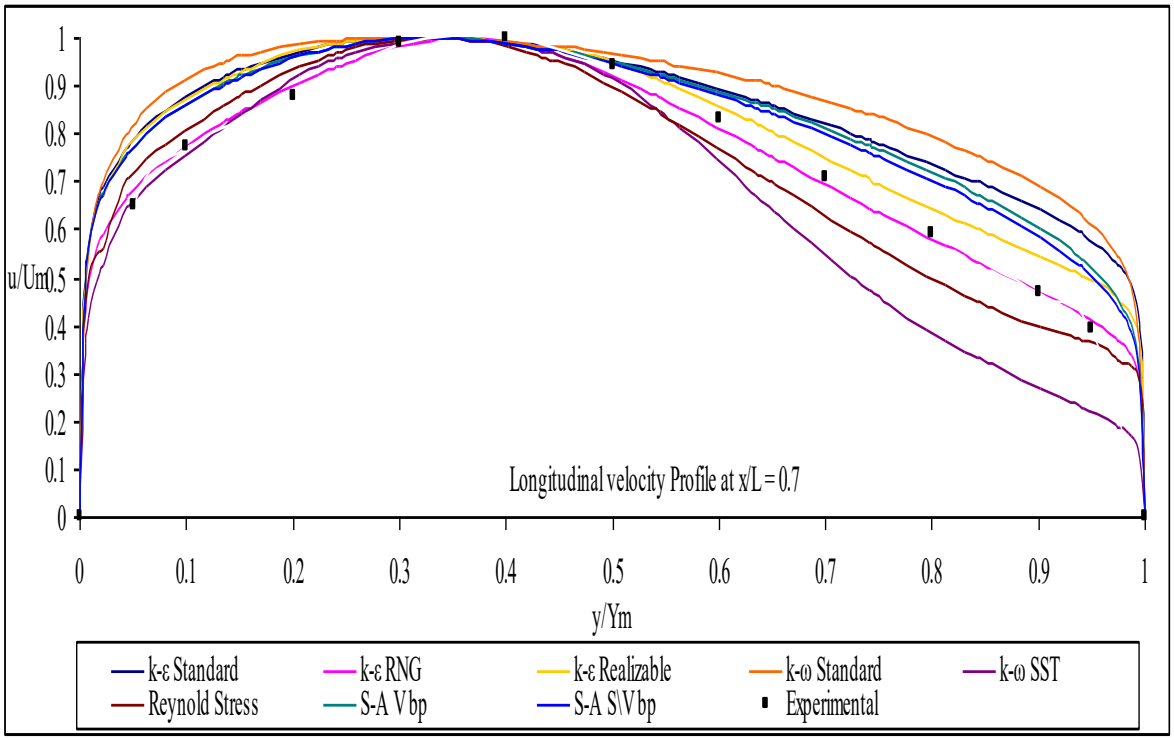

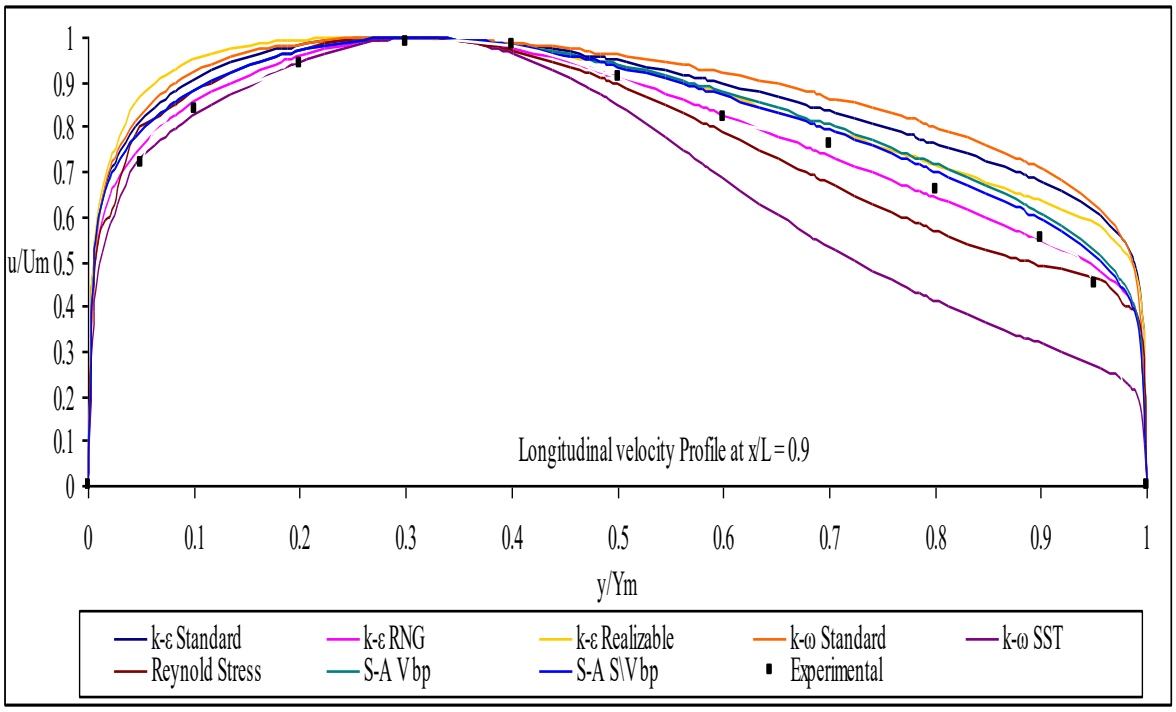

Fig. 5.2(b) Validation of Turbulence Model with Experimental Results at x/L = 0.7 and 0.9

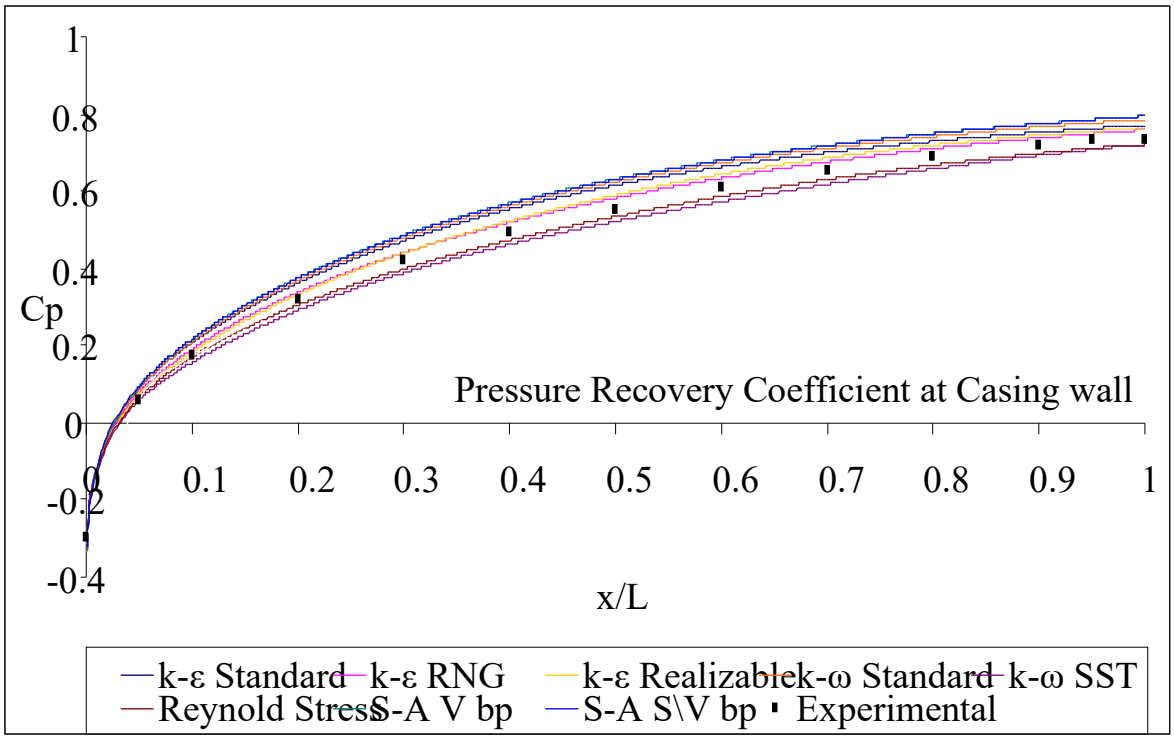

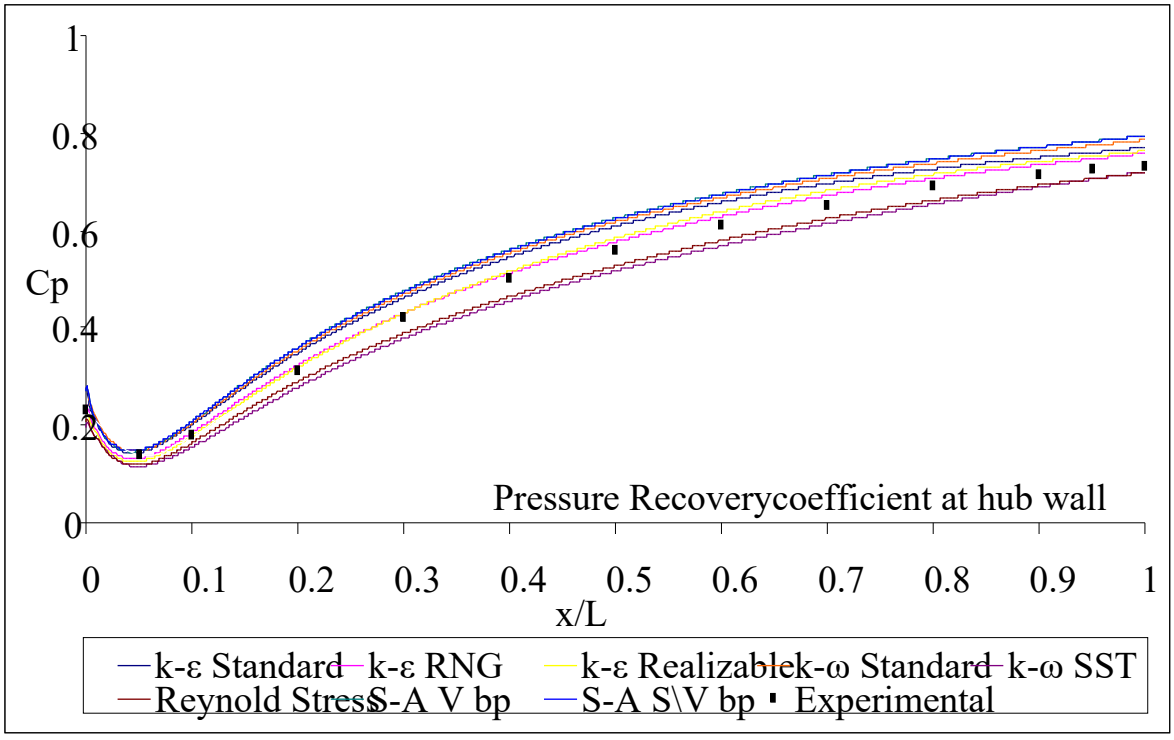

Fig. 5.3 Validation of Pressure Recovery Coefficient with experimental Results at the casing and hub wall

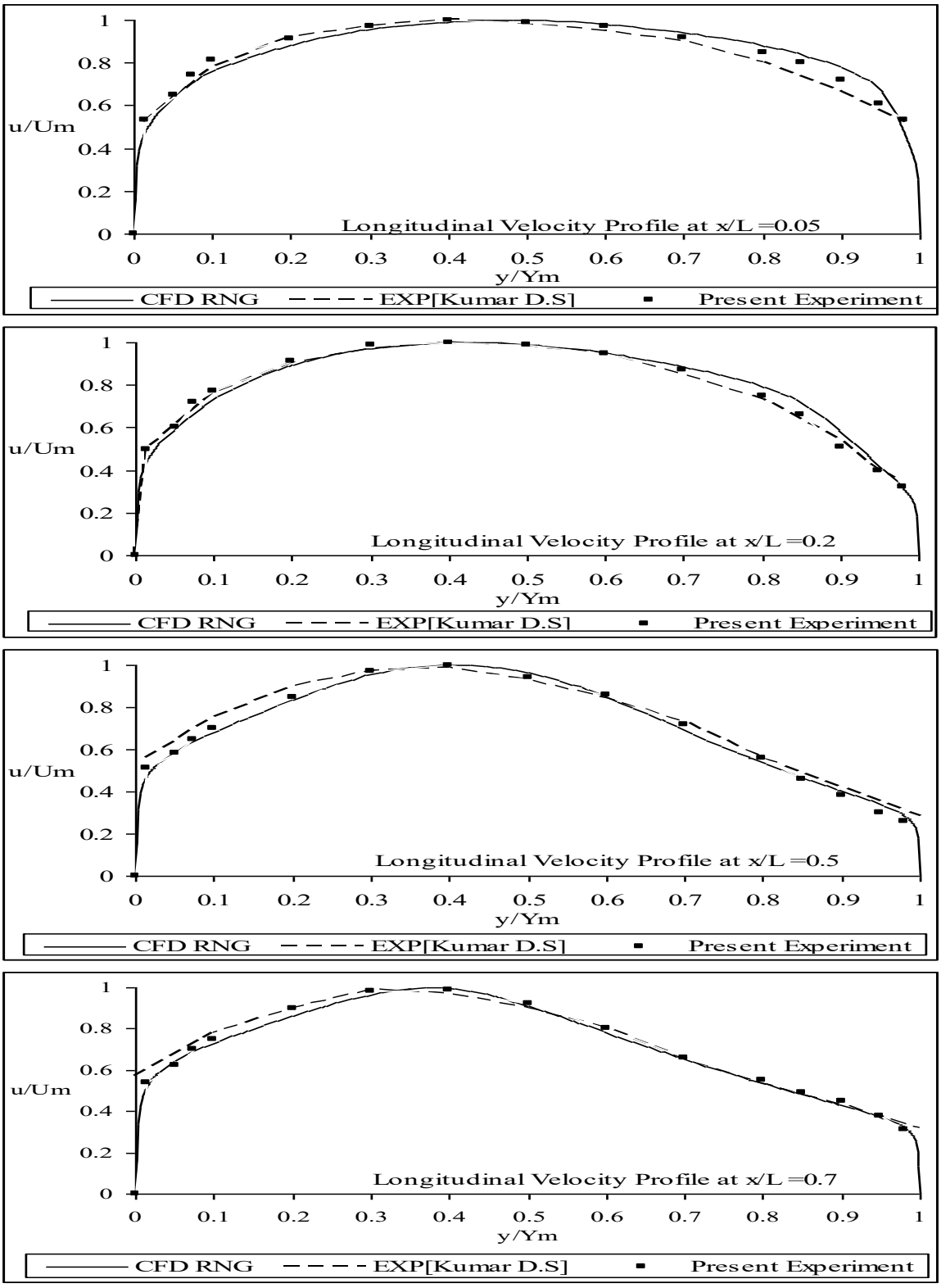

Fig. 5.4 Validation of Longitudinal velocity profile for 10° equivalent cone angle diffuser B without swirl

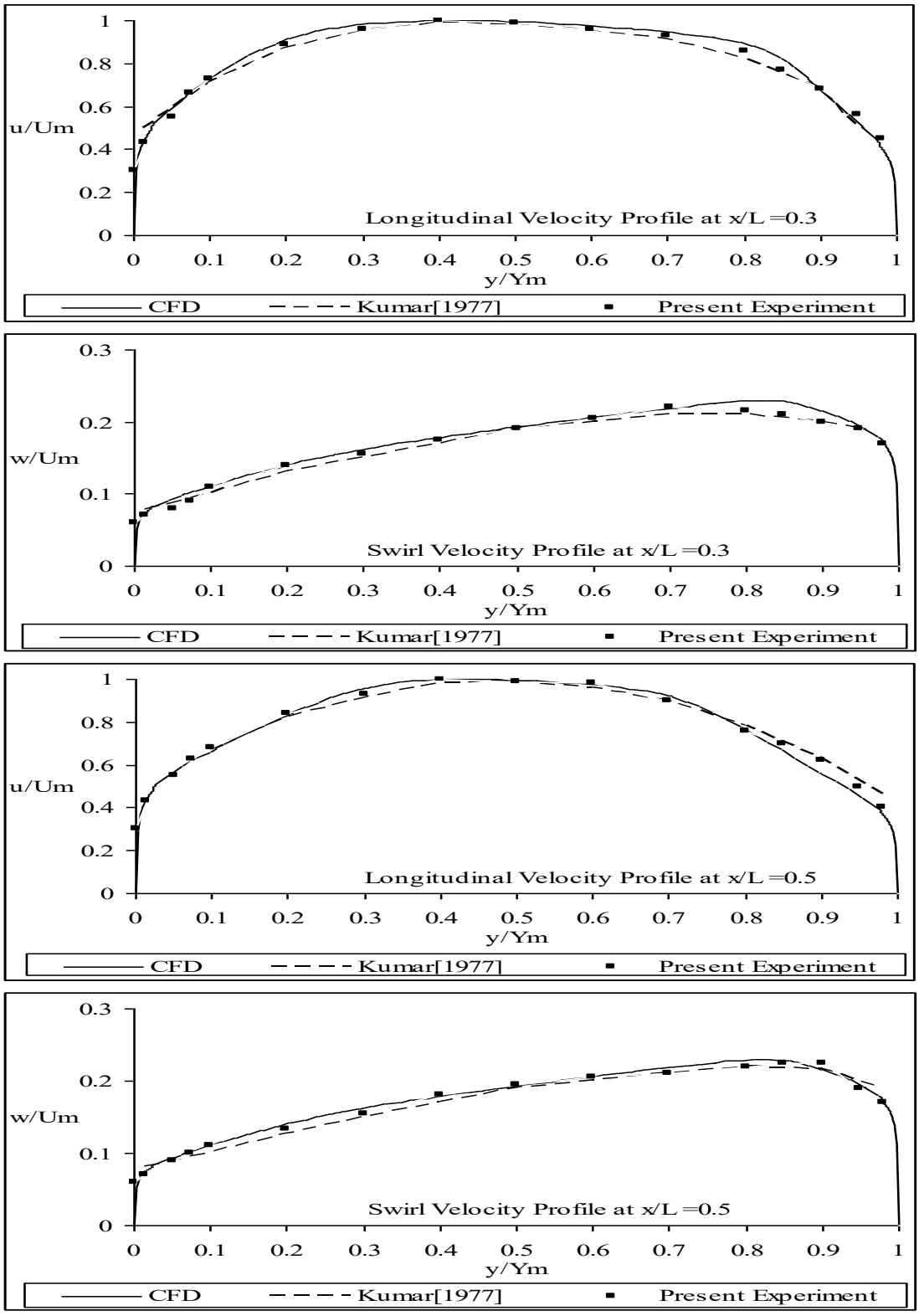

Fig.5.5 Validation of Longitudinal and swirl velocity profile for 10° equivalent cone angle diffuser B with 12° inlet swirl

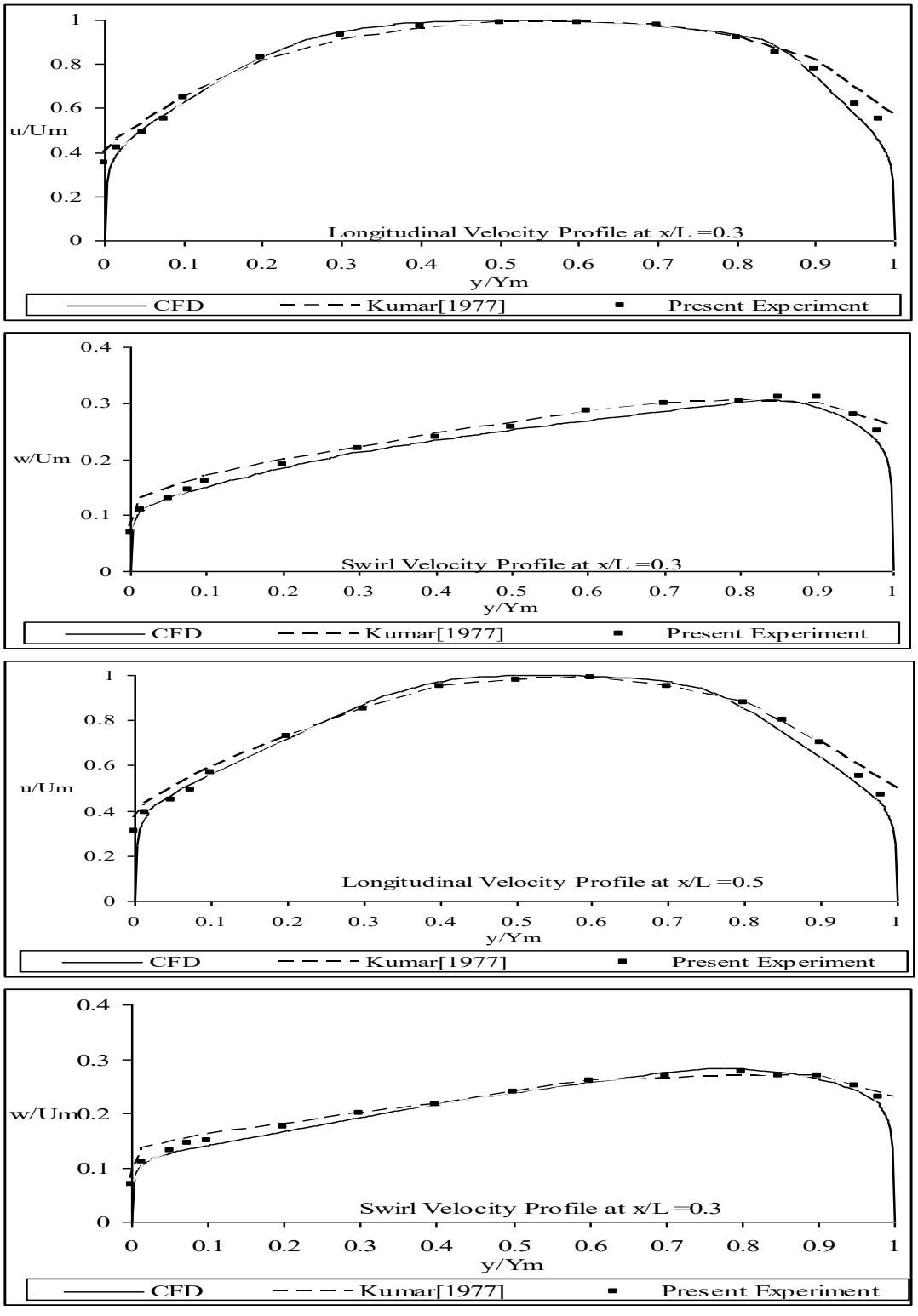

Fig. 5.6 Validation of Longitudinal and swirl velocity profile for 10° equivalent cone angle diffuser B with 17° inlet swirl

CHAPTER 6

RESULTS AND DISCUSSION

In this section, outcomes of theoretical studies are shown and examined. As previously mentioned in chapter 4, the goal of the computational study was to gather information regarding the flow and efficiency features of annular diffusers. CFD analysis was performed both with and without inlet swirl in all the diffusers, utilizing the inlet velocity profile that was derived from experiments. The same CFD model used in these investigations was applied, which confirmed the experimental findings closely as explained in the earlier chapter. The findings have been displayed in terms of non-dimensional flow and performance metrics to emphasize the general behavior of the diffusers.

Initially, the flow development in the diffusers is detailed for varying inlet conditions, concluding with a discussion and graphical representation of the performance parameters of the diffusers.

6.1 Velocity Profile

The flow within a diffuser occurs due to an unfavorable pressure gradient. The longitudinal velocity steadily declines as the flow moves downstream, regardless of whether the incoming flow is swirling or not. This reduction in velocity happens because

the cross-sectional area of the diffuser increases in the direction of flow, which aligns with the Principle of Continuity; at the same time, the static pressure will also increase.

The drop in velocity is directly related to the ratio of the area increase, and simultaneously, the static pressure distribution rises within the diffuser. The upcoming sections will present the progression of velocity profiles in the flow passage of the diffuser in a sequential manner. All velocity profiles will be represented as non-dimensional velocity, defined as local longitudinal or local swirl velocity divided by the local maximum longitudinal velocity at that particular transverse. The transverses considered are perpendicular to the hub at each position.

The non-dimensional velocity is depicted as a function of non-dimensional diffuser passage height (y/Ym) of the specific transverse, where y indicates the local diffuser passage height and Ym is the maximum diffuser passage height, both measured from the hub wall. Therefore, y/Ym = 0 corresponds to the hub position, while y/Ym = 1 refers to the casing position. Graphs will illustrate various transverses at non-dimensional diffuser lengths of x/L = 0.1, 0.3, 0.5, 0.7, and 0.9 for all area ratios and inlet swirl angles. The velocity profiles demonstrate conditions without swirl (0°) and include inlet swirl angles of 7.5°, 12°, 17°, and 25°.

6.2 Velocity distribution in 10° Equivalent cone angle diffusers

6.2.1 Diffuser A (Parallel hub and Diverging Casing)

Figures 6.1 and 6.2 depict the velocity patterns for Area ratios 2 and 3 respectively, corresponding to 10° cone angles for diffuser A (which features a straight hub and a diverging casing). In diagrams 6.1(a) and 6.2(a), the Longitudinal velocities are shown, while 6.1(b) and 6.2(b) illustrate the swirl velocity patterns for their respective area ratios. The data in figures 6.1(a) and 6.2(a) highlight that the Longitudinal velocity profiles decrease more quickly near the hub and the casing wall as the flow moves through the diffuser passage, attributed to the expansion of the boundary layer. The increase in the boundary layer is clear from the longitudinal velocity profiles, showing that the velocity reduces close to both the hub and casing wall as the diffuser passage shifts from x/L=0.1 to 0.9.

The non-swirl flow graphs (0°) reveal that the position of the peak non-dimensional velocity moves towards the hub in the downstream section of the diffuser passage, as illustrated in figures 6.1(a) and 6.2(a) for area ratios 2 and 3 respectively. As the area ratio rises for the same inlet velocity profile, the shift towards the hub grows more significant. This effect occurs due to the increased development of stall near the casing wall with a higher area ratio for the same cone angle diffusers. With the introduction of swirl, the stall migrates from the casing wall to the hub wall. The figures demonstrate that with a greater inlet swirl, the longitudinal velocity profile flattens, and the peak shifts from the hub towards the casing side. Analyzing figures 6.1(a) and 6.2(a) shows that this

shift becomes more pronounced as the area ratio increases. Additionally, flow reversal is noted at the hub wall with a 25° inlet swirl for area ratio 2 at x/L= 0.7, reaching y/Ym= 0.09, and at x/L= 0.9, up to y/Ym= 0.19. In the case of area ratio 3, flow reversal is observed at 17° and 25° inlet swirls. For area ratio 3, the reversal at 17° inlet swirl starts at x/L=0.9, while for the 25° swirl, it commences at x/L=0.3. The 17° inlet swirl reversal for area ratio 3 at x/L=0.9 reaches y/Ym= 0.09. For the 25° inlet swirl and area ratio 3, the reversal occurs at x/L=0.3, 0.5, 0.7, and 0.9, achieving y/Ym=0.01, 0.19, 0.25, and 0.28 respectively. The findings suggest that the introduction of swirl encourages the stall to move from the casing towards the hub, with significant separation at the hub wall becoming noticeable as the area ratio increases.

Figures 6.1(b) and 6.2(b) demonstrate that the swirl velocity without dimensions rises as we progress through the diffuser passage. Figure 6.1(b) shows that the highest point of the non-dimensional velocity moves toward the hub as we advance down the passage for a 7.5° inlet swirl, suggesting that the swirl diminishes within the passage. This shift and reduction happen more rapidly for larger area ratios, as observed in Figure 6.2(b). For greater swirl angles, the peak of the velocity moves toward the casing, and the slight rise in velocity through the diffuser passage decreases, turning negative for significant inlet swirl. The reduction in swirl indicates the likelihood of a separation bubble and a tendency for flow reversal.

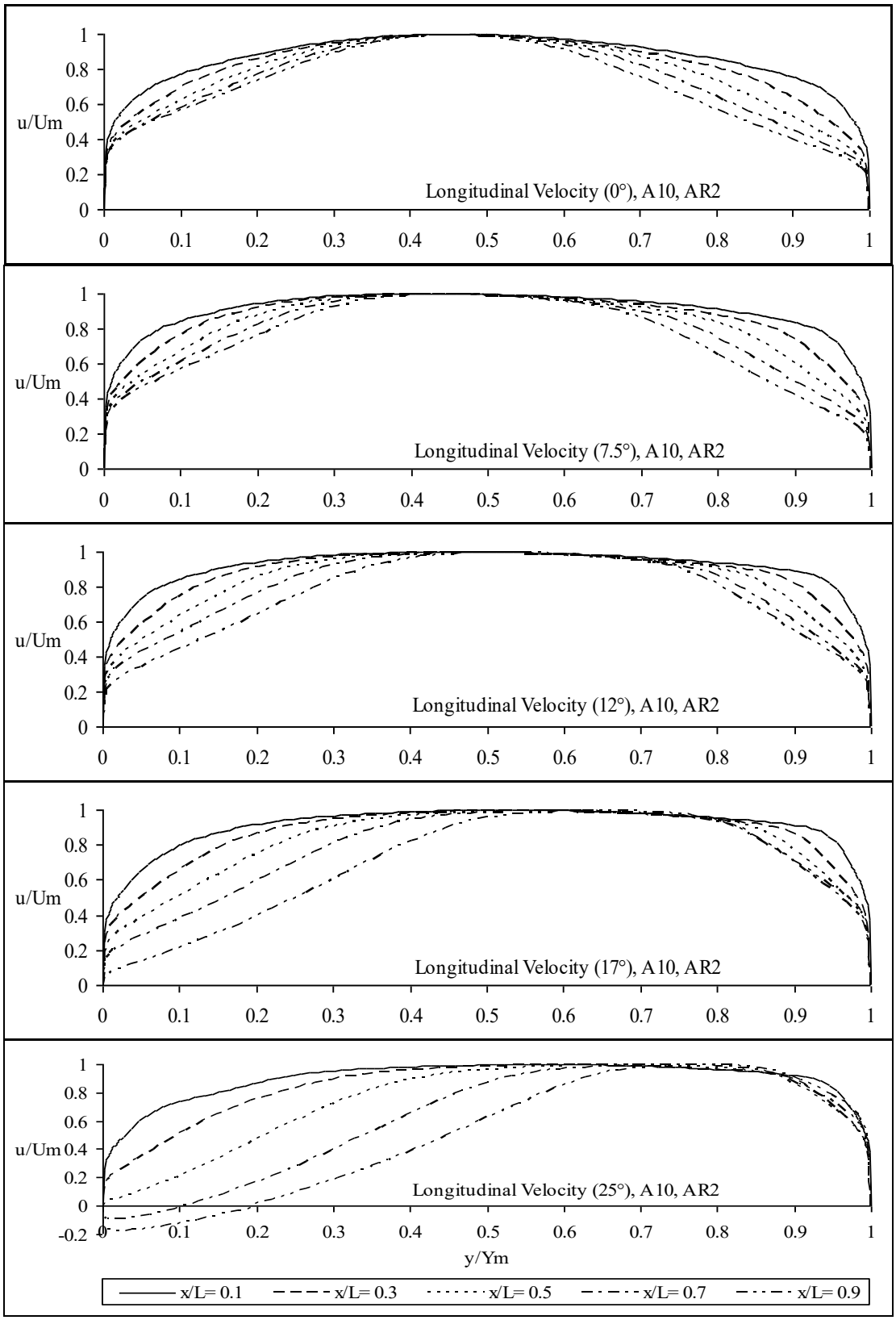

Fig. 6.1(a) Non-dimensional Longitudinal Velocity versus diffuser passage height for diffuser A, equivalent cone angle 10º, Area ratio 2 for inlet swirl angles (0º to 25º) at various transverses at x/L = 0.1 to 0.9.

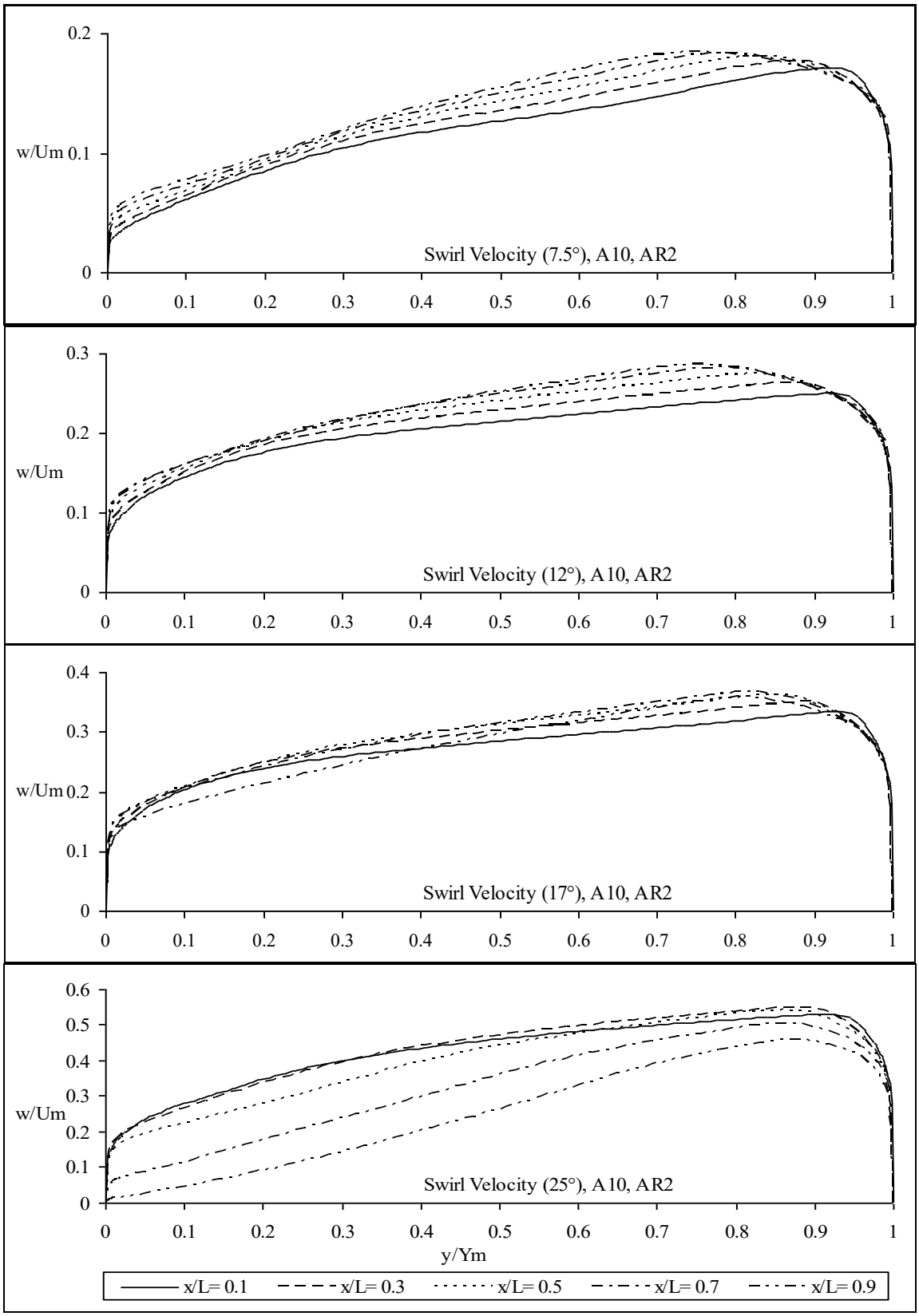

Fig. 6.1(b) Non-dimensional Swirl Velocity versus diffuser passage height for diffuser A, equivalent cone angle 10º, Area ratio 2 for inlet swirl angles (7.5º to 25º) at various transverses at x/L = 0.1 to 0.9.

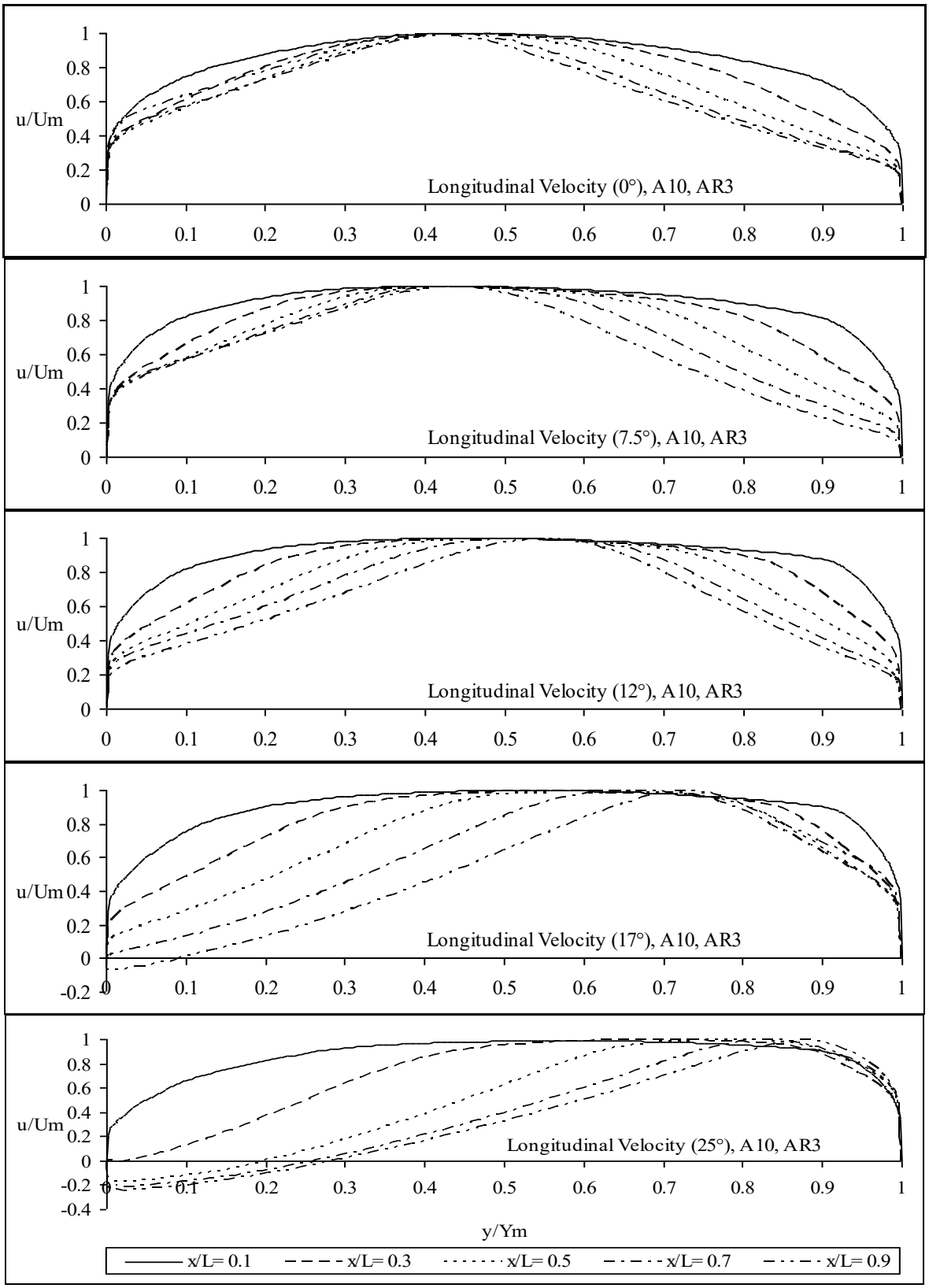

Fig. 6.2(a) Non-dimensional Longitudinal Velocity versus diffuser passage height for diffuser A, equivalent cone angle 10º, Area ratio 3 for inlet swirl angles (0º to 25º) at various transverses at x/L = 0.1 to 0.9.

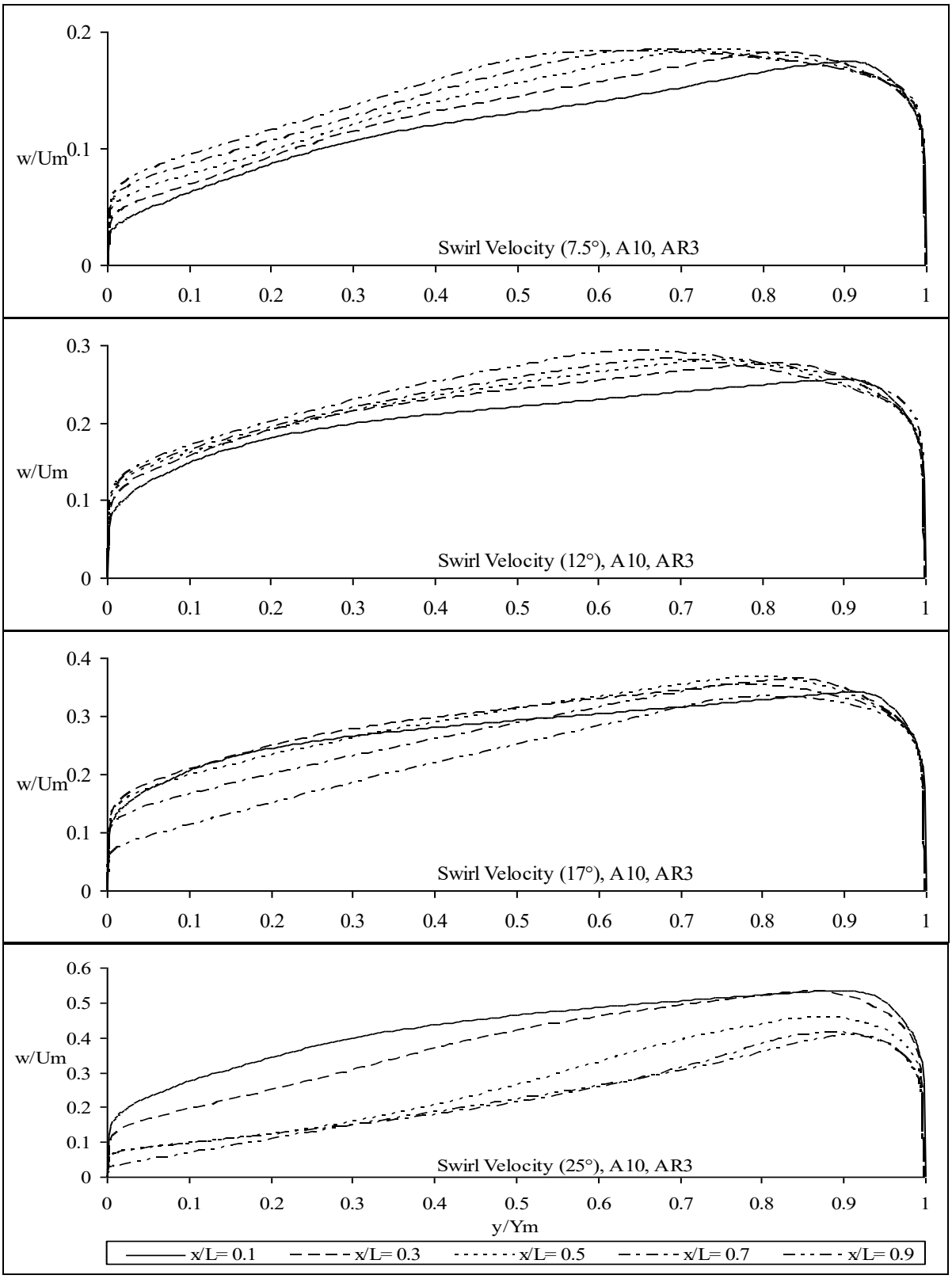

Fig. 6.2(b) Non-dimensional Swirl Velocity versus diffuser passage height for diffuser A, equivalent cone angle 10º, Area Ratio 3

6.2.2 Diffuser B (Both hub and casing diverging with equal angles)

Figures 6.3 and 6.4 display the velocity patterns for area ratios 2 and 3, respectively, using a 10° equivalent cone angle for diffuser B (which has both hub and casing diverging at the same angles). In this scenario, the flow without swirl is generated by the hub and moves towards the casing when swirl is introduced. The non-dimensional longitudinal and swirl velocities drop within the diffuser passage; however, the reduction in swirl velocity is small compared to diffuser A. This occurs because the height of the diffuser passage remains consistent throughout. The drop in longitudinal velocity near the casing wall happens at a quicker pace than at the hub wall due to a larger resistance area, which further amplifies as the area ratio increases, as shown in Figures 6.3(a) and 6.4(a). In this diffuser type, there is no observed separation or reversal of flow on either the hub or the casing wall, even when a 25° inlet swirl is applied. This is linked to the diffuser passage height being constant throughout.

Figures 6.3(b) and 6.4(b) show that the non-dimensional swirl velocity declines as it travels through the diffuser passage for all inlet swirl angles considered. The decline is more significant with higher inlet swirl angles and further increases with a higher area ratio.

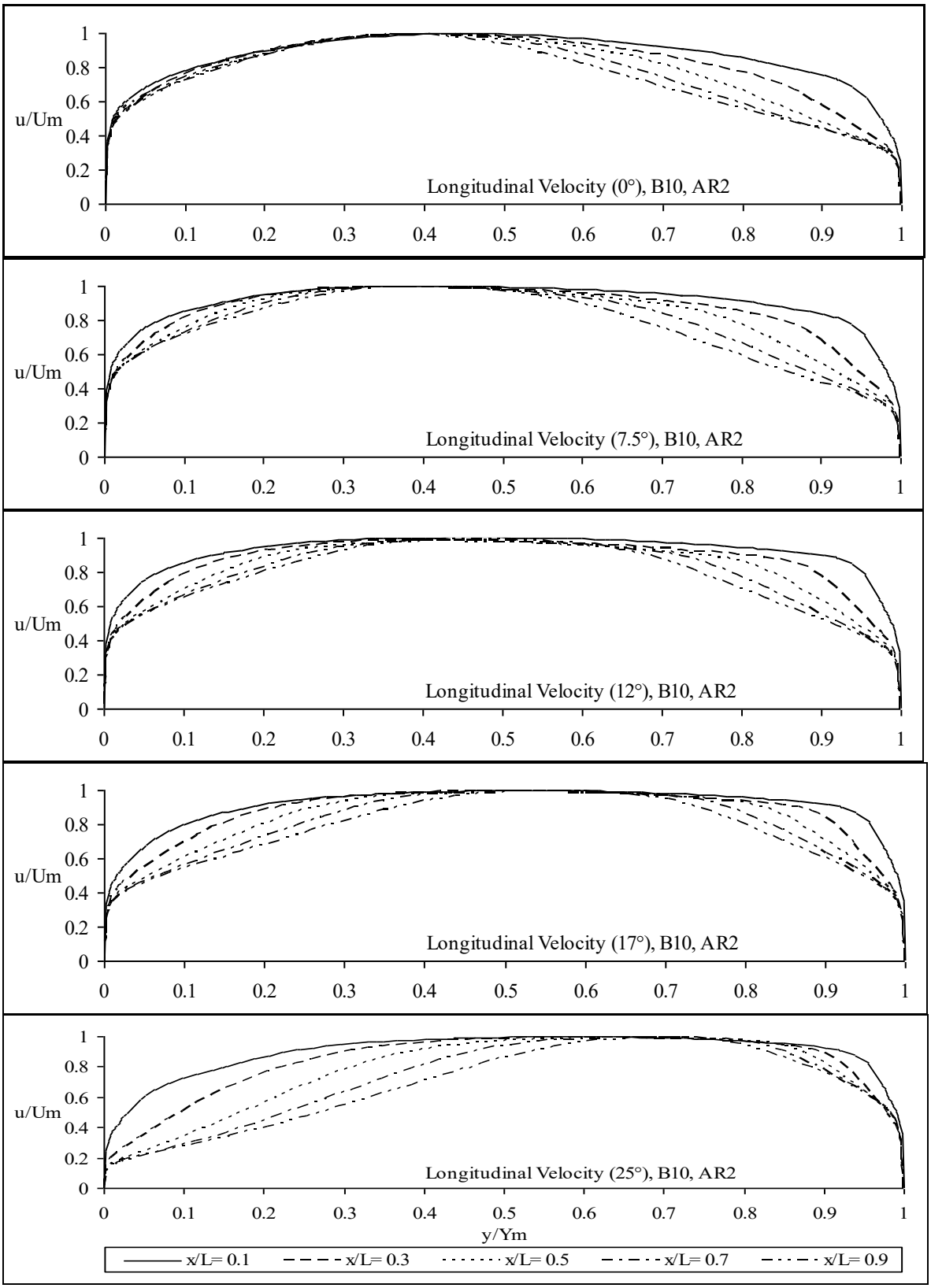

Fig. 6.3(a) Non-dimensional Longitudinal Velocity versus diffuser passage height for diffuser B, equivalent cone angle 10º, Area ratio 2 for inlet swirl angles (0º to 25º) at various transverses at x/L = 0.1 to 0.9.

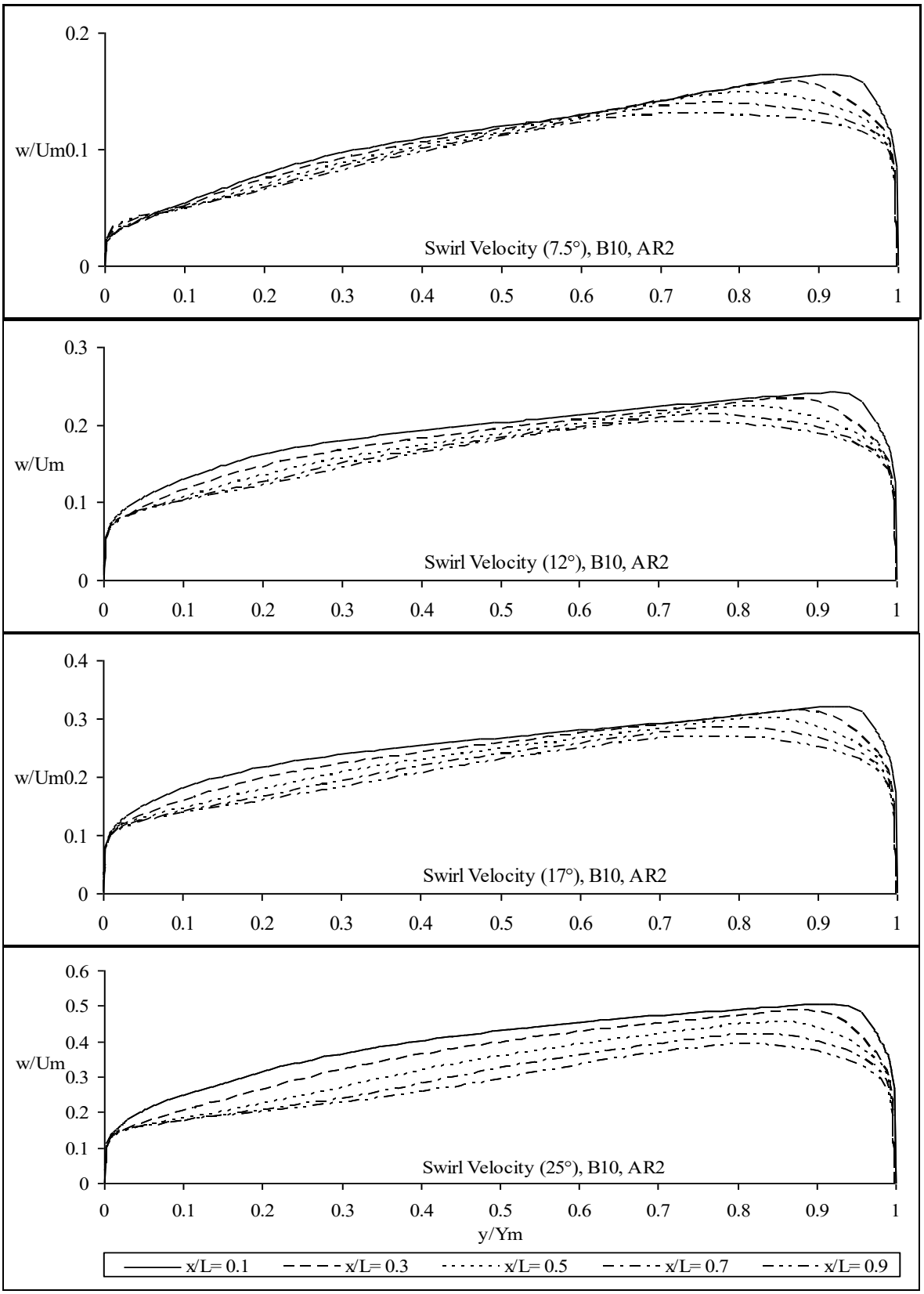

Fig. 6.3(b) Non-dimensional Swirl Velocity versus diffuser passage height for diffuser B, equivalent cone angle 10º, Area ratio 2 for inlet swirl angles (7.5º to 25º) at various transverses at x/L = 0.1 to 0.9.

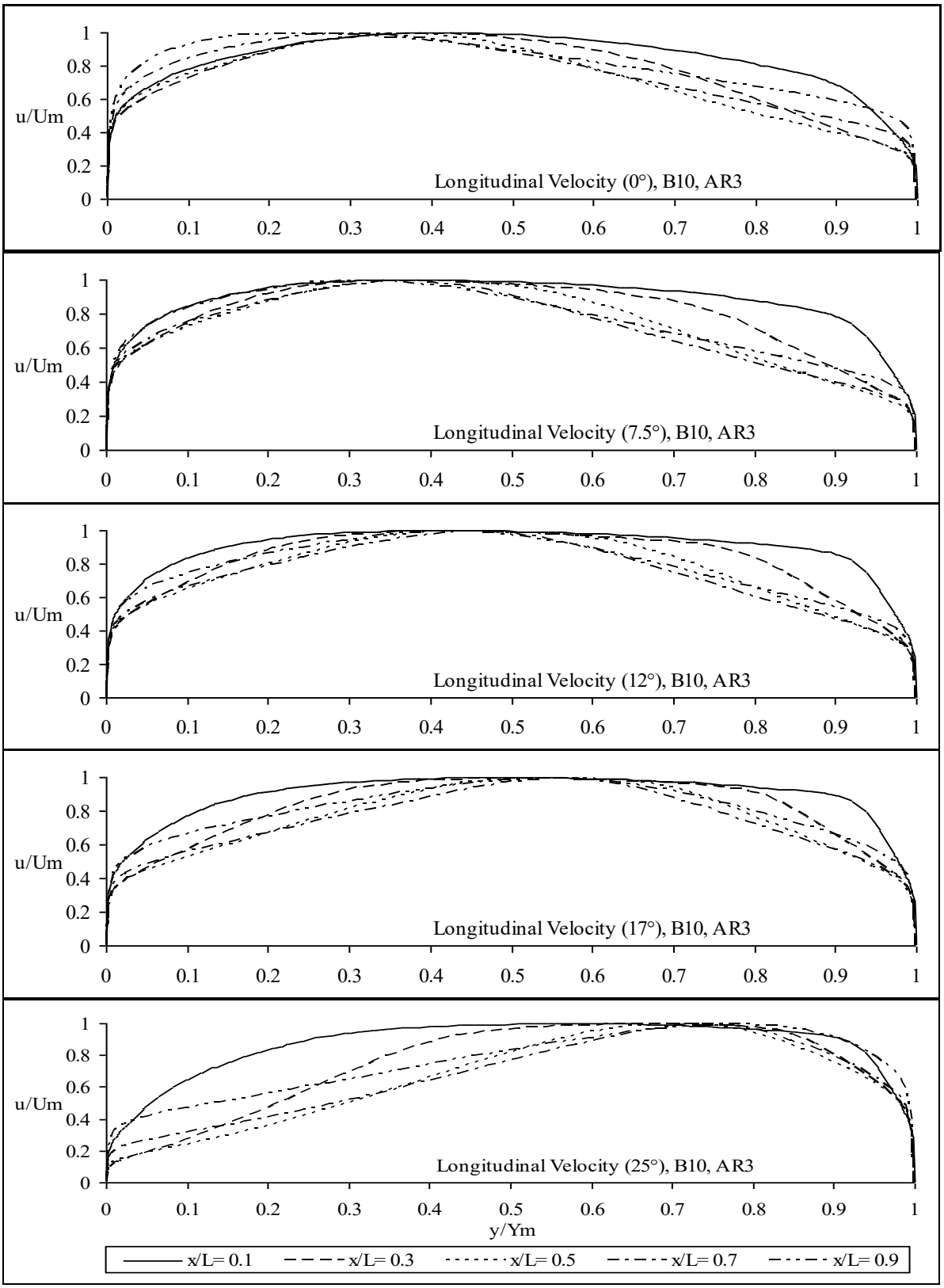

Fig. 6.4(a) Non-dimensional Longitudinal Velocity versus diffuser passage height for diffuser B, equivalent cone angle 10º, Area ratio 3 for inlet swirl angles (0º to 25º) at various transverses at x/L = 0.1 to 0.9.

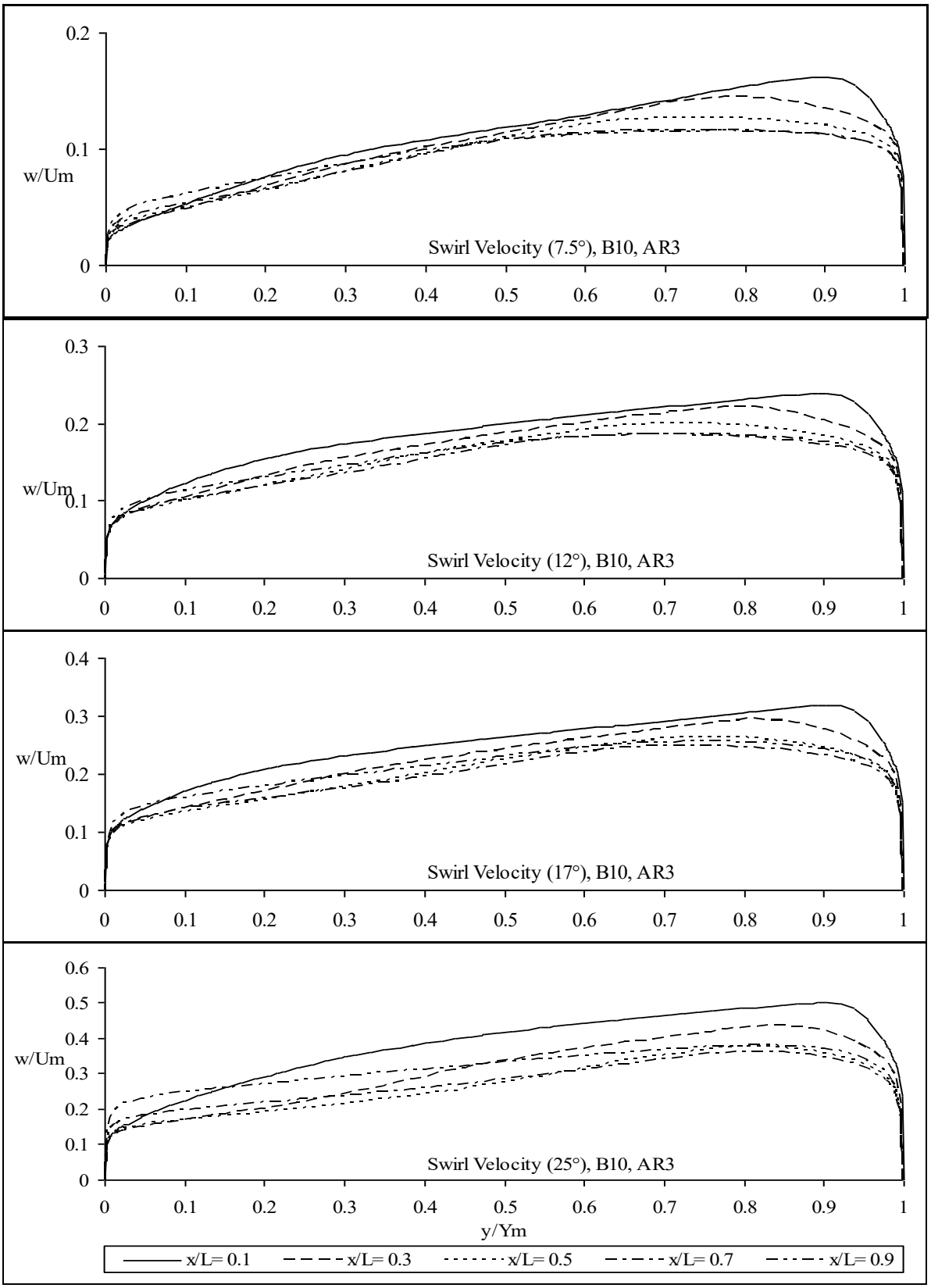

Fig. 6.4(b) Non-dimensional Swirl Velocity versus diffuser passage height for diffuser B, equivalent cone angle 10º, Area ratio 3 for inlet swirl angles (7.5º to 25º) at various transverses at x/L = 0.1 to 0.9.

6.3 Velocity distribution in 20° Equivalent cone angle diffusers

6.3.1 Diffuser A (Parallel hub and diverging casing)

Figures 6.5 and 6.6 show the velocity profiles for Area ratios 2 and 3, respectively, for the 20° equivalent cone angle diffuser A (meaning parallel hub and diverging casing). In Fig. 6.5(a) and 6.6(a), the Longitudinal flow is represented, while 6.5(b) and 6.6(b) depict the swirl velocity profiles.

In Fig. 6.5(a) and 6.6(a), it can be seen that the flow is generated by the hub when there is no swirl effect, and this shift becomes more pronounced towards the hub as the area ratio increases, even with the same inlet velocity profile. Compared to the 10° equivalent cone angle diffuser A, the movement of the peak velocity towards the hub for the no swirl condition is more significant in this case. The peak velocity at x/L = 0.9 for area ratios 2 and 3 is found at y/Ym = 0.45 and 0.41 for the 10° equivalent cone angle, whereas for the 20° equivalent cone angle, it occurs at y/Ym = 0.4 and 0.34. Additionally, the velocity at the casing decreases more rapidly in this scenario than with the 10° equivalent cone angle diffuser. The flow is directed towards the casing when swirl is introduced.

In Fig. 6.5(a) for area ratio 2, it can be seen that the flow reverses at the casing wall for a 7.5° inlet swirl at x/L = 0.9, moving from casing to y/Ym = 0.98, while for an inlet swirl of 12° or more, the reversal happens at the hub wall. The reversal occurs at x/L = 0.7 for a 12° inlet swirl and at x/L = 0.5 and 0.3 for 17° and 25° respectively. For a 12° inlet swirl, the flow reverses up to y/Ym = 0.05 and 0.13 at x/L = 0.7 and 0.9 correspondingly.

For a 17° inlet swirl, the flow reverses to y/Ym = 0.05, 0.15, and 0.23 at x/L = 0.5, 0.7, and 0.9 respectively. For a 25° inlet swirl, the flow reverses to y/Ym = 0.004, 0.09, 0.18, and 0.26 at x/L = 0.3, 0.5, 0.7, and 0.9 correspondingly.

Figure 6.6 (a) for an area ratio of 3 shows that the flow changes direction at the casing wall with no swirl (0°) and at 7.5° of inlet swirl occurring at x/L= 0.7 and 0.5, respectively. In the no swirl scenario, the reversal happens from the casing to y/Ym= 0.98 and 0.94 at x/L=0.7 and 0.9, while for the 7.5° inlet swirl, it transpires from casing to y/Ym= 0.98, 0.91, and 0.87 at x/L=0.5, 0.7, and 0.9, respectively. For swirl angles of 12° and higher, the change happens at the hub wall. The reversal occurs at x/L= 0.5 for a 12° inlet swirl and at x/L= 0.3 for both 17° and 25°. For the 12° inlet swirl, the flow reverses to y/Ym= 0.13, 0.25, and 0.34 for x/L = 0.5, 0.7, and 0.9, respectively. With a 17° inlet swirl, the flow shifts back to y/Ym= 0.07, 0.23, 0.33, and 0.38 for x/L = 0.3, 0.5, 0.7, and 0.9, respectively. In contrast, for the 25° inlet swirl, it reverses to y/Ym= 0.18, 0.32, 0.39, and 0.44 for x/L = 0.3, 0.5, 0.7, and 0.9, respectively.

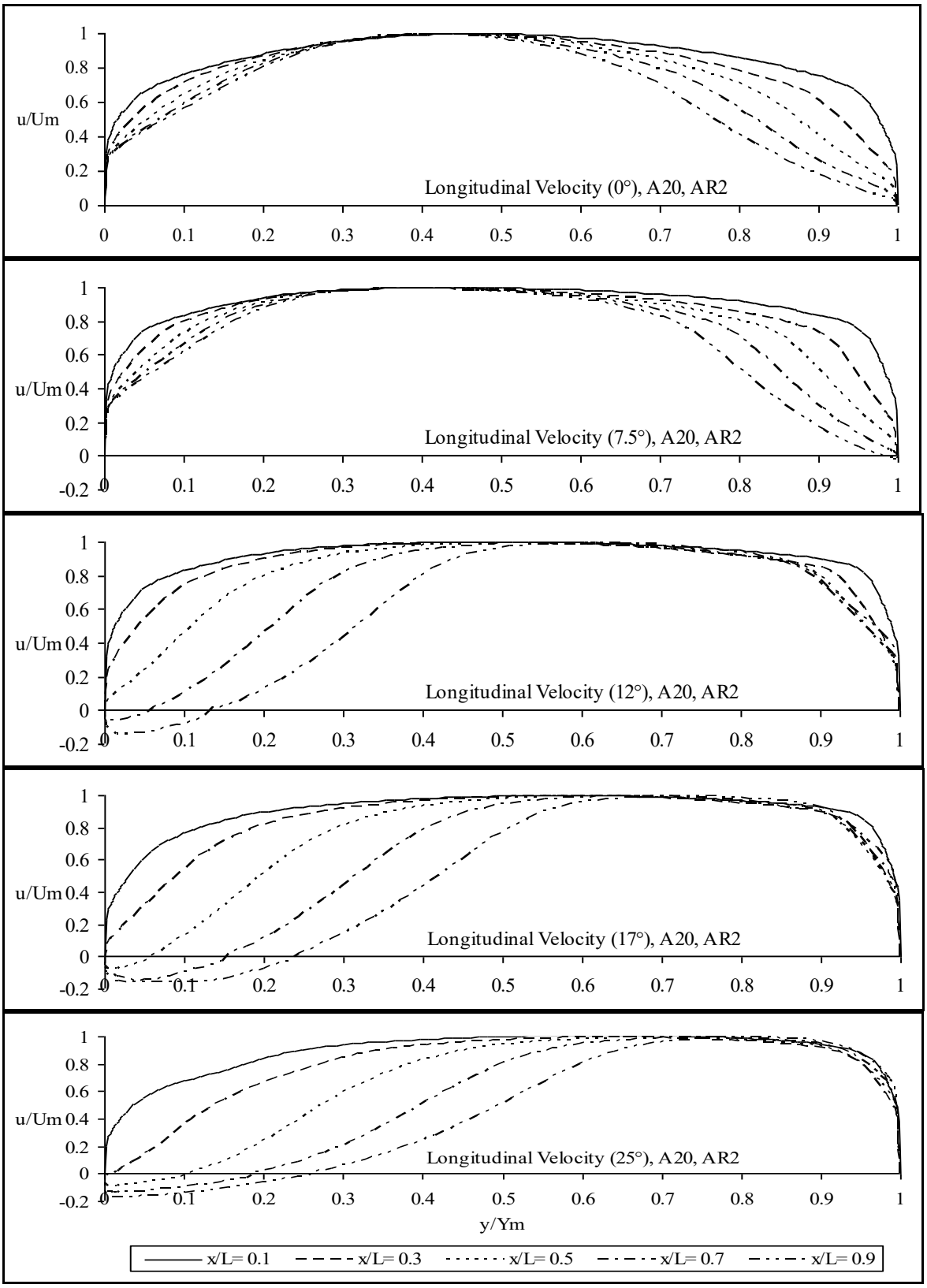

Fig. 6.5 (a) Non-dimensional Longitudinal Velocity versus diffuser passage height for diffuser A, equivalent cone angle 20º, Area ratio 2 for inlet swirl angles (0º to 25º) at various transverses at x/L = 0.1 to 0.9.

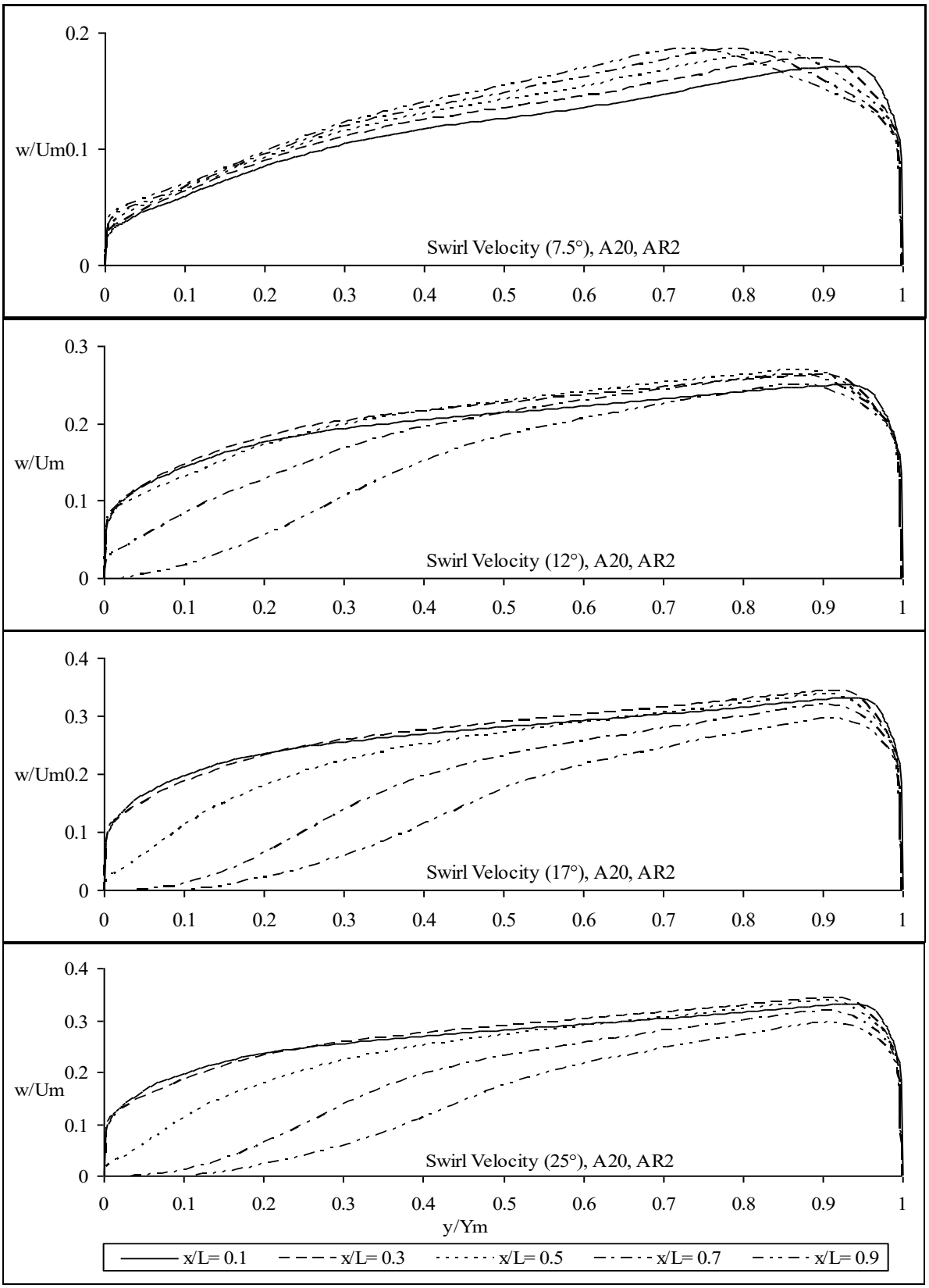

Fig. 6.5 (b) Non-dimensional Swirl Velocity versus diffuser passage height for diffuser A, equivalent cone angle 20º, Area ratio 2 for inlet swirl angles (7.5º to 25º) at various transverses at x/L = 0.1 to 0.9.

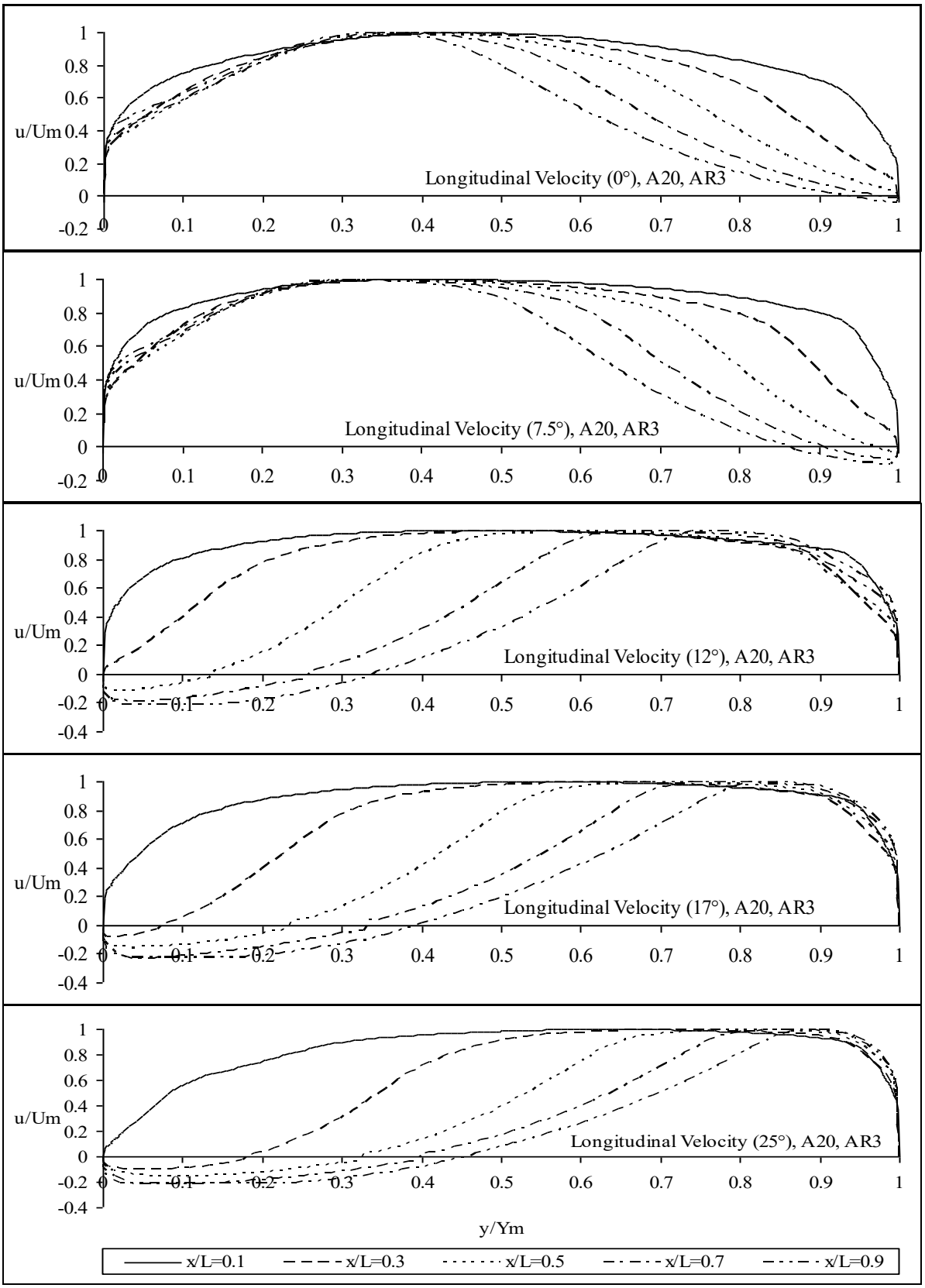

Fig. 6.6 (a) Non-dimensional Longitudinal Velocity versus diffuser passage height for diffuser A, equivalent cone angle 20º, Area ratio 3 for inlet swirl angles (0º to 25º) at various transverses at x/L = 0.1 to 0.9.

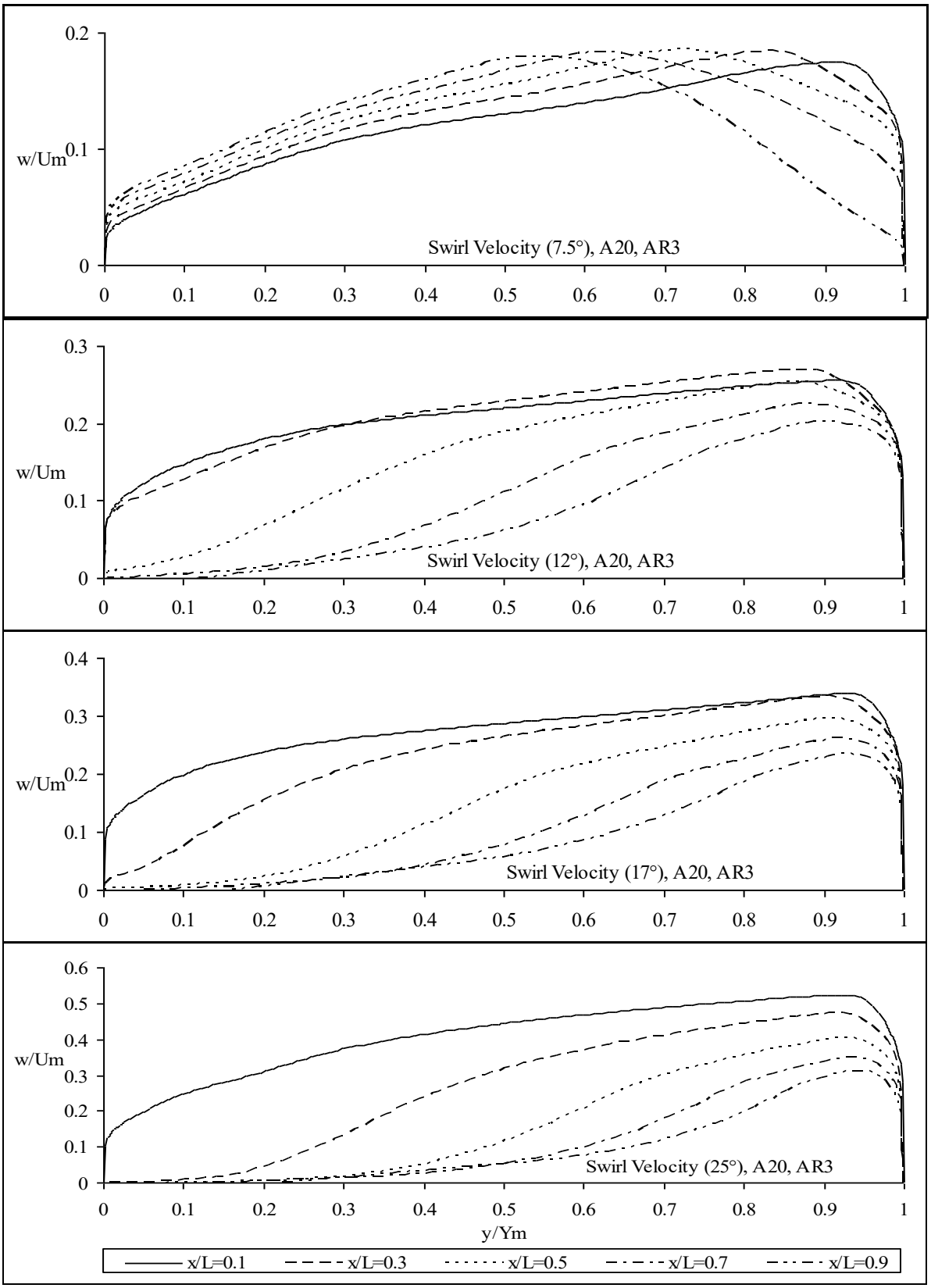

Fig. 6.6 (b) Non-dimensional Swirl Velocity versus diffuser passage height for diffuser A, equivalent cone angle 20º, Area ratio 3 for inlet swirl angles (7.5º to 25º) at various transverses at x/L = 0.1 to 0.9.

6.3.2 Diffuser B (Both hub and casing diverging with equal angles)

Figures 6.7 and 6.8 depict the speed profiles for area ratios of 2 and 3, respectively, in a diffuser B with a cone angle of 20° (where both the hub and casing diverge at the same angle). In this diffuser type, neither the hub nor the casing wall shows signs of flow separation or reversal, even when a 25° inlet swirl is introduced.

As the area ratio grows from 2 to 3, the flow becomes increasingly generated by the hub, which is observable in figures 6.7(a) and 6.8(a). When inlet swirl is added, the flow does start to move toward the casing, but this movement is minimal compared to a 10° equivalent cone angle diffuser A at the same area ratio. Figure 6.7(a) demonstrates that the longitudinal velocity shifts toward the casing is weak compared to 10° cone angle diffusers, and it is only with the 25° inlet swirl that a more significant shift occurs. Comparing figures 6.7(a) to 6.8(a), it is evident that the movement toward the casing diminishes even at 25° inlet swirls as the area ratio increases. There is no reversal of flow noted, even with the addition of the 25° inlet swirl, which is the maximum observed in this study.

Figures 6.7(b) and 6.8(b), which illustrate swirl velocity profiles, show that the swirl velocity is generated by the casing and consistently reduces as one moves along the length of the diffuser passage. The highest point of the swirl shifts toward the hub as the passage length increases, indicating a decline in swirl intensity. Although the swirl velocity falls with greater inlet swirl at a fixed area ratio, the reduction becomes less significant as the area ratio increases for the same inlet swirl.

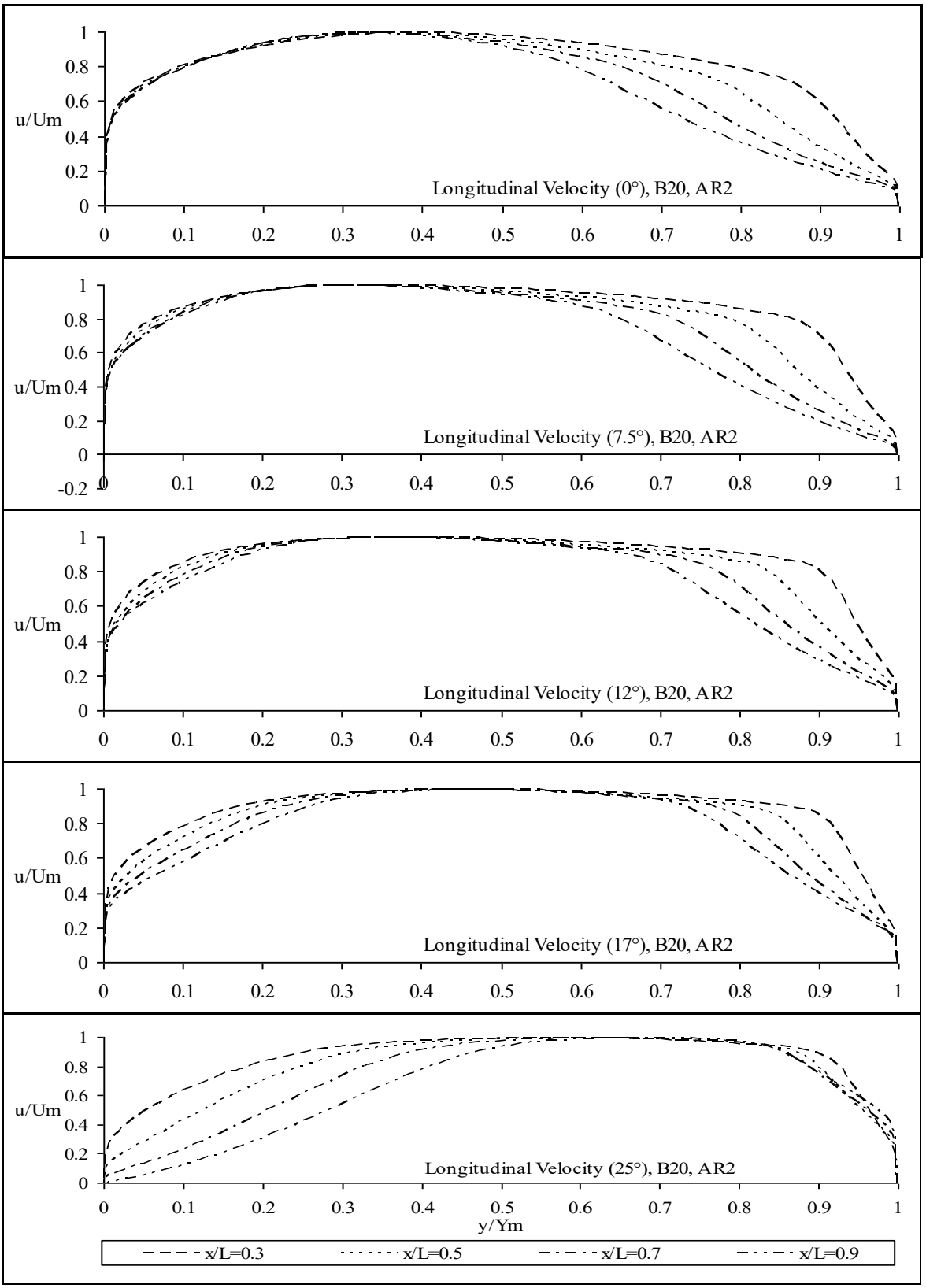

Fig. 6.7(a) Non-dimensional Longitudinal Velocity versus diffuser passage height for diffuser B, equivalent cone angle 20º, Area ratio 2 for inlet swirl angles (0º to 25º) at various transverses at x/L = 0.1 to 0.9.

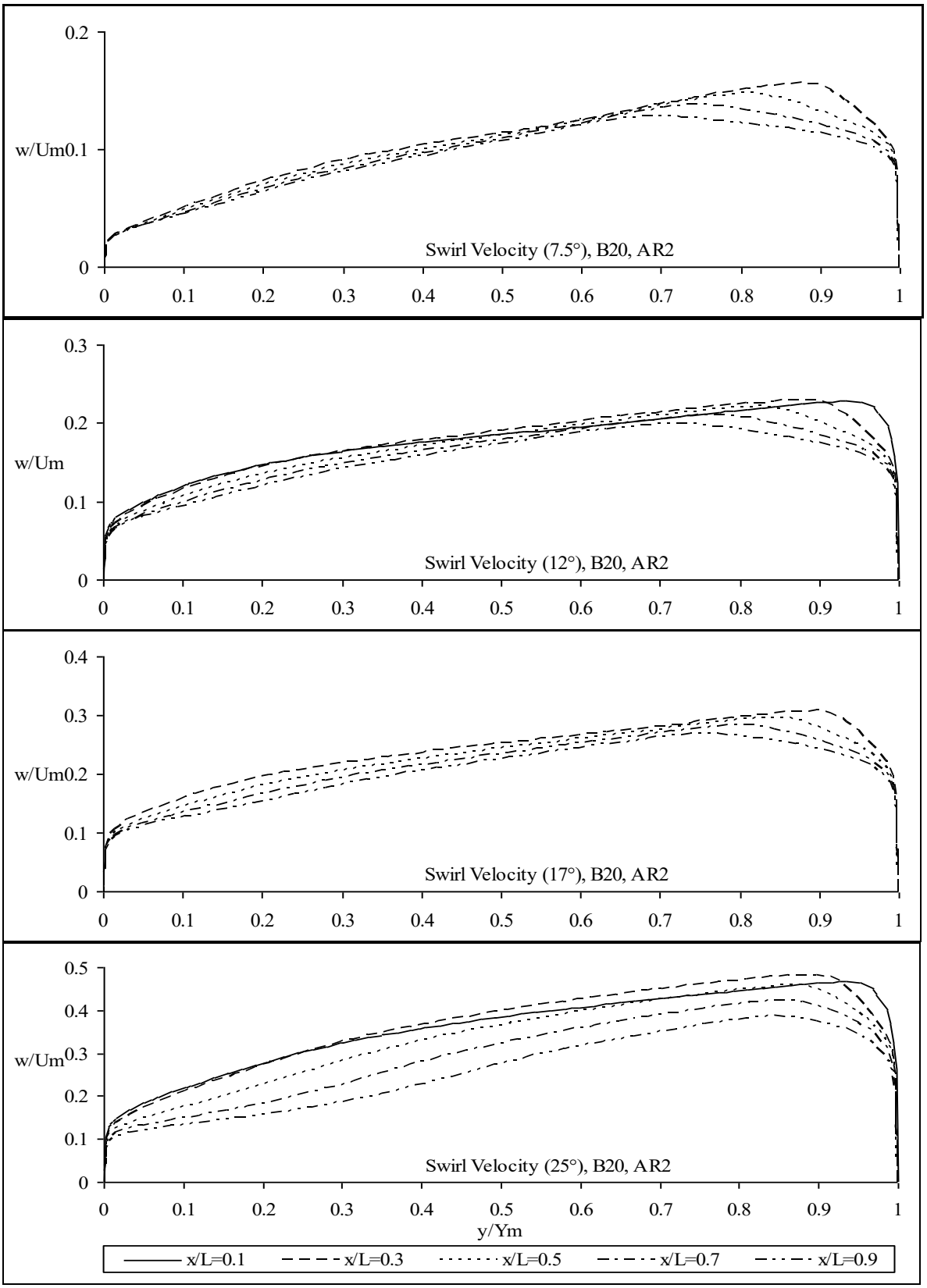

Fig. 6.7(b) Non-dimensional Swirl Velocity versus diffuser passage height for diffuser B, equivalent cone angle 20º, Area ratio 2 for inlet swirl angles (7.5º to 25º) at various transverses at x/L = 0.1 to 0.9.

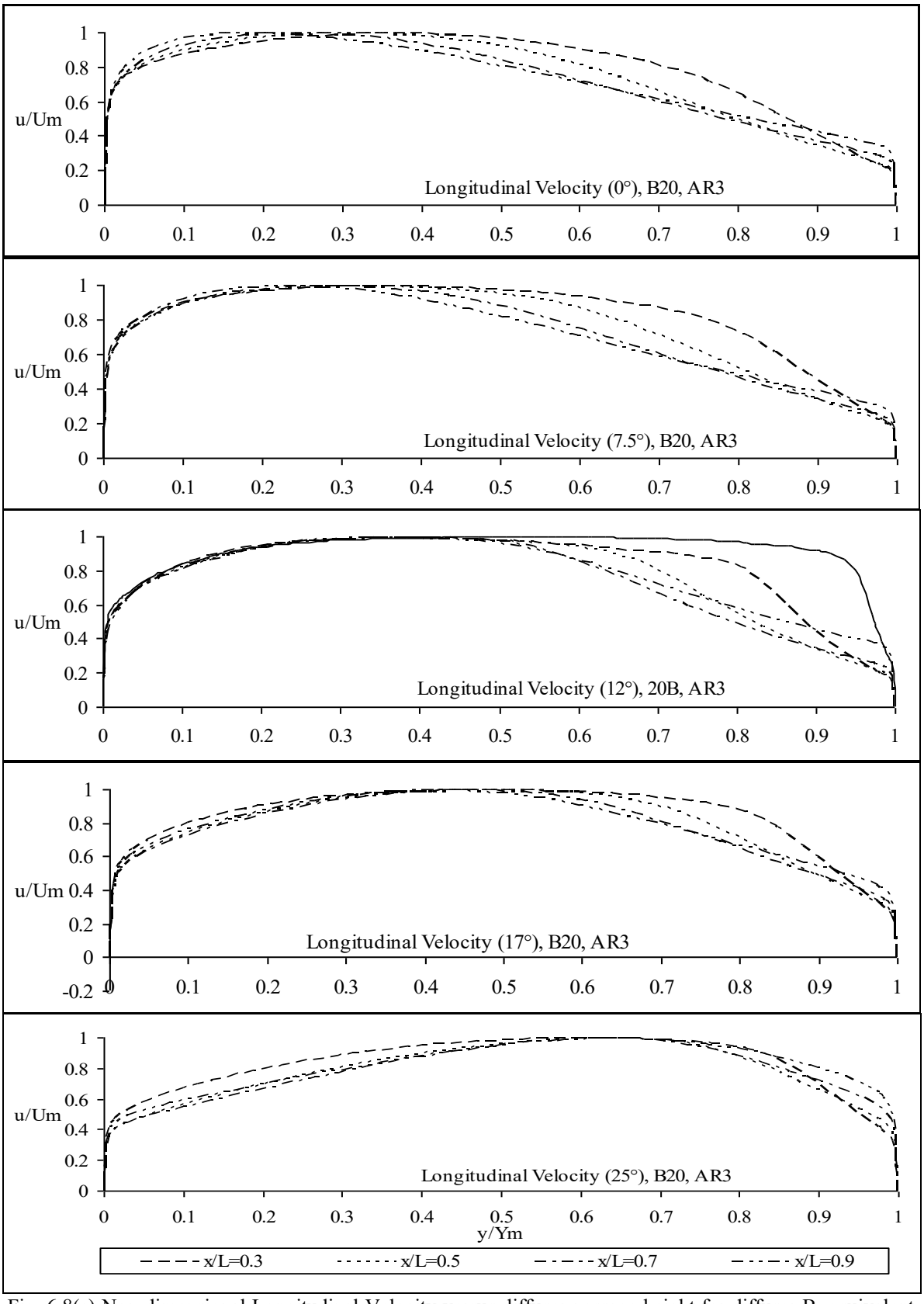

Fig. 6.8(a) Non-dimensional Longitudinal Velocity versus diffuser passage height for diffuser B, equivalent cone angle 20º, Area ratio 3 for inlet swirl angles (0º to 25º) at various transverses at x/L = 0.1 to 0.9.

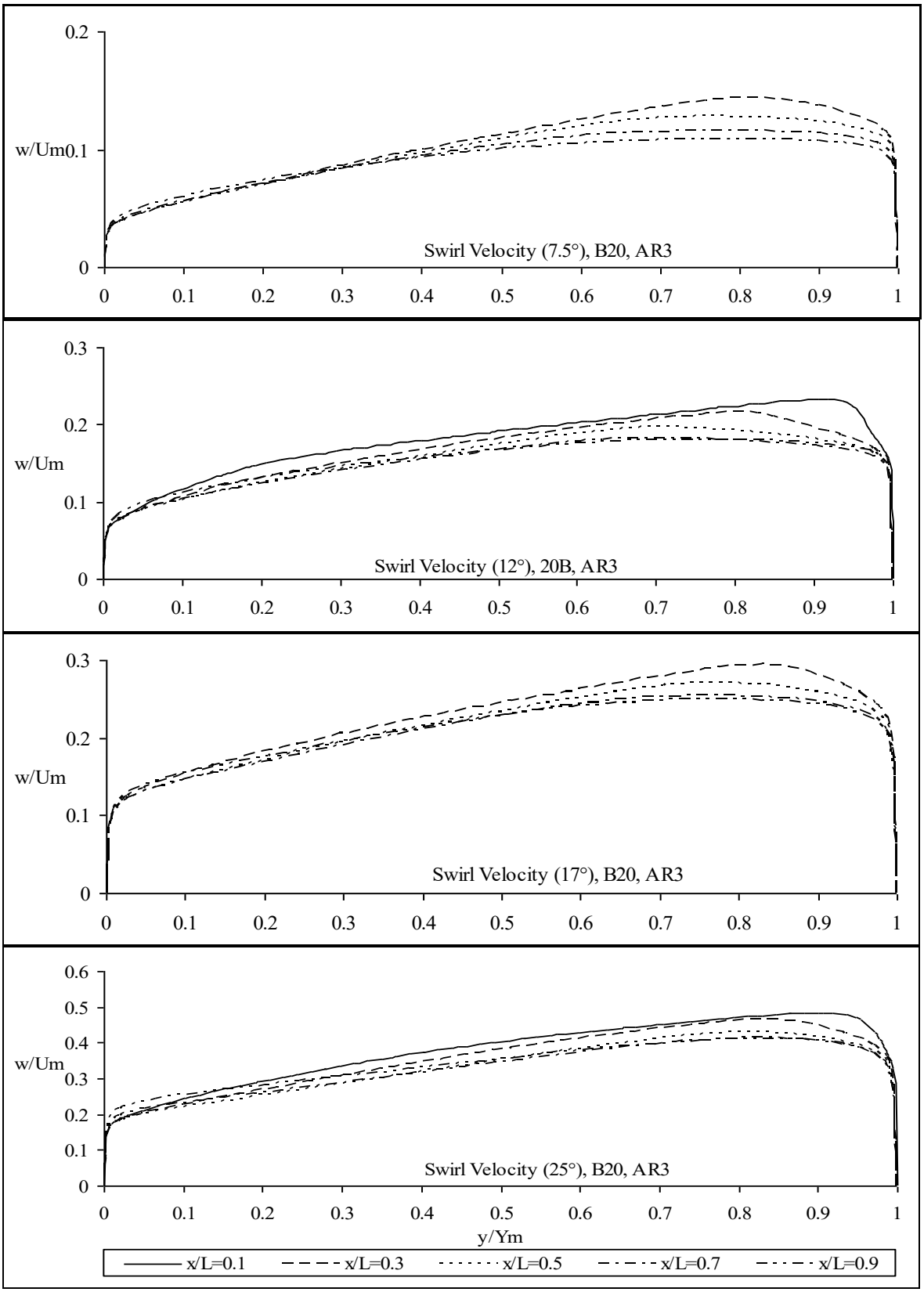

Fig. 6.8(b) Non-dimensional Swirl Velocity versus diffuser passage height for diffuser B, equivalent cone angle 20º, Area ratio 3 for inlet swirl angles (7.5º to 25º) at various transverses at x/L = 0.1 to 0.9.

6.4 Performance parameters

The Performance or effectiveness of a diffuser is evaluated based on certain performance indicators like Pressure recovery coefficient, Diffuser effectiveness, and Pressure loss coefficient, which were discussed previously. The Pressure recovery coefficient indicates the percentage of kinetic energy that has been successfully transformed into pressure energy through the diffusion process. Diffuser effectiveness shows the part of the ideal pressure recovery coefficient that has been achieved, while the pressure loss coefficient represents the gap between the ideal and actual pressure recovery coefficients.

6.5 Pressure Recovery Coefficient in 10º Equivalent cone angle

6.5.1 C_p in 10º Equivalent cone angle Area ratio 2

Figure 6.9 shows the pressure recovery coefficient related to the non-dimensional length of the diffuser passage for a 10-degree equivalent cone angle and an area ratio of 2, at different levels of inlet swirl for four kinds of axial annular diffusers. In diffuser A, which features a parallel hub and a diverging casing, the pressure recovery coefficient (C_p) rises with a longer diffuser passage length under non-swirling flow conditions. Initially, C_p increases with added swirl when compared to non-swirl flow at the start of the diffuser passage. However, for 7.5°, 12°, 17°, and 25° of inlet swirl, C_p falls below that of the non-swirling flow past x/L = 0.82, 0.95, 0.78, and 0.47, respectively. The highest C_p value is observed up to a diffuser passage length of 0.36 for a 25° inlet swirl. From x/L = 0.36 to 0.56, it hits its maximum for 17° inlet swirl, then from 0.56 to 0.95, it peaks for 12° inlet swirl, followed lastly by the flow without swirl.

In the case of diffuser B, which both diverges in hub and casing at equal angles, it shows that C_p is higher with greater swirl across all conditions looked at in this study. Yet for a 25° inlet swirl, C_p remains below that of the non-swirl flow after x/L = 0.73. This suggests that swirl diminishes as the length of the diffuser passage increases. For the inlet swirls of 7.5°, 12°, 17°, and 25°, C_p also drops below the non-swirling flow past x/L = 0.82, 0.95, 0.78, and 0.47, respectively. The greatest C_p is reached up to a diffuser passage length of 0.32 for a 25° inlet swirl. Beyond x/L = 0.32, it peaks for 17° inlet swirl.

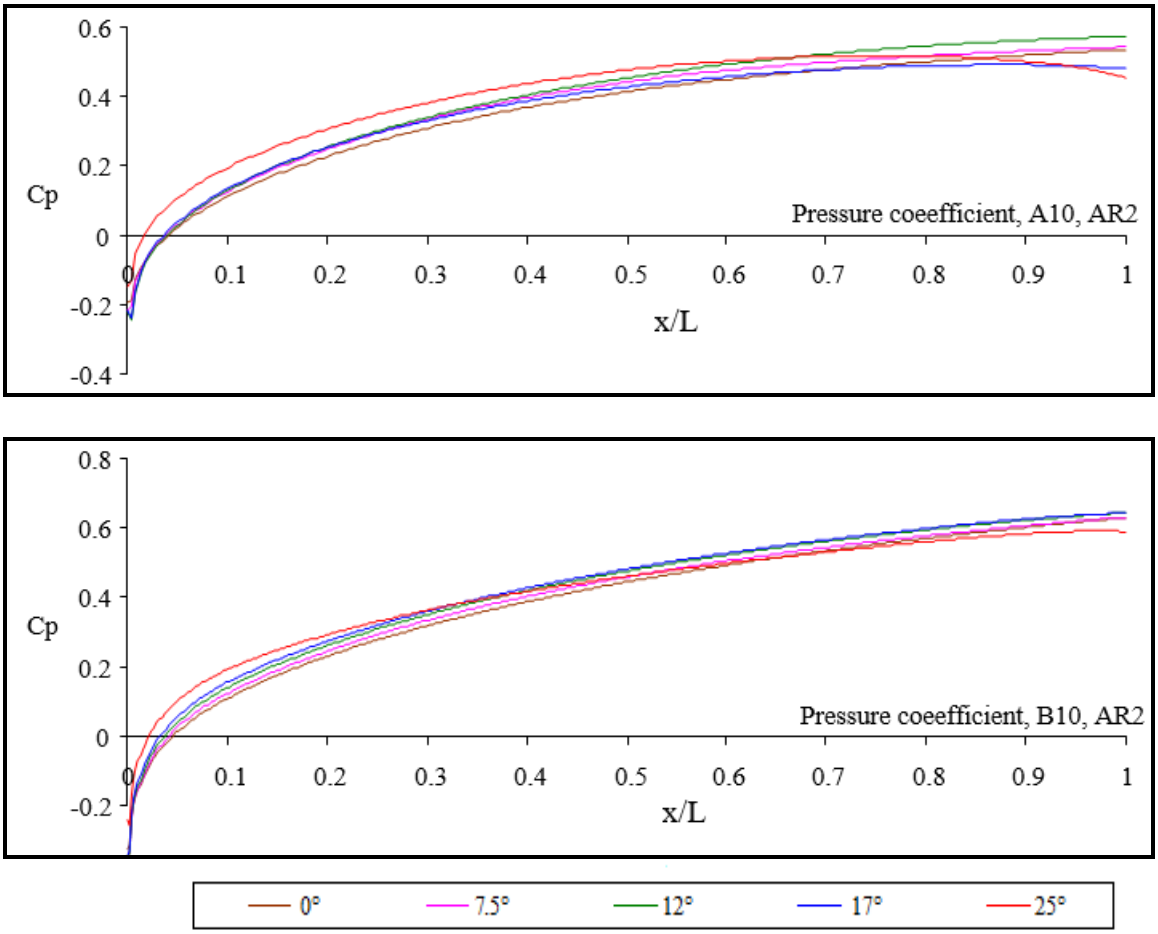

Fig. 6.9 Pressure coefficient versus non-dimensional diffuser passage length for equivalent cone angle 10º, Area ratio 2 at various inlet swirls for different types of diffusers.

6.5.2 C_p in 10º Equivalent cone angle Area ratio 3

Figure 6.10 shows how the pressure recovery coefficient varies with the non-dimensional length of the diffuser passage for a 10º equivalent cone angle and an area ratio of 3 under different levels of inlet swirl for all four designs of axial annular diffusers.

For diffuser A, the C_p improves when compared to the scenario with no swirl as the swirl increases initially along the length of the diffuser passage, and the increase is greater compared to the diffuser with an area ratio of 2. Yet, for inlet swirls of 7.5°, 12°, 17°, and 25°, the C_p is less than for the no swirl case after the points x/L = 0.67, 0.97, 0.60, and 0.25, respectively. The C_p reaches its peak at a diffuser passage length of 0.18 for the 25º inlet swirl. Between x/L=0.18 and 0.28, it is highest for the 17º inlet swirl, while from 0.28 to 0.97, it is maximum for the 12º inlet swirl, and finally, for the flow without swirl. This behavior occurs because the swirl diminishes as the flow progresses downstream in the diffuser.

In diffuser B, from x/L= 0.16, the C_p is greatest with a 25º inlet swirl, but after this point until the end, it is highest for the 17º inlet swirl. In this scenario, the C_p is lower than the no swirl case only for the 25º inlet swirl, noted at x/L= 0.34.

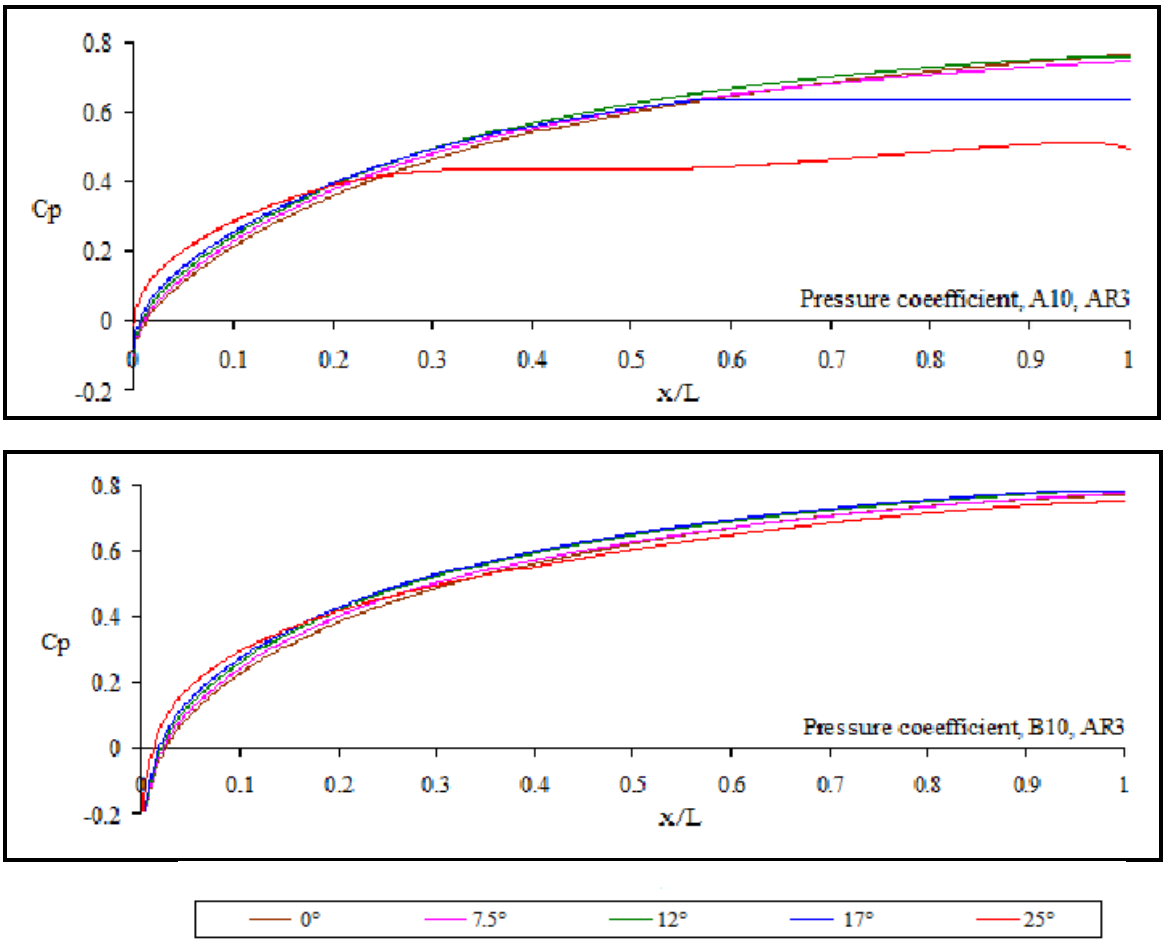

Fig. 6.10 Pressure coefficient versus non-dimensional diffuser passage length for equivalent cone angle 10º, Area ratio 3 at various inlet swirls for different types of diffusers.

6.6 Pressure Recovery Coefficient in 20º Equivalent cone angle

6.6.1 C_p in 20º Equivalent cone angle Area ratio 2

Figure 6.11 demonstrates the recovery coefficient of pressure as it relates to the non-dimensional length of the diffuser passage for a 20º equivalent cone angle and an area ratio of 2, considering different levels of inlet swirl across four types of axial annular diffusers.

In diffuser A, for inlet swirl angles of 17º and 25º, the coefficient C_p is less than that of the flow without swirl beyond x/L = 0.72 and 0.85, respectively. For a 25º inlet swirl, C_p reaches its peak up to a diffuser passage length of 0.65. From x/L=0.65 to the end, the maximum C_p occurs for a 12º inlet swirl.

In diffuser B, until x/L= 0.35, the highest C_p is recorded for a 25º inlet swirl, after which, from this point onward, the highest value is for the 17º inlet swirl. In this scenario, C_p consistently rises in accordance with increasing inle swirl throughout the length of the diffuser passage, except for the range from x/L= 0.35 to the end, where C_p for a 17º inlet swirl exceeds that of a 25º inlet swirl.

6.6.2 C_p in 20º Equivalent cone angle Area ratio 3

Figure 6.12 shows the coefficient of pressure recovery related to the non-dimensional length of the diffuser passage with a 20º equivalent cone angle and an area ratio of 3, under different inlet swirl conditions for all four types of axial annular diffusers.

In diffuser A, for inlet swirl angles of 7.5°, 12°, 17°, and 25°, the C_p value is below that of the flow without swirl beyond x/L = 0.61, 0.50, 0.16, and 0.11 respectively. The C_p reaches its peak at a diffuser passage length of 0.08 for the 25º inlet swirl. Between x/L=0.08 and 0.13, the maximum C_p occurs for a 12º inlet swirl, from x/L=0.13 to 0.61 it is highest for a 7.5º inlet swirl, and from 0.61 to the end, it reverts to the flow without swirl.

In diffuser B, for a 7.5° inlet swirl, the C_p becomes lower than the flow without swirl after x/L = 0.81. The peak C_p is achieved at a diffuser passage length of 0.58 for the 25º inlet swirl. From x/L=0.58 to the end, the C_p remains maximum for the 12º inlet swirl.

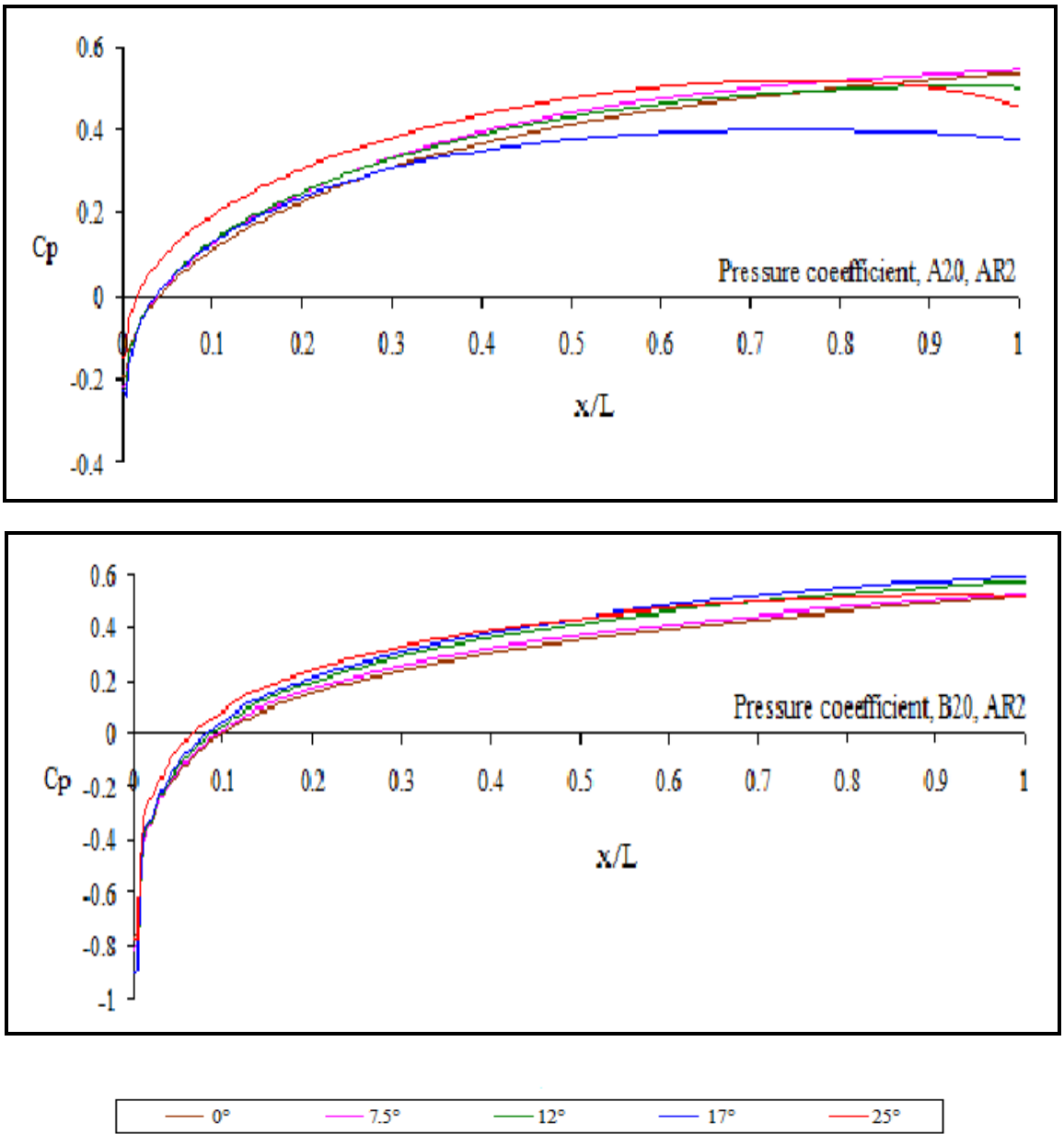

Fig. 6.11 Pressure coefficient versus non-dimensional diffuser passage length for equivalent cone angle 20º, Area ratio 2 at various inlet swirls for different types of diffusers.

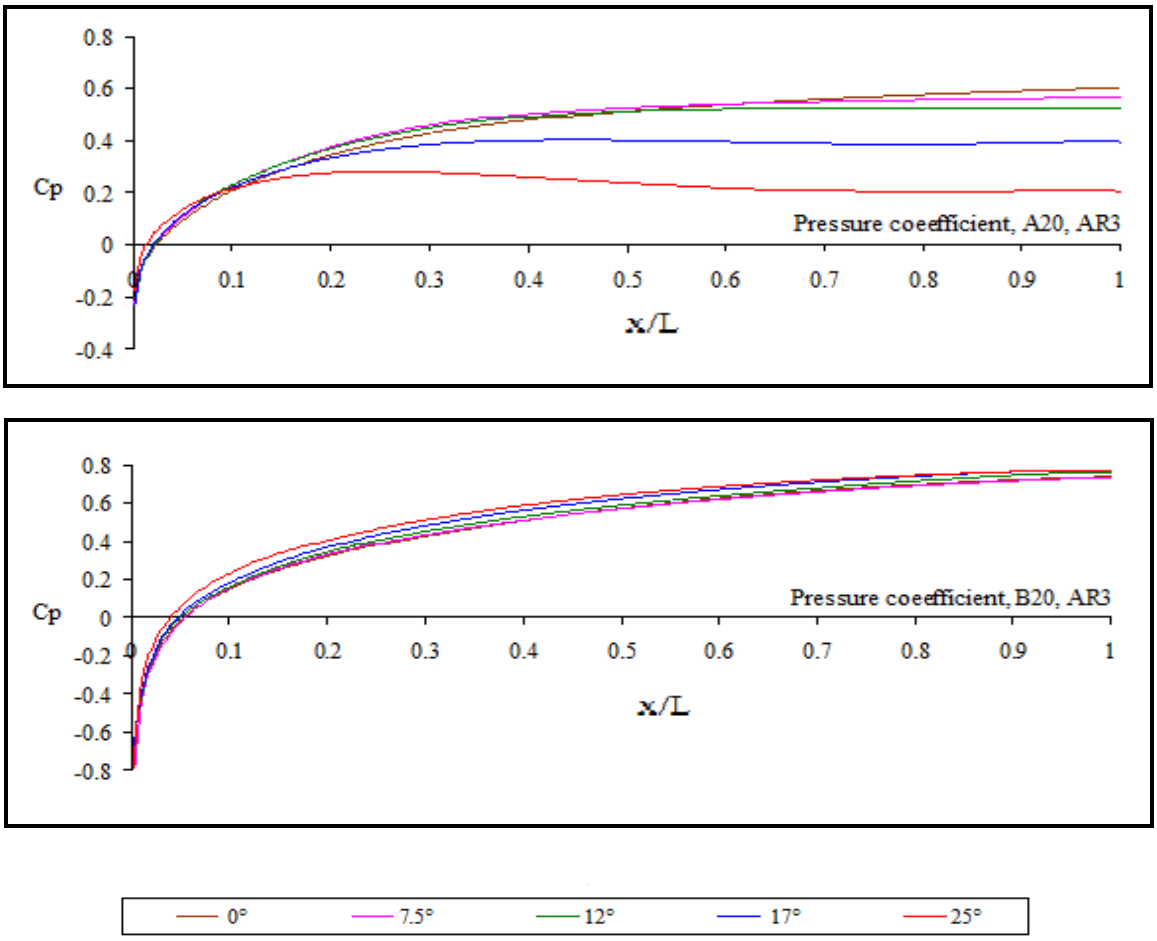

Fig. 6.12 Pressure coefficient versus non-dimensional diffuser passage length for equivalent cone angle 20º, Area ratio 3 at various inlet swirls for different types of diffusers.

6.7 Effect of swirl on Performance parameters

6.7.1 Pressure Recovery Coefficient

Figure 6.13 and Figure 6.14 show how swirl affects performance metrics in a diffuser with a 10° equivalent cone angle. The pressure recovery coefficient rises with the addition of inlet swirl until it reaches a specific point, after which it starts to drop. For a given inlet swirl, the pressure recovery coefficient grows as the area ratio increases, but

the additional increase becomes less significant as the area ratio gets larger. For diffuser B, pressure recovery continues to improve with more swirl, even reaching 25º inlet swirl, suggesting that it operates effectively.

Figures 6.15 and 6.16 show that the pressure recovery in a diffuser with a 20° equivalent cone angle follows a similar pattern, where the best swirl occurs at an inlet swirl of 12° for diffuser A. In contrast, diffuser B achieves this optimal condition at a 17° inlet swirl. Additionally, it shows that introducing swirl significantly enhances the pressure recovery compared to the earlier scenario.

6.7.2 Diffuser effectiveness

The efficiency of a diffuser is influenced by how close it is to the optimal pressure recovery coefficient. For a diffuser with a cone angle of 10°, the efficiency rises as the area ratio grows, reaching an ideal point for the highest efficiency. This rise in efficiency with a larger area ratio is clearly seen in diffuser B. In the case of diffuser A, however, after a certain level of inlet swirl, the efficiency drops as the area ratio increases. Diffusers with a cone angle of 20° show similar patterns, and the slight increase in efficiency grows with a larger equivalent cone angle. The rise in efficiency based on the area ratio is observed first in A, followed by B when there is low inlet swirl.

6.7.3 Pressure Loss Coefficient

The coefficient for pressure loss is the opposite of the effectiveness of the diffuser. When the effectiveness of the diffuser rises, the coefficient for pressure loss falls, and the

reverse is also true. A low value for the pressure loss coefficient shows the best performance of the diffuser. For every diffuser, the best value is found between 10° and 20° of inlet swirl, which has been mentioned before.

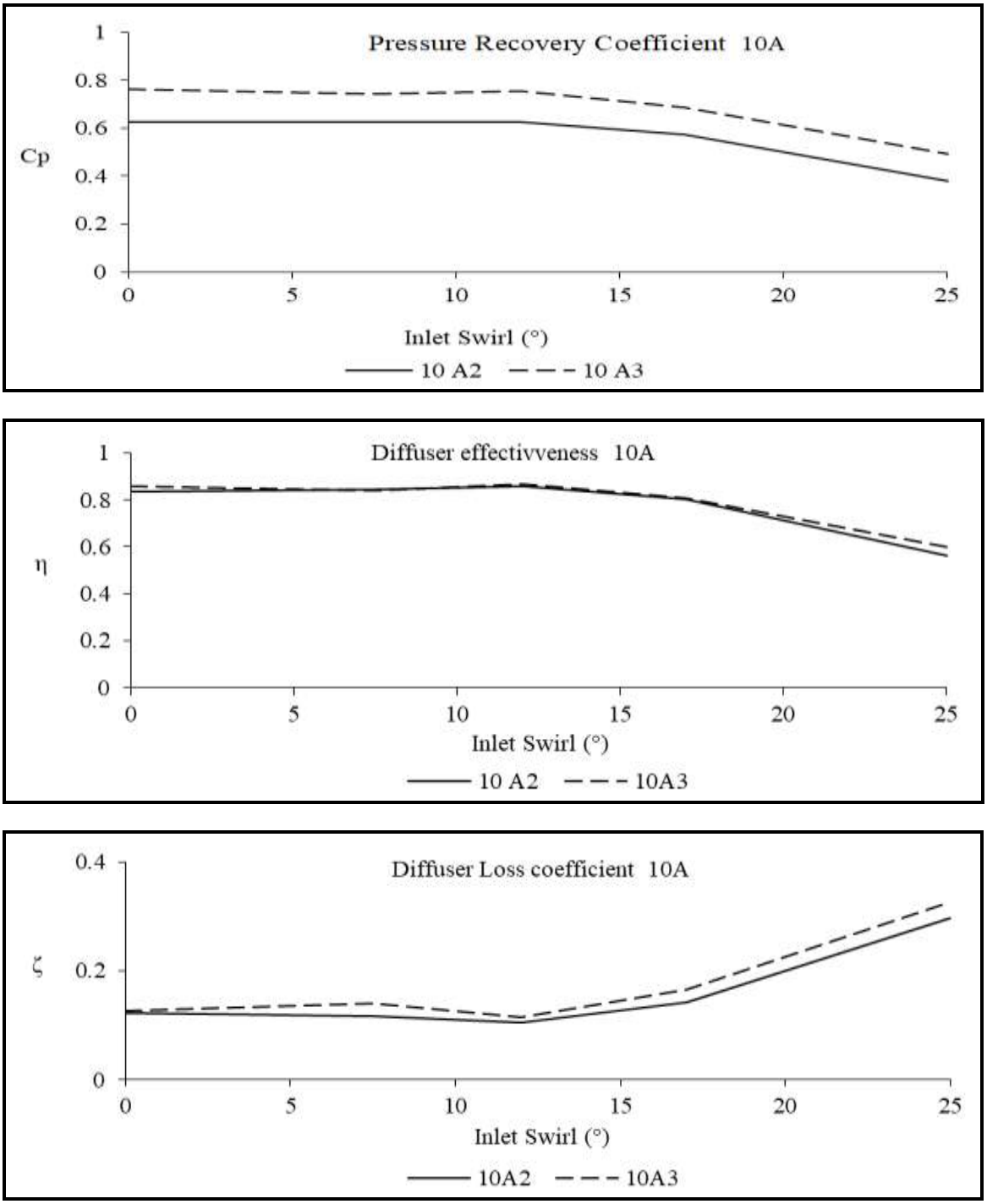

Fig. 6.13 Performance parameters of 10° equivalent cone angle Diffuser A

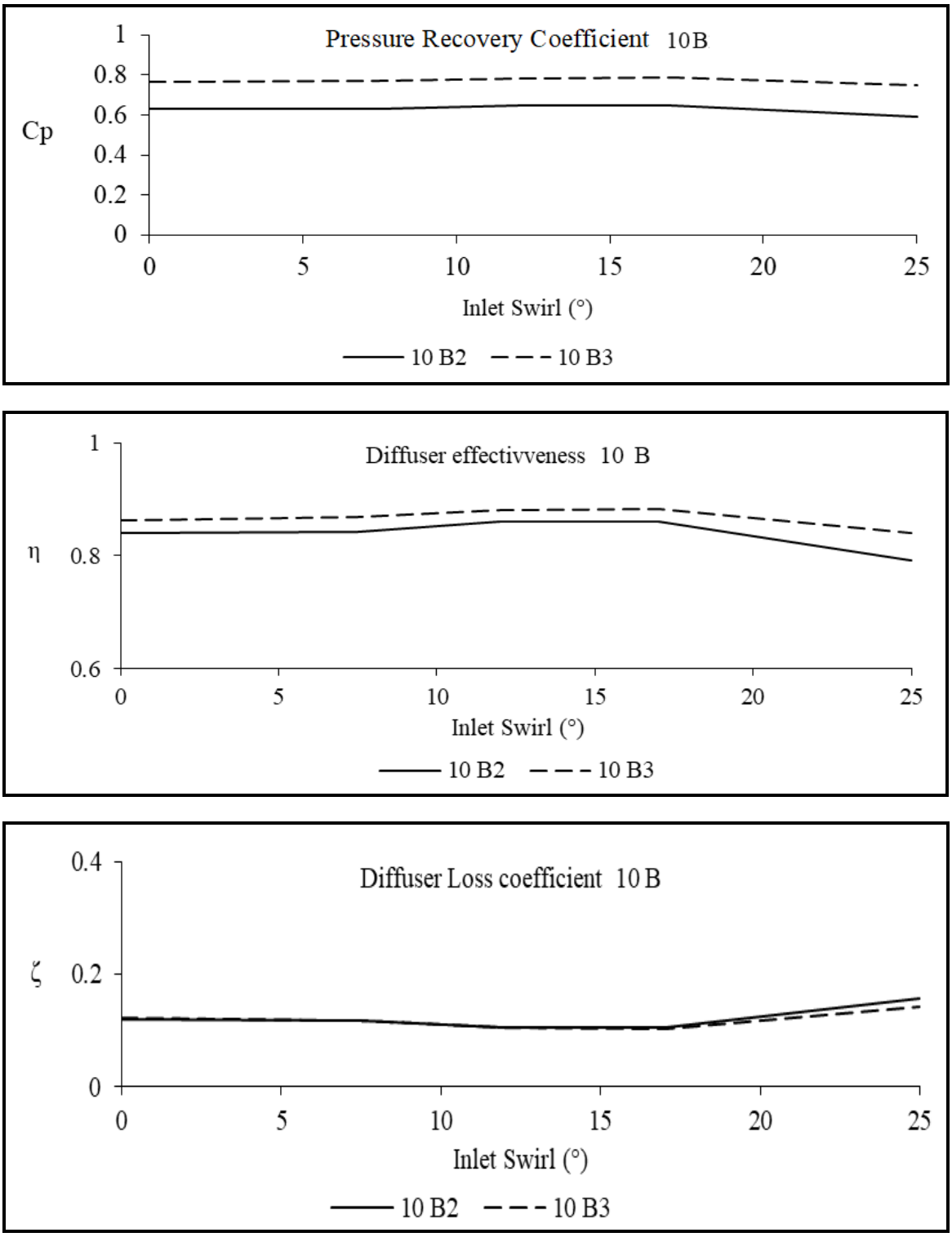

Fig. 6.14 Performance parameters of 10º equivalent cone angle Diffuser B

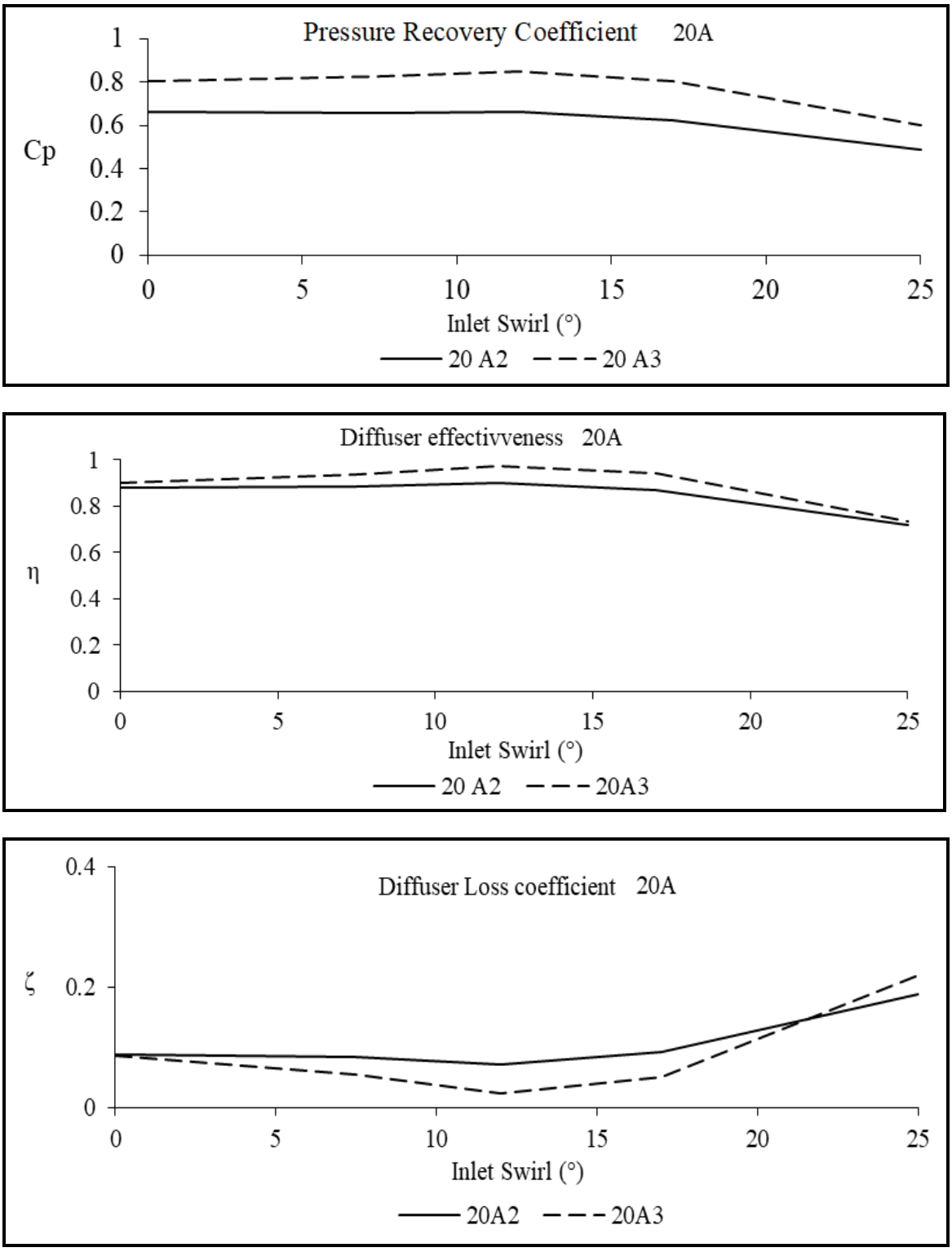

Fig. 6.15 Performance parameters of 20º equivalent cone angle Diffuser A

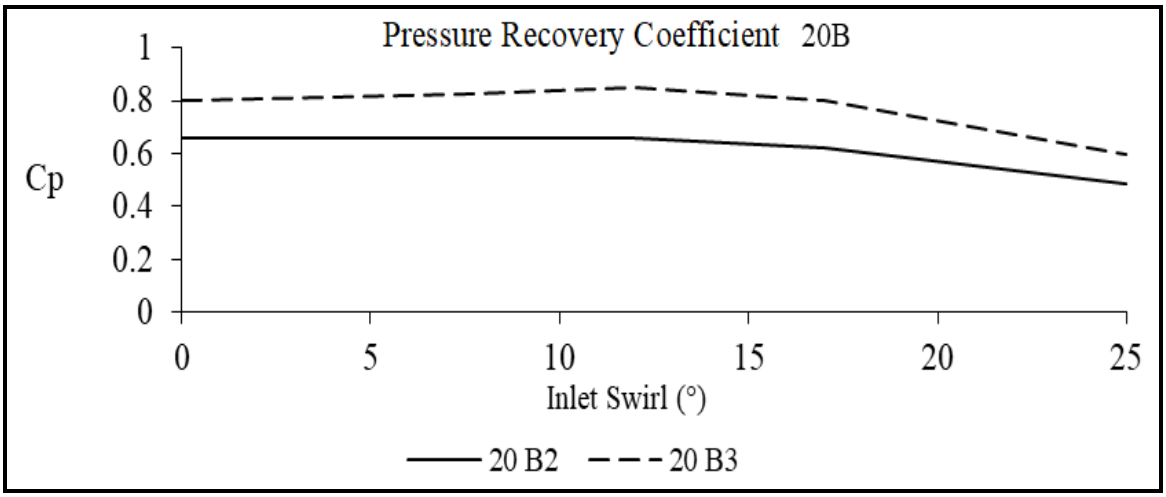

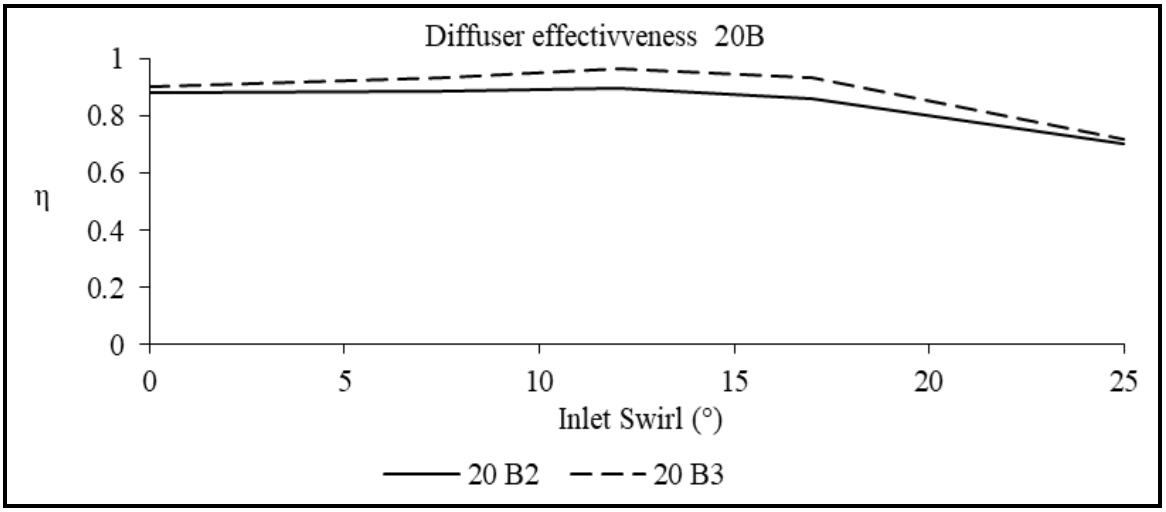

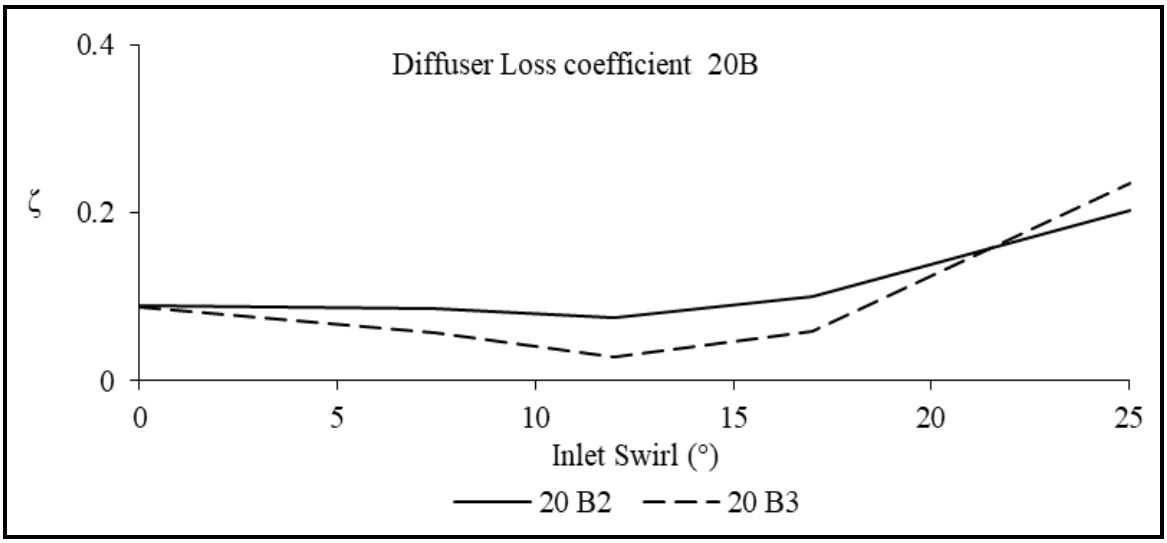

Fig. 6.16 Performance parameters of 20º equivalent cone angle Diffuser B

CHAPTER 7

CONCLUSION AND RECOMMENDATION FOR FUTURE WORK

The movement of fluid through different designs of annular diffusers has been explored, both with and without swirl at the entrance, in this study. The research was conducted using both experimental and analytical methods. The main findings from the current analysis, along with suggestions for further research, are provided below:

7.1 Conclusions

1. As the flow moves downstream, the speed in the direction of flow continuously drops, regardless of whether the entrance flow is swirling or not. As the speed decreases, the pressure recovery increases while the flow continues. However, the growth rate of pressure recovery diminishes as the distance from the inlet becomes greater.

2. The shapes of velocity profiles vary at different points within the flow path due to the formation of the boundary layer.

3. The peak velocity at any cross-section of the diffuser is not found in the center; rather, it is located towards the hub for non-swirling flow, which moves towards the casing as swirl is introduced.

4. When swirl is added, the flow is directed toward the casing wall, which results in a stronger flow near the casing than near the hub wall.

5. With swirl being introduced, recovery occurs more rapidly near the casing wall. The influence of swirl seems to gradually lessen as the flow goes downstream, and the recovery becomes insignificant or absent by the time the flow reaches the diffuser exit.

6. The overall pressure recovery for a stalled diffuser is lower compared to well-functioning diffusers. In this study, diffuser B (with both hub and casing diverging at equal angles) generally performs better than diffuser A (with a parallel hub and diverging casing).

7. Stalling is typically not detected on the hub wall in most cases with non-swirling flow, but it does occur on the casing wall and is worsened with an increasing area ratio. However, in diffuser A, stalling happens on the hub wall even with an inlet swirl of 17°, which increases as the swirl intensifies.

8. With the presence of inlet swirl, stalling tends to move away from the casing wall and can completely disappear with a high level of inlet swirl.

9. The effectiveness of the diffuser and the diffuser loss coefficient rise with a greater area ratio for a specific equivalent cone angle and level of inlet swirl.

10. The pressure recovery coefficient, diffuser effectiveness, and pressure loss coefficient reach their best values at a certain inlet swirl.

11. CFD analysis aligns well with the experimental results. The modeling applied in this study can predict flow behavior ahead of time, and pressure recovery along with diffuser effectiveness can be calculated for a specific type of diffuser.

7.2 Recommendation for future work

The current study has been conducted both with and without varying degrees of inlet swirl; future research might focus on the following areas.

1. The current research could be broadened to explore the influence of swirl generated at the hub, with or without inlet swirl.

2. The correlation between non-dimensional length and inlet swirl could be examined.

3. The impact of the tailpipe on diffuser performance can be analyzed.

4. The effects of different levels of inlet turbulence can be researched.

5. The influence of friction and roughness combined with inlet swirl could be analyzed to find the ideal swirl level.

6. The relationship between Mach number and swirl can be investigated.

7. The study can also be conducted using other fluids, such as water, among others.

REFRENCES

Adenubi S. O., (1975), “Performance and Flow Regime of Annuar Diffusers with Axial-Turbomachine-Discharge Inlet Conditions,” Paper 75-WA/FE 5, ASME, New York.

Adenubi S. O., (1976), “Performance and flow regime of annular diffusers with axial Turbo machine discharge inlet conditions,” Journal of fluids Engineering, Trans ASME, pp.236-243, June 1976.

Adkins R. C. and Wardle M. H., (1992), “A method for the design of optimum Annular diffusers of canted configuration,” Journal of Engineering for Gas turbine and Power, Trans ASME, Vol.114, pp. 8-12, Jan 1992.

Adkins R. C., (1975), “A short diffuser with low pressure loss,” Journal of fluids Engineering, Trans. ASME, pp. 297-302, Sep 1975.

Agrawal D. P., Singh S. N., Sapre R .N. and Malhotra R. C., (1989), "Effect of Hub Rotation on the Mean Flow of Wide Angle Annular Diffusers", Hydro Turbo 1989, 89, Vol. 1, pp. 231–240, Ostrava., Czechoslovakia.

Agrawal D. P., Singh S. N., Sapre R. N. and Malhotra R. C., (1994), "Effect of Casing angle Flow development in Annular Diffuser with hub rotation", Journal of Aeronautical. Society of India, Vol.46, No.3 pp.144-153, Aug. 1994.

Agrawal D. P., Yahya S. M. and Thankappan K. V., [(991), "Effect of inlet velocity distribution on the vaned radial diffuser performance," ASME FED-119.

Ainley D. G., (1946), "Investigation of air flow through some annular diffusers," Power Jets Report No, R 1151.

Al-Mudhafar M.M., Ilyas M. and Bhinder F.S., (1982), "Investigation of flows in a rectangular diffusers with inlet flow distortions," ASME paper No. 82-GT-67.

Armfield S. W. and Fletcher C. A. J., (1986), ''Simulation of Internal Swirling Flow Using Mixing Length and k-ε Turbulence Models,'' Proceeding. Int. Symposium Computational Fluid Dynamics in Tokyo, pp. 740–751, Amsterdam, North Holland.

Armfield S. W. and Fletcher C. A. J., (1986), "A Comparison of Single and Multi-Sweep Techniques for Reduced Navier-Stokes Equations," Computer Technology and Applications. CTAC 85, pp. 431–442, Amsterdam, North Holland.

Armfield S. W., (1990), "Prediction of Turbulence quantities of swirling flow in conical diffusers," AIAA Journal Vol.28, No.3, pp. 453–460.

Armfield, S. W. and Fletcher, C. A. J., (1986), "Numerical simulation of swirling flow in diffusers," Int. J. Numerical Methods in Fluids, Vol.6, pp. 541–556.

Arora B. B. and Pathak B. D., (2011), “CFD analysis of axial annular diffuser with both hub and casing diverging at unequal angles”, International Journal of Dynamics of Fluids, 7(1), 109-122.

Arora B. B, Kumar M. and Mazi S., (2010), “A Study of Inlet Conditions on Diffuser Performance” Journal International Journal of Theoretical and Applied Mechanics” ISSN 0973-6085 Volume 5 Number 2(2010) pp. 201-221, 2010

Arora B. B, Kumar M. and Mazi S., (2010), “Analysis of Flow Separation in Wide Angle Annular Diffusers” International Journal of Applied Engineering Research ISSN 0973-4562 Volume 5 Number 20, pp. 3419– 3428.

Arora B. B. (2014), “Performance analysis of parallel hub diverging casing axial annular diffuser with 20° equivalent cone angle” Australian Journal of Mechanical Engineering, Vol 12 No 2.

Arora B. B. and Pathak B. D., (2009), “*Effect of Geometry on the Performance of Annular Diffuser*” International Journal of Applied Engineering Research,2009, Vol. 4, 2639–2652.

Arora B. B. and Pathak B. D., 2005 “Flow characteristics of parallel hub diverging casing axial annular diffusers”. ISME publication pp 794-798.

Arora B. B., 2007, “Aerodynamic Analysis of Diffuser”, PhD Thesis, 2007, DU, Delhi.

Ashjee J. and Johnston J. P., (1979), “Transitory stall in diffusers,” presented at the symposium on flow in primary, non rotating passages in turbo machines. ASME winter annual meeting.

Ashjee J. and Johnston J. P., (1980), “Straight walled two dimensional diffusers-transitory stall and peak pressure recovery,” Journal of fluids Engineering, Trans. ASME, Vol.110, pp.275-282.

Azouz I. and Shirazi S. A., (1997), “Numerical simulation of drag reducing turbulent flow in annular conduits,” Journal of fluids Engineering, Trans. ASME, vol.119, pp.838-846

Badawy M. T. S and Aly M. E., (2000), “Gas dynamic analysis of the performance of diffuser augmented wind turbine,” Mechanical Engineering Department, National Research Center, Dokki, Cairo, Egypt, Vol. 25, Part 5, October 2000, pp. 453-461.

Bansal S. C. and Khanna J. K. (1977), “On the factors affecting the performance of straight conical diffusers,” Presented at the 7th National conference on Fluid Mechanics and Fluid Power, Baroda, India.

Barbosa D. L., Vaz J. R., Figueiredo, S. W., Silva M. D. O. E., Lins E. F. and Mesquita

A. L., (2015), “An investigation of a mathematical model for the internal velocity profile of conical diffusers applied to DAWTs”, Anais da Academia Brasileira de Ciências, 87(2), 1133-1148.

Bardina .J, Lyrio A. and Kline. S. J. (1981), “A prediction model for planer diffuser flows,” ASME journal of fluid Engineering, Vol.103, pp.315-321.

Barker A. G. and Carrotte J. F. (2001), “Influence of compressor exit conditions on combustor annular diffusers, Part 2: Flow redistribution.” Journal of Propulsion and Power, 17, No. 3, pp. 687-694.

Batchelor G. K. (1967), “An Introduction to Fluid Dynamics”, Cambridge University Press, Cambridge, England. Pp.348.

Benedict R. P., Gleed A. R. and Sehulte R. D., (1973), “Air and water studies on a diffuser modified flow nozzle” Journal of fluids Engineering, Trans ASME, pp.169-179, June 1973.

Bhaskarone E. A., (1991), “Finite element analysis of Turbulent flow in annular exhaust diffuser of gas turbine Engines,” Journal of fluids Engineering, Trans ASME, Vol.113, pp104-110, March 1991.

Bose T. K., Thanawala R. H. and Annamalai K., (1992), “CFD analysis of A Rocket

Exhaust Diffusers," Journal of Aeronautical Society of India, Vol.44, No.4, pp.355-359, Nov. 1992.

Bradshaw P, (1972), "The understanding and prediction of turbulent flow," J. Royal Aeronautical Society Vol.6. pp. 403-408.

Bradshaw P., (1963) "Performance of a diffuser with fully developed, pipe flow at entry," J. Royal Aeronautical Society, Vol.67, P.733-736.

Brighton J. A. and Jones J. B., (1964), "Fully-developed turbulent flow in annuli," ASME J. Basic Engineering., Vol.86, pp.835-839.

Bryer D. W. and Pankhurst R. C., (1971), "Pressure Probe methods for determining wind speed and flow direction," H.M.S.O., London.

Bryer D. W., Walshe D. E. and Garner M. C., (1958), "Pressure probes selected for three-dimensional flow measurements," Aeronautical Research Council, R&M 3037.

Buice C. U. and Eaton J. K., (1997), "Experimental Investigation of Flow Through an Asymmetric Plane Diffuser", Report No.TSD-107, Thermo sciences Division, Department of Mechanical Engineering, Stanford University, Stanford, CA, USA.

Buice C. U. and Eaton J. K., (2000), "Experimental Investigation of Flow through an

Asymmetric Plane Diffuser," Journal of fluids Engineering, Trans. ASME, Vol.122, pp.433-435, Jun 2000.

Carlson J. J., Johnston J. P. and Sagi C. J., (1967), "Effects of wall shape on flow regimes and performance in straight, two-dimensional diffusers. ASME J,. Basic Engg., Vol 89., P 151.

Chithambaran V. K, Aswatha, Narayana P. A, Chandrashekra Swamy N. V, (1984), "Mean velocity characteristics of plane diffuser flows with inlet velocity distortion." Journal of Indian Institute of Science, 65(A):79-93.

Choudhury D. (1993), "Introduction to the Renormalization Group Method and Turbulence Modeling." Fluent Inc. Technical Memorandum TM-107.

Clausen P. D., Koh S. G. and Wood D. H. (1993), "Measurement of a swirling boundary layer developing in a conical diffuser," Journal Experimental Thermal and Fluid Sciences, Vol.6, pp.39-48.

Cockrell D. J. and Markland E., (1963), "A review of incompressible diffuser flow," Journal Aircraft Engineering, Vol.35, pp.286-295.

Coladipietro R., Schneider J. H. and Shridhar K., (1974), "Effects of inlet flow conditions on the performance of equiangular annular diffusers", CSME Paper No.73, CSME 84.

Constantinescu G., Mahesh K., Apte S., Iaccarino G., Ham F. and Moin P., (2003), "A new paradigm for simulation of turbulent combustion in realistic gas turbine combustors using LES," ASME Turbo Expo 2003, GT2003-38356

Dau K., McLood M. and Surry D., (1968), "Two probes for the measurement of complete velocity vector in subsonic flow," J. Royal Aeronautical Society, Vol.72, pp.1066.

Davis R., Yao J., Clark J. P., Stetson G, Alonso J. J., Jameson A., Halde-man C. and Dunn M., (2002), "Unsteady interaction between a transonic turbine stage and downstream components," ASME Turbo Expo 2002, GT-2002-30364.

Davis, R., Yao, J., Alonso, J. J., Paolillo, R. and Sharma O. P., (2003), "Prediction of main/secondary-air system flow interaction in a high pressure turbine," AIAA Paper 2003-4833.

Dean Jr, R. C., and Runstadler Jr, P. W. (1969), "Straight channel diffuser performance at high inlet Mach numbers", Creare, Inc., Hanover, NH, TN-88.

Dellenback P. A., Metzger D. E. and Neitzel G. P., (1988), "Measurements in turbulent swirling flow through an abrupt axisymmetric expansion," AIAA J., Vol. 26, pp. 669-681.

Dolan F. X. and Runstadler P. W., (l973), “Pressure recovery Performance of conical diffusers at high subsonic Mach numbers,” NASA, CR-2299.

Dovzhik S. A. and Kartavenko V. M., (1975), “Measurements of the effect of flow swirl on the efficiency of annular ducts and exhaust nozzles of axial turbo machines,” Fluid Mechanics, Soviet Research, Vol. 4, pp.156-172.

Duggins R. K. (1975), “Conical diffusers with annular injection,” J. Mechanical Engineering Science, Vol.17, pp.237-245.

Duggins R. K., (1970), “The performance of conical diffusers discharging through tailpipes,”Journal Aircraft Engineering, Vol.42, pp.28-30.

Duncan Walker A., Denman Paul A. and McGuirk James, J., (2004)**, “**Experimental and Computational Study of Hybrid Diffusers for Gas Turbine Combustors”, ASME Journal of Engineering for Gas Turbines and Power, Vol. 126, No. 4, pp. 717–725, October 2004.

El-Askary W. A., Ibrahim K. A., El-Behery S. M., Hamed M. H. and Al-Agha M. S., (2015), “Performance of vertical diffusers carrying Gas-solid flow: experimental and numerical studies”, Powder Technology, 273, 19-32.

Filipenco V. G., Deniz D., Johnston J. M. and Greitzer E. M., (2000), “Effects of Inlet Flow Field Conditions on the Performance of Centrifugal Compressor Diffusers: Part 1

— Discrete-Passage Diffuser", Journal of Turbomachinery, 122(1), DOI:10.1115/1.555418

Frendikov I. A. and Yanko A. K., (1972), "Some results of experiments with conical diffusers," Fluid Mechanics/ Soviet Research 1(5):72.

Gartner J., & Amitay M., (2016). "Vortex generator's effectiveness compared to active flow control techniques in a transonic diffuser", In the 8th AIAA Flow Control Conference (p. 3770).

Ginevsskiy A. S, Kolesnikov A. V, Podolnyy I. N. and Smolyaninova A. N., (1975), "Aerodynamic performance of flat diffuser with no flow separation," Fluid Mechanics, Soviet Research, Begall house Vol. 4, No. 3, pp. 68-88.

Gorman J. M., Sparrow E. M., Abraham J. P. and Minkowycz W. J. (2016), "Evaluation of the efficacy of turbulence models for swirling flows and the effect of turbulence intensity on heat transfer", Numerical Heat Transfer, Part B: Fundamentals, 70(6), 485-502.

Hah C., (1983), "Calculation of Planar, Conical and Annular diffuser flows with inlet swirls and inlet distortion effects," AIAA journal, vol. 21, No.8, pp.223-253.

Hestermann R., Kim S., Ben Khaled A. and Wittig S., (1995), " Flow field and

performance characteristics of combustor diffusers: A basic study," Journal of Engineering for Gas Turbine and Power, Trans. ASME, Vol.117, pp.686-694.

Hoadley D. and Hughes D. W., (1969), "Swirling flow in an annular diffuser," Department of Engineering, University of Cainbridge, London. Report CUED/A-Turbo/TR5.

Hoadley D., (1970), "Three-Dimensional Turbulent Boundary Layers in an Annular Diffuser", Ph.D. Thesis, Department of Engineering, University of Cainbridge, London.

Hoffmann J. A. and Fang L. W., (1988), "Influence of the structure of inlet free stream turbulence on diffuser performance," AIAA paper No. 88-3673 CP.

Hoffmann J. A. and Gonzales G, (1984), "Effect of small scale high intensity turbulence on flow in a two dimensional diffuser," Journal of fluids Engineering, Trans. ASME, Vol.106, pp.121-124.

Hoffmann J. A., (1981), "Effect of free stream Turbulence on diffuser performance," Journal of fluids Engineering, Trans. ASME, Vol.103, pp.385-390, Mar1974.

Howard J. H. G., Thronton-Trump A. B. and Henseler H. J., (1967), "Performance and flow regimes of annular diffusers," ASME Paper No. 67-WA/FE 21.

Ishida M., Sakaguchi D. and Ueki H., (2001), “Suppression of Rotating Stall by Wall Roughness Control in Vane less Diffusers of Centrifugal Blowers,” ASME Journal of Turbo machinery, Vol. 123, No. 1, pp. 64–72, January 2001.

Ishikawa K. and Nakamura I., (1989), “Performance charts and optimum geometries of conical diffusers with uniform inlet flow and free discharge,” JSME international Journal, series II, Vol. 32, No. 4, pp.559-567.

Ishikawa K. and Nakamura I., (1990), “Performance charts and optimum geometries of conical diffusers with uniform inlet flow and tailpipe discharge,” JSME international Journal, series II, Vol. 33, No. 1, pp.97-105.

Japikse D. and Pampreen R., (1979), “Annular diffuser performance for an automotive Gas Turbine.” ASME journal of Engineering for power, Vol.101, pp.358-372.

Japikse D., (1986), “ A new diffuser mapping technique Part 1 – Studies in component performance “, Journal of fluids Engineering, Trans ASME, Vol.108, pp.148-156

Ji-jun Y., Zhao-gang Y. and Ming-de W., (1992), ‘‘On the Through flow with Swirling Flow in Annular Diffuser,’’ Applied. Mathematical. Mechanics, Vol. 13, No. 3, Shanghai, China, pp. 241–254.

Johnston I. H., (1954), “The effect of inlet conditions on flow in annular diffusers,”

Report No. ARC CP 178.

Johnston J. P., (1998), “Review: Diffuser Design and performance analysis by a unified integral method,” Journal of fluids Engineering, Trans. ASME, Vol. 120, pp 6-18

Kanemoto T. and Toyokura T., (1983), “Flow in Annular Diffusers : 2nd Report, Flow Analysis and Effect of Inlet Boundary Layer Thickness,” JSME, Vol. 26, No.218(19830800) pp.1323-1329.

Kanemoto T., Toyokura T. and Kurokawa J., (1982), “Flow in Annular Diffuser : 1st Report, Internal Flow and Performance,” JSME, Vol. 25, No.204(19820600) pp.912-918.

Kano F., Tazawa N. and Fukao Y., (1982), “Aerodynamic performance of large centrifugal compressors,” ASME paper No. 82-GT-17.

Karanja K. and Anthony S, (2008). Experimental Measurements of the Mean Flow Field in Wide-Angled Diffusers: A Data Bank Contribution. International Journal of Mechanical, Aerospace, Industrial, Mechatronic and Manufacturing Engineering, Vol: 2, No: 7.

Kelnhofer W. J. and Derick C. T., (1971), “Tailpipe effects on gas turbine diffuser performance with fully developed inlet conditions,” Journal of Engineering for power, Trans. ASME Vol. 93, No. 1, pp.57–62.

Kenny D. P., (1972), “A comparison of predicted and measured performance of high pressure ratio centrifugal compressor diffusers,” ASME paper No. 72-GT-54.

Klein A., (1981), “Review: Effects of inlet conditions on conical diffuser performance,” Journal of fluids Engineering, Trans ASME, Vol.103, pp. 250-257.

Klein A., (1995), “Characteristics of combustor diffusers,” Programme, Aerospace Science, Vol.31, pp.171.

Kochevsky A. N., (2001), “Numerical investigation of swirling flow annular Diffusers with a rotating hub installed at the exit of hydraulic machines,” Journal of fluids Engineering, Trans ASME, Vol.123,pp 484-489, Sep.2001

Kochevsky A. N., (2004), “Computation of internal fluid flows in channels using the CFD software tool flow vision,” Paper No. 2134

Kumar D. S. and Kumar K. L., (1978), “Effect of swirling flow through annular diffusers,” Ist International conference on centrifugal compressors Technology, pp. D1-1 to D1-10.

Kumar D. S., (1977), “Effect of swirl on flow through annular diffusers,” Ph.D. Thesis, I.I.T. Delhi.

Kumar M., Arora B. B., Maji S. and Maji S., (2011), “Effect of Inlet Swirl on the Flow Behavior inside Annular Diffuser”, International Journal of Dynamics of Fluids., Vol. 7, pp 181-188.

Kwon O. B., Kim M. K., Kwon H. C. and Bae D. S., (2002), “Two-dimensional Numerical Simulations on the Performance of an Annular Jet Pump,” The Visualization Society of Japan and Ohmsha, Ltd., Journal of Visualization, Vol. 5, No. 1 (2002), pp. 21-28.

Kwong A. H. M. and Dowling A. P., (1994), “Active Boundary Layer control in diffusers,” AIAA Journal Vol.32, No.12, pp. 2409-2414, Dec 1994.

Kwong A. H. M. and Dowling A.P., (1994), “Unsteady flow in diffusers,” Journal of fluids Engineering, Trans. ASME, Vol. 116, pp. 842-847, Dec 1994

Lai Y. G. and So R. M. C., (1989), “Calculation of planer and conical diffuser flows,” AIAA journal , Vol. 27, No. 5, pp. 542-548.

Lee Y-T., Luo L. and Bein T., (2000), “Direct Method for Optimization of a Centrifugal Compressor Vaneless Diffuser,” Journal of Turbomachinery-transactions of The ASME, DOI: 10.1115/1.1308571

Liepe F., (1960), “Efficiency of thin conical diffusers in swirling flows,” Maschinenbautechnik, Vol.9, pp.405-412

Lipeng L., Luyang Z. and Yangwei L., (2016), "Turbulence models assessment for separated flows in a rectangular asymmetric three-dimensional diffuser". Engineering Computations, Vol. 33 No. 4 pp 978–994.

Little B. H. Jr. and Wilbur S. W., (1954), “Performance and boundary layer data from 12deg and 23 deg conical diffuser of area ratio 2.0 at Mach Numbers up to choking and Reynolds Numbers up to $7.5x10^6$,” NACA report 1201.

Little B. H., JR. and Wilbur S. W., (1950), “Performance area ratio and boundary-layer data from 12° and 23° conical diffusers 2.0 at Mach numbers up to choking and Reynolds numbers up to $7.5x10^6$ ”, National advisory committee for aeronautics.

Livesey J. L. and Odukewe A. O., (1973), “Some effects of pipe flow generated entry conditions on the performance of straight walled conical diffusers with high subsonic entry Mach Number,” Israel Journal of Technology, Vol.11, No. 4, pp.217-222.

Lohmann R. P., Markowski S. J. and Brookman E. T., (1979), ‘‘Swirling Flow through Annular Diffusers with Conical Walls,’’ ASME J. Fluids Engineering, Vol.101, No. 2, pp. 224–229.

Mansour N. N, Kim J. and Moin P., (1989), “Near wall k-ε Turbulence Modeling,” Journal AIAA, Vol.27, pp.1068-1073, Aug. 1989.

Masuda S., Ariga I. and Watanabe I., (1971), “On the behavior of uniform shear flow in diffusers and its effects on diffuser performance,” Journal of Engineering for Power, Trans ASME, pp377-385, Oct 1971.

Masuda S., Ariga I. and Watanabe I., (1975), “Uniform shear flow with rectangular parallel walled diffusers,” ASME paper No.75-FE-34

McDonald A. T and Fox R. W., (1965), “An experimental investigation of incompressible flow in conical diffusers,” ASME Paper No. 65-FE-25.

McDonald A. T., Fox R. W. and Van Dowoestine R. V., (1971), “Effects of, swirling inlet flow on pressure recovery in conical diffusers,” AIAA Journal Paper No. 71-84. Vol.9, No.10.pp.2014-2018.

Mcmillan O. J. and Johnston J. P., (1973), “Performance of low aspect ratio diffuser with fully developed Turbulent inlet flows, Part 2- Development and application of a performance prediction method,” Journal of fluids Engineering, Trans. ASME, pp.393-400, Sep.1973.

Michel J. C. and Engstrom F. T., (2004), “Factorial Design Applied to CFD,” ASME

Journal of Fluids Engineering, Vol. 126, No. 5, pp. 791–798, September 2004.

Miler D. S., (1971), “Performance of straight diffusers,” Internal flow: A guide to losses in pipe and duct systems, Part II, British Hydrodynamic Research Association.

Mohan, R., Singh, S. N. and Agrawal D. P., (1998), “Optimum inlet swirl for annular diffuser performance using CFD,” Indian journal of engineering and materials sciences 1998, vol. 5, pp. 15-21

Moller P. S. (1966). A radial diffuser using incompressible flow between narrowly spaced disks. Journal of Basic Engineering, vol. 88(1), pp. 155-162.

Moyle K. R., Antiga L. and Steinman D. A. (2006) “Inlet Conditions for Image-Based CFD Models of the Carotid Bifurcation: Is it Reasonable to assume fully developed Flow?” ASME Journal of Biomechanical Engineering, Vol. 128, No. 3, pp. 371–379, June 2006.

Neve R. S., (1993), “Computational fluid dynamics analysis of diffuser performance in gas powered jet pumps,” Int. Journal of Heat and fluid flow, Vol. 14, No. 4, pp. 401-407

Nordin N., Karim A., Ambri Z., Othman S. and Raghavan V. R., (2015), “Effect of varying inflow Reynolds number on pressure recovery and flow uniformity of 3-D turning diffuser”. Applied Mechanics and Materials, Vol. 699, pp. 422-428, Trans Tech

Publications.

Nordin N., Karim Z. A. A., Othman S., Raghavan V. R., Batcha M. F. M., Hariri A. and Basharie S. M., (2017, April). Flow characteristics of 3-D turning diffuser using particle image velocimetry. In AIP Conference Proceedings (Vol. 1831, No. 1, p.020021). AIP Publishing.

Noui-Mehidi M. N., Wu J. and Sutalo I., (2004), "Velocity distribution in an asymmetric diffuser with perforated plates," 15th Australasian Fluid Mechanics Conference, The University of Sydney, Sydney, Australia, 13-17 December 2004

Patterson G. N., (1938), "Modern diffuser design-Aircraft Engineering," Vol.10, pp.267-270.

Perry J. H., (1974), "Calibration and comparison of cobra probe and hot wire anemometer for flow measurements in turbo machinery," Tech. Report No. TRI, Division of Mechanical Engineering, CSIRO Australia.

Peters, H., (1934), "Conversion of energy in cross sectional divergence under different conditions of inflow," NACA TM 737.

Poroseva, S. and Iccarino, G., (2001) "Simulating separated flows using the k-ε model," Center for Turbulence Research Annual Research Briefs 2001.

Raghunathan, S. and Cooper, R. K., (2000), “Passive Boundary layer control with slots in short diffuser,” Journal of fluids Engineering, Trans. ASME, Vol.122, pp.177-179

Reneau L. R., Johnston J. P. and Kline S. J., (1967), “Performance and design of straight, two dimensional diffusers,” ASME J. Basic Engg. Vol. 90, pp.141-150.

Reneau, L. R. and Johnston, J. P., (1966), “A Performance prediction method for unstalled, two dimensional diffusers,” ASME J. Basic Engg. Vol. 89, pp.643-654.

Reneau, L. R., Johnston, J. P. and Kline, S. J., (1964), “Performance and design of straight, two dimensional diffusers,” Report PD-8, Thermo sciences Division, Mechanical Engineering Department, Stanford University.

Ripple E., (1958), “Experimental investigations concerning the efficiency of slim conical diffusers and their behavior with regard to flow separation,” Monthly Technical Review, Vol. 2, pp. 64.

Runstadler P. W. Jr and Dean R. C. Jr., (1969), “Straight channel diffuser at high inlet Mach numbers," ASME Journal Basic Engineering. Vol.91, pp.397-401.

Runstadler P. W. Jr. and Dolan F. X., (1973), “Further data on the pressure recovery performance of straight channel, plane divergence diffuser at high subsonic mach

numbers," Journal of fluids Engineering, Trans ASME, pp.373-384, Sep.1973.

Sajben, M., Kroutil, J. C., Sedrick, A. V. and Hoffman G. H., (1974), "Experiment on conical diffuser with distorted inflow," AIAA paper 74-529.

Sapre R. N., Singh S. N., Agrawal D. P and Malhotra R. C., (1987), "Flow Through Equiangular Wide Angle Annular Diffusers", 15th NCFMFP, Srinagar, July, 1987.

Schlauter J. U., Wu X., Kim S., Alonso J. J. and Pitsch H., (2003), "Integrated RANS-LES computations of turbo machinery components: Generic compressor/diffuser," Center for Turbulence Research Annual Research Briefs 2003, pp.357-368.

Schwartz I. R., (1949), "Investigation of an annular diffuser fan combination handling rotating flow," NACA RM No. L9B28.

Selvakarthick C., Ajith S., Nagaraju D. H., Kumar S. V. R., Rangaraj V. and Allen, J. K., (2016), "Parametrical Optimization of a three-dimensional Dump Diffuser with Aerodynamically-shaped Flame Tube for Modern Aircraft Engines", In 52nd AIAA/SAE/ASEE Joint Propulsion Conference (p. 5009).

Senno, Y., Kawaguachi, N. and Nagata, T., (1978), "Swirl flow in conical diffusers," Bulletin JSME, Vol. 21, pp.112-119.

Sharan, V. K., (1972), “Diffuser performance correlation,” J. Aeronautical Society of India, Vol.24, pp.415-419.

Sharan, V. K., (1972), “Improving diffuser performance by artificial means,” AIAA Journal 10, pp.1105-1106.

Sharan, V. K., (1976), “Factors influencing the performance of a diffuser,” Indian jornal of technology Vol.14, No.2, pp. 63-66.

Shi F. and Tsukamoto H., (2001), “Numerical study of pressure fluctuations caused by impeller-diffuser interaction in a diffuser pump stage,” Journal of fluids Engineering, Trans. ASME, Vol. 123, pp. 466-474.

Shimizu, Y., Kuzuhara, S. and Nagafusa, M., (1982), “Effects of approaching flow on the performance of straight conical diffusers,” Bulletin JSME 25, pp. 1506-1512.

Shulleray R. K., Ashok V. and Shantharam K. V. (1992), “Effect of inlet flow distortion on performance of vortex controlled diffusers,” Journal of fluids Engineering, Trans. ASME, Vol. 114, pp. 191-197, June1992.

Singh H. and Arora B. B., (2021), “Effect of swirl flow on the performance of parallel hub axial annular diffuser,” Journal of Engg. Research Vol.10 No. (1B) pp. 240-251

Singh H. and Arora B. B., (2023), “Effects of casing angle on the performance of parallel hub axial annular diffuser” International Journal of Turbo & Jet-Engines, 40(1): 31–41, Elsevier

Singh S. N, Agarwal D. P. and Gosman A. D., (1995), "Flow Prediction in Axisymmetric Axial Diffusers", Institution of Engineers(I) Journal MC, vol. 76, pp 24-29, May 1995.

Singh, H. and Arora B. B., (2019) “Optimization of inlet swirl for separation in annular diffuser” International Conference on Emerging Trends in Electro-Mechanical Technologies and Management, HMR Institute of Technology & Management, Delhi(26-27 July 2019), Lecture Notes in Mechanical Engineering, ISSN 2195-4356.

Singh, H. and Arora B. B., (2019), “Review: effect of inlet condition on diffuser performance” International Journal of Mechanical and Production Engineering Research and Development (IJMPERD), Vol. 9, Issue 5, pp. 813–832

Singh, S. N., Agrawal, D. P., Sapre, R. N., and Malhotra, R. C., (1994), ‘‘Effect of inlet swirl on the performance of wide-angled annular diffusers,’’ Indian Journal of Engineering and Materials Sciences, Vol.1, pp. 63–69.

Sitaram N. and Treaster A. L., (1985), “ A Simplified method using Four hole Probes to measure Three dimensional flow fields,” Journal of fluids Engineering, Trans. ASME, Vol.107, pp.31-35, Dec 1985.

So, K. L., (1967), “Vortex phenomena in conical diffuser,” AIAA Journal, vol,5, pp.1072-1076.

Sovran, G. and Klomp, E. D., (1967), “Experimentally determined optimum geometries for rectilinear diffusers with rectangular, conical or annular cross-section,” Fluid Mechanics of Internal Flow, Ed. G. Sovran, Elsevier, Amsterdam, pp.270.

Spall, R. E. and Ashby, B. M., (2000), “A Numerical study of vortex breakdown in turbulent swirling flows,” Journal of fluids Engineering, Trans. ASME, Vol.122, pp.179-181, Jun 2000.

Sprenger H., (1959), “Experimental research on straight and carved diffusers,” Mitt. Inst., Aero, E.T.H. Zurich, Translation TIL/T.5134, Min, of Aviation, U.K., 1962.

Srinath T., (1968), “An investigation of the effects of swirl on flow regimes and performance of annular diffusers with equal inner and outer cone angles. Thesis,” University of Waterloo, Canada.

Stevens S. J. and Markland E., (1968), “The effect of inlet conditions on the performance of two annular diffusers,” ASME Paper No68-WA/FE-38.

Stevens S. J. and Williams G. J., (1971), “Measurements of the overall performance and

boundary layer growth in an annular diffuser," Symposium on Internal Flows, Salford University, England, 1971.

Stevens S. J. and Williams G. J., (1980), "The influence of inlet conditions on the performance of annular diffusers," Journal of fluids Engineering, Trans. ASME, Vol.102, pp. 357-363.

Stevens S. J., (1968), "The Performance of Annular Diffusers". Proceedings Institution of Mech. Engineers., Vol. 182, Part 31, pp. 58-62.

Su K. and Zhou C. Q., (2000), "Numerical modeling of Gas Turbine Combustor integrated with Diffuser," Proceedings of NHTC'00,34th National Heat Transfer Conference, Pittsburgh, Pennsylvania, August 20–22, 2000.

Suzuki T. and Colonius T., (2003), "Large-scale unsteadiness in a two-dimensional diffuser: numerical study toward active separation control," AIAA Paper 2003-1138

Thakker A., (1986), "Effect of solid body swirl on wide angle diffusers," J. Fluid control and Management," Pergamon, Vol.1, pp. 503-514.

Thakker A., Frawwley P., Jambunathan K. and Ashiforth-Frost S., (1991), "Axial and swirling flow in a diffuser: A comparison of simulation and LDA experimental results," ASME Journal Laser Anemometry, Vol. 1, pp.211-216.

Thayer E. B., (1971), “Evaluation of curved wall annular diffusers,” ASME paper No. 71-WA/FE-35.

Tsui Y. Y. and Wang C., (1995), “Calculation of laminar separated flow in symmetric Two dimensional diffusers” Journal of fluids Engineering, Trans. ASME, Vol.117, pp. 612-616.

Tsurusaki H. and Kinoshita T, (2001), “Flow control of rotating stall in a radial vaneless diffuser,” Journal of fluids Engineering, Trans. ASME, Vol.123, pp.281-286, Jun 2001.

Tyler R. A and Williamson R. G., (1973), “Conical diffusers with inflow distortions: estimated peak velocity at exit,” National Research Council of Canada, Report No. 13716.

Tyler R. A. and Williamson R. G., (1968), “Diffuser performance with distorted flow,” Proceedings Institution of Mechanical Engineers 182(3D), pp. 115-125.

Ubertini S. and Desideri U., (2000), “Experimental performance analysis of an annular diffuser with and without struts,” Elsevier, J. Experimental Thermal and Fluid Science Vol. 22, Number 3, September 2000, pp. 183-195(13).

Van Dewoestine, R. V. and Fox, R. W., (1966), “An experimental investigation on the

effect of subsonic inlet Mach number on the performance of conical diffusers," International Journal of Mechanical Sciences, Vol.8. No.12, pp.759-769.

Vassiliev V., Irmisch S. and Florajancic S., (2002), "CFD analysis of Industrial Gas Turbine Exhaust Diffusers," Proceedings of ASME Turbo Expo 2002, June3-6, 2002, Amsterdam, The Netherlands Paper No. 2002-GT-30597.

Vlahostergios Z. and Yakinthos K., (2015), "Modeling the Flow in a Transonic Diffuser with One Reynolds-Stress and Two Eddy-Viscosity Models", Flow, Turbulence and Combustion, vol. 94, no. 3, pp 619-642.

Waitman B. A, Reneau L. R. and Kline S. J., (1961): Effects of inlet conditions on performance of two-dimensional subsonic diffusers. J. Basic Engg. Vol.83, P.349.

Wen C., Cao X., Yang Y. and Li W. (2012), "Numerical simulation of natural gas flows in diffusers for supersonic separators. Energy", 37(1), 195-200.

Wolf S. and Johnston J. P., (1969), "Effects of non uniform inlet velocity profile on flow regimes and performance in two dimensional diffusers," Journal of fluids Engineering, Trans. ASME, Vol.91, pp. 462-474.

Xu H. T. and Niu J. L., (2003), "A new method of CFD simulation of airflow characteristics of swirling floor diffusers," Eighth International IBPSA Conference

Eindhoven, Netherlands, August 11-14, 2003

Yeung, W. W. H. and Parkinson, G. V., (2004), "Analysis and Modeling of Pressure Recovery for Separated Reattaching Flows," ASME Journal of Fluids Engineering, Vol. 126, No. 3, pp. 355–361, May 2004**.**

Yongsen H., Kobayashi T., and Morinishi Y., (1992), "Numerical prediction of turbulent flow in a conical diffuser using *k*-ε model," Journal Applied Mathematics and Mechanics, Vol. 8, No.2. pp. 117-126.

Yoshinaga Y., Kaneki T., Kobayashi H. and Hoshino M., (1985), "A study of performance improvement for high speed centrifugal compressors by using diffusers with half guide vanes," ASME FED-32.

Yu J. J., Yang Z. G. and Wang M. D., (1992), "On the through flow with swirling inflow in annular diffuser," J. Applied Mathematics and Engineering, Vol.13. No.3, pp. 241-254.

Details of SCIE Publications

S. No.	Title of the Paper	Authors	Name of Journal	Indexation / Ranking of Journal (with proof)	Published / Accepted	Publisher	DOI
1.	EFFECT OF INLET SUBSONIC VELOCITY AND AREA RATIO ON THE PRESSURE RECOVERY IN EQUIVALENT CONE ANGLE ANNULAR DIFFUSER	Priya & B. B. Arora	International Journal of Maritime Engineering ISSN/ eISSN: 1479-8751 / 1740-0716	SCIE Indexed Journal	2025	UNIV BUCKINGHAM PRESS	10.5750/ijme.v167iA3(S).1711
2.	ANALYSIS OF SWIRLING FLOW IN ANNULAR DIFFUSER	Priya & B. B. Arora	International Journal of Maritime Engineering ISSN/ eISSN: 1479-8751 / 1740-0716	SCIE Indexed Journal	Accepted	UNIV BUCKINGHAM PRESS	N.A.

Participation in International Conferences

S. No.	Title of the Paper	Authors of Paper	Title of Conference	Organizers Conference	Date	National / International	Venue of Conference
1.	EFFECT OF INLET SWIRL ON STRAIGHT ANNULAR DIFFUSER	Priya & B. B. Arora	International Conference of Advance Research and Innovation (ICARI-2024)	International Journal of Advance Research and Innovation	28th January 2024	International	Delhi State Center, Institution of Engineers (India), New Delhi, India
2.	EFFECT OF INLET SUBSONIC VELOCITY AND AREA RATIO ON THE PRESSURE RECOVERY IN EQUIANGULAR CONICAL DIFFUSER	Priya & B. B. Arora	International Conference of Advance Research and Innovation (ICARI-2024)	International Journal of Advance Research and Innovation	28th January 2024	International	Delhi State Center, Institution of Engineers (India), New Delhi, India